MÉTODOS MATEMÁTICOS PARA ESTUDIAR EL PROCESAMIENTO DE LA INFORMACIÓN EN LA RETINA

MATHEMATICAL METHODS TO STUDY INFORMATION PROCESSING IN THE RETINA

José Ángel Bolea Oliván

MEMORIA DE TESIS DOCTORAL

DIRECTOR: Eduardo Fernández Jover

Año 2017

Instituto de Bioingeniería

Universidad Miguel Hernández

UNIVERSITAS
Miguel
Hernández

Instituto de Bioingeniería
Universidad Miguel Hernández

UNIVERSITAS Miguel Hernández

El Prof. Dr. D. Eugenio Vilanova Gisbert, Director del Instituto de Bioingeniería de la Universidad Miguel Hernández,

HACE CONSTAR

Que da su conformidad a la lectura de la Tesis Doctoral presentada por D. José Ángel Bolea Oliván, titulada "Modelos matemáticos para estudiar el procesamiento de la información en la retina", que se ha desarrollado dentro del Programa de Doctorado de Bioingeniería, bajo la dirección del Prof. Dr. D. Eduardo Fernández Jover.

Lo que firma en Elche, a instancias del interesado y a los efectos oportunos, a diez de mayo de dos mil diecisiete.

Fdo.: Eugenio Vilanova Gisbert
Director del Instituto de Bioingeniería

UNIVERSITAS
Miguel
Hernández

Instituto de Bioingeniería
Universidad Miguel Hernández

UNIVERSITAS Miguel Hernández

Eduardo Fernández Jover, Catedrático de Biología Celular y Director del Grupo de Neuroingeniería Biomédica de la Universidad Miguel Hernández,

CERTIFICA

Que la memoria presentada para optar al grado de Doctor por la Universidad Miguel Hernández por D. José Ángel Bolea Olivan titulada "Modelos matemáticos para estudiar el procesamiento de la información en la retina", ha sido realizada bajo su dirección.

Que ha supervisado los contenidos científicos y los aspectos formales del trabajo y da su conformidad para su presentación y defensa pública.

Elche a 9 de Mayo de 2017

Fdo.: Eduardo Fernández

UNIVERSITAS
Miguel
Hernández

A Ignacio, José, Pedro y Lupe,

a los que tanto admiro

y, aún más, quiero.

UNIVERSITAS
Miguel
Hernández

Agradecimientos

Todo el trabajo que he realizado a lo largo de estos años y que ha dado lugar a las publicaciones que conforman esta Tesis se debe al interés y motivación por el mismo instigado y apoyado por Eduardo Fernández. Su contagioso entusiasmo para abordar ambiciosos proyectos científicos y su interés por enriquecerlos con aproximaciones interdisciplinares hicieron que me embarcara en esta fascinante aventura y que haya perseverado en ella intentando compatibilizarla con la enseñanza de las matemáticas, mi profesión y mi otra gran pasión .

Es mucho, y difícil de expresar, lo que tengo que agradecerle a Eduardo; sobre todo recuerdo con añoranza, ahora que por los compromisos laborales y la distancia no podemos apenas mantenerlas, esas conversaciones tan científicas y amistosas –en las que yo tanto aprendía– sobre lo que se sabía y lo que no, lo que necesitaba confirmarse o explorarse, las posibilidades de hacerlo, con qué tipo de experimentos… De ahí, de esos momentos, surgieron poco a poco gran parte de mis aproximaciones desde las matemáticas al estudio de la retina.

Otra razón para seguir investigando fue que siempre he encontrado en su laboratorio un muy buen ambiente de trabajo, propiciado por gente entusiasta con la que daba gusto colaborar: Marce, Raquel, Vicen, Arantxa, Montse y Antonio en los primeros tiempos; Paula y Markus poco después; Cristina y Ariadna recientemente. Y varios más a los que apenas conozco pero que creaban ese entorno a la vez afable y laborioso en el que se realizaban los

experimentos y se obtenían los datos con los que después podíamos trabajar. A todos, muchas gracias.

Mención aparte merecen dos personas, ambas dedicadas al campo de las Ciencias de la Computación, con las que también conviví en el laboratorio en aquellos añorados comienzos: José Manuel Ferrández y Óscar Martínez.

José Manuel es, como Eduardo a mi parecer, otro gran científico, con inquietudes semejantes, de las que buena muestra está dejando en sus responsabilidades en la Universidad Politécnica de Cartagena. Es una satisfacción haber podido compartir con él muchos trabajos e ideas, unos que han visto la luz y otros que no. Tengo mucho que agradecer a su sensatez, a su capacidad de trabajo y a sus conocimientos, siempre al día y de primera línea.

Óscar pasó de ser brillante alumno en el Instituto a compañero de fatigas en ese par de asignaturas más "biológicas", tan difíciles para nosotros, en los cursos del Doctorado de Bioingeniería. Conseguíamos acabar de entender todo aquello gracias a la eficaz ayuda y la sabiduría de Marcelino Avilés, que fue nuestro tutor y ejercía de tal. Quiero agradecerle a Óscar que, mientras progresaba en su exitosa e internacional carrera científica, encontrara suficiente tiempo para que desarrolláramos y validáramos el método de la *V-proporción*, que se recoge en un par de los artículos que aparecen en esta memoria de Tesis.

En fin, son muchas las deudas contraídas a lo largo de los años en que se realizaron los trabajos reflejados en las publicaciones que aquí se recogen. Quiero resaltar mi gratitud hacia todos los coautores de las mismas por lo sencillo e instructivo que ha resultado colaborar con ellos y la facilidad con que iban aceptando y asumiendo mis aportaciones e indicaciones.

También me gustaría mencionar a Juan Monterde, en otro tiempo compañero de estudios en la Facultad de Matemáticas de la Universidad de Valencia y actualmente profesor de la misma, por su ayuda ante una dificultad surgida cuando trabajaba en ciertos detalles finales del método ya citado basado en el diagrama de Voronoi. Su aportación hizo que buscáramos un enfoque distinto para su resolución.

No puedo terminar sin agradecer a Eduardo Sánchez-Villaseñor, Jesús Salas y, especialmente, Manuel Carretero, actuales compañeros en el Grupo de Matemática Aplicada de la Universidad Carlos III de Madrid el haber depositado su confianza en mí para formar parte del mismo y su gran ayuda para hacerme fácil mi docencia universitaria. Esto me ha permitido, además de compaginarla con mis clases en el Instituto, poder seguir con mis trabajos de investigación. También para ello compartir despacho, zozobras e inquietudes con José Manuel Pérez Morales ha sido un acicate. A él le agradezco que con su ejemplo me haya mostrado que hacer ciencia vale siempre la pena por muy adversas que puedan ser las circunstancias.

UNIVERSITAS
Miguel
Hernández

Resumen

La aplicación de métodos y herramientas matemáticas ha contribuido con éxito a los avances en neurociencia desde mediados del siglo XX. En los últimos años diversos progresos tecnológicos han permitido una mayor exploración del sistema nervioso, lo que ha provocado un llamativo aumento en el empleo de las matemáticas para investigar los numerosos datos ahora disponibles para los neurocientíficos.

En esta tesis doctoral hemos utilizado diversos métodos matemáticos para estudiar y analizar imágenes neuronales y señales fisiológicas obtenidas en experimentos con el objetivo de conocer cómo se procesa la información visual en la retina y analizar con que códigos se transmite al cerebro.

Inicialmente abordamos el estudio de varios aspectos morfológicos de las células de la retina para conocer con más precisión ciertas particularidades de los circuitos retinianos. En este sentido hemos estudiado la posible caracterización de las neuronas como multifractales (Fernández *et al.*, 1999) y hemos desarrollado un nuevo método -la *V-proporción*, basada en el diagrama de Voronoi- que permite estudiar las relaciones espaciales entre los mosaicos neuronales de la retina (Ahnelt *et al.*, 2000; Martínez *et al.*, 2010).

Paralelamente hemos analizado registros simultáneos de respuestas de poblaciones de células ganglionares de la retina, que son las encargadas de codificar la información visual y enviarla al cerebro. Usando Redes Neuronales Artificiales (Ferrández *et al.*, 1999) y Teoría de la Información (Ferrández *et al.*,

2002) hemos encontrado que los parámetros más relevantes en la codificación son el número de potenciales de acción y el tiempo exacto en que se produce el primero de ellos tras el estímulo. Además, la información se transmite utilizando un código poblacional y redundante.

Para reducir los datos poblacionales sin perder información relevante hemos desarrollado un método que permite detectar grupos de neuronas con respuestas semejantes (Bonomini *et al.*, 2005a). Posteriormente lo hemos incorporado a un programa libre de código abierto que facilita el análisis de los datos registrados con multielectrodos (Bonomini *et al.*, 2005b).

Por último, hemos diseñado un proceso para decodificar la información visual que procesa la retina evaluando cuantitativamente la reconstrucción conseguida del estímulo (Díaz-Tahoces *et al.*, 2015).

Abstract

The application of mathematical methods and tools has successfully contributed to advances in neuroscience since the last mid century. In recent years, a diversity of technological developments has allowed a greater exploration of the nervous system, causing a striking increase in the use of mathematics to investigate the large number of data now available to neuroscientists.

In the present doctoral thesis our objective is to determine how visual information is processed in the retina and how this is coded and transmitted to the brain. This has been achieved using several mathematical methods to study and analyze neuronal images as well as physiological signals.

Initially, we addressed the study of several morphological aspects of retinal cells to better understand certain particularities of the retinal circuits. In this sense we have studied the possible characterization of neurons as multifractals (Fernández et al., 1999) and have developed a new method - the V-proportion, based on the Voronoi diagram, this permits to study the spatial relationships between neural mosaics of the retina (Ahnelt et al., 2000; Martínez et al., 2010).

Furthermore, we have analyzed simultaneous responses of populations of retinal ganglion cells, which are responsible for encoding the visual information and sending it to the brain. Using Artificial Neural Networks (Ferrández et al., 1999) and Information Theory (Ferrández et al., 2002) we

found that the most relevant parameters in the coding process are the number of action potentials and the exact time in which the first of them occurs after the stimulus. This information is transmitted using a redundant population code.

In order to reduce population data without losing relevant information, we have developed a method to detect groups of neurons with similar responses (Bonomini et al., 2005a). We then incorporated this into an open source free program that facilitates the analysis of data recorded with multielectrodes (Bonomini et al., 2005b).

Finally, we have designed a process to decode the visual information from the retina by quantitatively evaluating the stimulus reconstruction achieved (Díaz-Tahoces et al., 2015).

Índice

Curriculum Vitae

A continuación, se adjunta un resumen del curriculum vitae del autor de la presente tesis doctoral. Se relacionan los proyectos de investigación en los que ha participado, las publicaciones derivadas total o parcialmente de los resultados expuestos en esta memoria de tesis, así como los foros científicos donde se ha dado difusión a los diferentes trabajos.

El autor es Licenciado en Matemáticas por la Universidad de Valencia (1984) y ejerce, por oposición, como Profesor de Secundaria desde el año 1985. Ha trabajado en varios institutos de la Comunidad Valenciana y, desde 2005, de la Comunidad de Madrid. Actualmente lo hace en el I.E.S. Jaime Ferrán de Collado Villalba.

De 1998 a 2003 fue además profesor colaborador honorífico del Departamento de Histología y Anatomía de la Universidad Miguel Hernández.

Desde 2012 es también profesor asociado en el grupo de Matemática Aplicada adscrito al Departamento de Ciencia e Ingeniería de Materiales e Ingeniería Química de la Universidad Carlos III de Madrid. Además, sigue colaborando con las investigaciones desarrolladas en la Unidad de Neuroprótesis y Rehabilitación Visual del Instituto de Bioingeniería de la Universidad Miguel Hernández de Elche.

Participación en proyectos de investigación financiados

- Método de Autoinstrucción asistido por ordenador para el aprendizaje de la Biología Neuronal. *Proyecto de Investigación de la Generalitat Valenciana nº GV-3160/95*. Periodo 1996.

- Acoplamiento eléctrico y circuitos neuronales en la plexiforme interna de la retina. *Proyecto de Investigación DGICYT nº PM94-1509*. Periodo 1996-1998.

- Estudio del diseño de la retina del roedor diurno Octodon Degus. *Proyecto de Investigación, HU1997-0045*. Periodo 1998-2000.

- Mecanismos de degeneración, regeneración y reparación en un modelo experimental neurodegenerativo. *Proyecto de Investigación CICYT SAF98-0098-CO2-02.* Periodo: 1998-2000.

- Development of a cortical visual neuroprosthesis for the blind. *Proyecto de Investigación financiado por la Comisión Europea QLK6-CT-2001-00279.* Periodo: 2001-2005.

- Sistema de apoyo a la visión mediante una retina artificial neuromórfica. *Proyecto de Investigación financiado por el Ministerio de Ciencia y Tecnología TIC2003-09557-C02-02.* Periodo: 2003-2005.

- Desarrollo de un dispositivo retinomórfico de alta resolución adaptado para baja visión y neuroprótesis visuales. *Proyecto de Investigación financiado por el Instituto de Mayores y Servicios Sociales.* Periodo: 2006-2007.

- Development of multifunctional microprobe arrays for cerebral applications. *Proyecto de Investigación de la Comisión Europea. FP7IST5.* Periodo: 2006-2010.

- Nuevos dispositivos de rehabilitación visual. *Proyecto de Investigación SAF2008-03694.* Periodo: 2009-2012.

- New therapeutic approaches for retinal dystrophies. *Proyecto de Investigación Intramurales del CIBER-BBN.* Periodo: 2011-2013.

- Nuevos tratamientos para las enfermedades degenerativas de la retina. *Proyecto de Investigación financiado por el Ministerio de Ciencia e Innovación (RTC-2014-2038).* Periodo: 2014-2017.

Revistas y publicaciones con índice de impacto (SCI)

- "V-Proportion: A method based on the Voronoi diagram to study spatial relations in neuronal mosaics on the retina". Martínez Mozos O., Bolea J.A., Ferrández J.M., Ahnelt P.K. y Fernández, E. (2010) *Neurocomputing*, 74 - 1-3, pp. 418- 427. Factor de impacto: 1.442

- "DATAMeans: An open source tool for the classification and management of neural ensemble recordings". Bonomini, M.P., Ferrández, J.M., Bolea, J.A. y Fernández E. (2005). *Journal of Neuroscience Methods*, 148(2), pp. 137-46. Factor de impacto: 1.784

- "Extracting common features from the responses of different ganglion cell populations". Bongard M., Ferrández J.M., Bolea J.A., Ammermüller

J. y Fernández E. (2002). *Ophthalmic Research* 34/S1: 363. Factor de impacto: 0.933

- "Irregular S-cone mosaics in non-primate retinas. Spatial interaction with axonless horizontal cells revealed by Voronoi based cross correlation". Ahnelt P.K., Fernández E., Martínez O., Bolea J.A. y Kübber-Heiss A (2000). *Journal of the Optical Society of America A*, 17(3), pp. 580–588. Factor de impacto: 1.481

- "Are neurons multifractals?". Fernández E., Bolea J.A., Ortega G. y Louis, E. (1999). *Journal of Neuroscience Methods*, 89, pp. 151-157. Factor de impacto: 1.362

- "Correlación espacial entre mosaicos de conos azules y células horizontales sin axón en retinas de felinos" Fernández E., Ahnelt P.K., Martínez O., Bolea J.A. y Kübber-Heiss A. (1999) *Revista de Neurología*, 30(S), 219. Factor de impacto: 0,265

- "Discriminant analysis of the population activity of turtle retinal ganglion cells". Fernández E., Normann R.A., Ferrández J.M., Bolea J.A. y Ammermüller J. (1998). *European Journal of Neuroscience* 10 (S10) 14.915. Factor de impacto: 3.820

Capítulos de libro

- Díaz-Tahoces A., Martínez-Álvarez A., García-Moll A., Humphreys L., Bolea J.A. y Fernández, E. (2015). Towards the Reconstruction of Moving Images by Populations of Retinal Ganglion Cells. En: Ferrández J.M. et al

(Eds), *Artificial Computation in Biology and Medicine*, (pp 220-227). Heidelberg: Springer. ISBN 978-3-319-18913-0.

- Bonomini M.P., Ferrández J.M., Bolea J.A. y Fernández E. (2005). Formulation and Validation of a method for classifying Neurons from multielectrode recordings. En: Mira J., Álvarez J.R. (Eds), *Mechanisms, Symbols and Models Underlying Cognition*, (pp 68-76). Berlin: Ed Springer. ISBN: 3-540-26298-5.

- Bolea J.A. (2004). Modelos estadísticos y geométricos en Matemáticas aplicadas a las Ciencias Naturales. En: García F.J. (Ed) *Jornades d'Educació Matemàtica en la Comunitat Valenciana*, (pp 549-555). San Vicente: Ed. Club Universitario, I.S.B.N.: 84-609-0029-0.

- Ferrández J.M., Bongard M., García-de-Quirós F., Bolea J.A. y Fernández, E. (2002). Neural Coding Analysis in Retinal Ganglion Cells Using Information Theory. En: Dorronsoro, J.R. (Ed), *Artificial Neural Networks - ICANN 2002*, (pp 174-179). London: Ed. Springer. ISBN: 3-540-44074-7.

- Bolea J.A. (2002). Modelos matemáticos: nueva asignatura para bachillerato. En: Palacián E., Sancho .J (Eds), *Actas X Jornadas para el Aprendizaje y Enseñanza de las Matemáticas,* (pp153-156). Zaragoza: I.C.E. Universidad de Zaragoza. I.S.B.N.: 84-7791-200-9.

- Ferrández J.M., Bongard M., García-de-Quirós F., Bolea J.A., Ammermüller J., Normann R.A. y Fernández E. (2001). Decoding the population responses of retinal ganglion cells using information theory. En: Mira J., Prieto A. (Eds), *Connectionist Models of Neurons, Learning*

Processes and Artificial Intelligence, (pp 55-62). London: Ed Springer. ISBN: 3-540-42235-8.

- Ferrández J.M., Bolea J.A., Ammermüller J., Normann R.A. y Fernández E. (1999). A Neural Network Approach for the Analysis of Multineural Recordings in Retinal Ganglion Cells. En: Mira J., Sanchez-Andres J.V. (Eds), *Engineering Applications of Bio-Inspired Artificial Neural Networks*, (pp 289-298). Berlin: Ed. Springer. ISBN: 3-540-66068-2.

Comunicaciones a Congresos Nacionales e Internacionales

- Díaz-Tahoces A., Martínez-Álvarez A., García-Moll A., Humphreys L., Bolea J.A. y Fernández, E. *Towards the Reconstruction of Moving Images by Populations of Retinal Ganglion Cells*. 6th IWINAC. Elche, 2015.
- M. Mozos O., Bolea J.A., Fernández E. y Ahnelt P.K. *V-Proportion: A method based on the Voronoi diagram to study spatial relations in neuronal mosaics on the retina*. XIII Encuentros de Geometría Computacional. Zaragoza, 2009.
- Ferrández J.M., Bongard M., García-de-Quirós F., Bolea J.A. y Fernández E. *Redundancy Analysis in Retinal Ganglion Cells using Information Theory*. 12th ICANN. Madrid, 2002.
- Bongard M., Ferrández J.M., Bolea J.A., Ammermuller J. y Fernández E. *Extracting common features from the responses of different ganglion cell populations*. 3rd Forum of European Neuroscience. Paris, 2002.

- Bongard M., Ferrández J.M., Bolea J.A., Ammermüller J., Normann R.A., Climent R., Ahnelt P.K., Belmonte J. y Fernández E. *In vivo massive parallel recordings of Human Retinal Ganglion Cell Populations*. EVER 2002 European Association for Vision and Eye Research. Alicante, 2002.

- Ferrández J.M., García de Quirós F., Bolea J.A., Ammermüller J., Normann R.A. y Fernández E. *Decoding the Population Responses of Retinal Ganglions Cells using Information Theory*. International Work Conference on Artificial and Natural Neural Networks. Granada, 2001.

- Ferrández J.M., García-de-Quirós F., Bolea J.A., Ammermüller J., Normann R.A. y Fernández E. *Análisis de la codificación distribuida en retina mediante el uso de redes neuronales*. IV Congreso Iberoamericano de Biofísica. Alicante, 2000.

- Bolea J.A., Martínez O., Ahnelt P.K. y Fernández E. *Estudio de las correlaciones espaciales en los mosaicos de la retina: un nuevo método basado en los diagramas de Voronoi*. IV Congreso Iberoamericano de Biofísica. Alicante, 2000.

- Jelinek H.F., Bolea J.A. y Fernández E. *Towards a useful fractal analysis methodology in biological research*. IV Congreso Iberoamericano de Biofísica. Alicante, 2000.

- Fernández E., Ahnelt P.K., Martínez O., Bolea J.A. y Kübber-Heiss A. *Correlación espacial entre mosaicos de conos azules y células horizontales sin axón en retinas de felinos*. VIII Congreso de la Sociedad Española de Neurociencias. Murcia, 1999.

- Ferrández J.M., Ammermüller J., Normann R.A., Bolea J.A. y Fernández E. *Management of color and luminance information by a network of ganglion cells in turtle retina*. 5th IWANN. Alicante, 1999.

- Ahnelt P.K., Fernández E., Martínez O., Bolea J.A., Kübber-Heiss A. *Räumliche Korrelation des Irregulären Blau-Zapfen Mosaiks in Säuger-Retinae mit Axon-losen Horizontalzellen*. 6th Meeting Austrian Neuroscience Association (ANA). Salzburg (Austria), 1999.

- Ammermüller J., Normann R.A., Ferrández J.M., Bolea J.A. y Fernández E. *Discriminant analysis of the activity of retinal ganglion cell populations*. EVER-1998 European Association for Vision and Eye Research. Palma de Mallorca, 1998.

- Bolea J.A. y Fernández E. *Implicaciones diagnósticas de la geometría Fractal en la Retinopatía Diabética*. I Congreso Internacional sobre Modelos y Métodos Matemáticos aplicados a la Biología y Medicina. Alicante, 1997.

Organización general de la tesis

El principal objetivo de esta tesis doctoral es conocer cómo se procesa la información visual dentro de la retina y desarrollar herramientas matemáticas para facilitar este análisis.

De acuerdo con la normativa interna de la Universidad Miguel Hernández para la presentación de tesis doctorales con un conjunto de publicaciones, esta memoria de tesis se ha estructurado en cuatro partes.

1. Introducción.

Tras presentar unas breves ideas sobre la utilización de las Matemáticas en Neurociencias exponemos como surgieron las investigaciones realizadas. Después se explican los conceptos e ideas principales relacionados con los problemas estudiados y cómo se han abordado: la clasificación de los tipos de células retinianas, las interacciones entre los mosaicos celulares, la codificación de la información que se realiza en la retina antes de transmitirla a los centros visuales superiores, la detección de grupos de neuronas que responden en sincronía y la posible decodificación de las respuestas neuronales registradas en presencia de estímulos.

2. Publicaciones.

Incluimos una copia de los ocho trabajos publicados que conforman esta memoria de tesis, los tres primeros relacionados con los diferentes aspectos morfológicos antes mencionados y los restantes con la codificación y decodificación.

3. Discusión y aportaciones.

Presentamos nuestras principales aportaciones y realizamos una revisión crítica de las mismas, resumiendo lo que a este respecto aparece en las publicaciones.

4. Conclusiones y líneas futuras.

Hacemos un extracto de las conclusiones presentes en las publicaciones enumerando las más relevantes. Tras ello se proponen una serie de líneas de investigación futura derivadas de nuestro trabajo.

Como último capítulo, en Referencias, se incluye una recopilación de la bibliografía consultada.

1. Introducción

"Las neuronas no han evolucionado
a comodidad de los matemáticos."
Francis Crick

1.1 Introducción

Uno de los grandes retos actuales de la neurociencia es comprender cómo funciona el cerebro. Aunque el interés por este tema viene desde varios siglos atrás, (figura 1.1), los primeros resultados significativos no se produjeron hasta el XIX y fue solo a partir del último cuarto del siglo pasado cuando los avances tecnológicos -la microscopía electrónica, la resonancia magnética, etc.- permitieron un gran desarrollo de los estudios científicos en este campo.

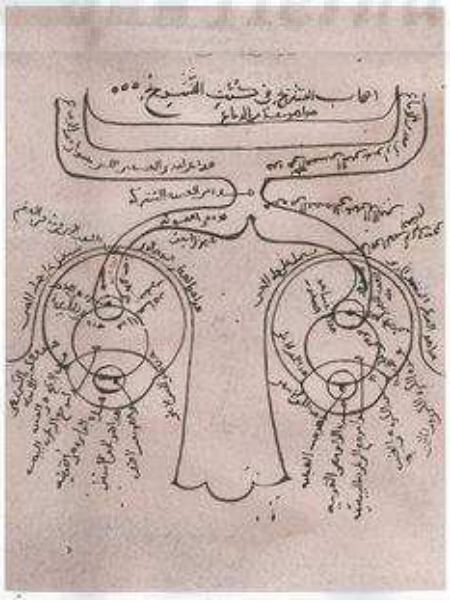

Figura 1.1: Diagrama del sistema visual, Ibn Al Haytham (965-1039)

Los años 90 supusieron un gran impulso al ser declarados "la década del cerebro" y más recientemente se están realizando grandes inversiones de recursos, tanto en EE.UU. (*BRAIN initiative*) como en Europa (*Human Brain Project*), para propiciar las investigaciones que permitan conseguir un mayor conocimiento de la estructura y el funcionamiento del cerebro y, como consecuencia, mejoras sustanciales en el diagnóstico y tratamiento de muchas enfermedades relacionadas con él.

El papel de la visión en las tareas que realiza el cerebro es de gran importancia y el estudio de cómo se produce la percepción visual se considera una de las estrategias más relevantes para entender cómo surge la consciencia (Crick, 2000; Koch, 2005). Pero lo que hace el cerebro para interpretar imágenes muy complejas en décimas de segundo no es una tarea sencilla: además de la mera adquisición de las imágenes hay que extraer información de ellas en tiempo real (por ejemplo, color, bordes, texturas,...), hay que adaptarse al movimiento, a los cambios de luminancia, etc. Contribuir a comprender cómo se realiza todo esto fue uno de los objetivos que nos planteamos al comenzar nuestras investigaciones dirigidas por el Dr. Eduardo Fernández en el Instituto de Bioingeniería de la Universidad Miguel Hernández.

Sus estudios, y por lo tanto los nuestros, se centran en la parte inicial de la vía visual, la retina. Es la parte más accesible del sistema nervioso central, aquella en la que más fácil resulta efectuar registros de la actividad neuronal. Estudiando el modo en el que la retina organiza y procesa la información respondiendo a estímulos visuales variables podemos obtener muchas ideas sobre cómo el cerebro capta y analiza las imágenes.

En esta búsqueda por conocer cómo se codifica la información en la retina, el uso de métodos matemáticos se hace imprescindible. Por un lado, para clasificar, ordenar y sistematizar los resultados obtenidos en los experimentos; y por otro, para asegurarnos de que nuestras teorías son consistentes. Así, diversos conceptos, principios y métodos propios de campos matemáticos tan diversos como el análisis de datos, las ecuaciones diferenciales, los procesos estocásticos, la teoría de la información, el procesamiento de señales, etc. se han venido usando en las últimas décadas en el estudio de la actividad neuronal en la retina.

Matemáticas y neurociencia.

Las aproximaciones matemáticas para estudiar el sistema nervioso comenzaron a mediados del siglo XX, especialmente tras el trabajo pionero de Hodgkin y Huxley (1952). Desarrollaron un modelo matemático de la corriente eléctrica que circula a través de la membrana de una neurona a partir de una serie de experimentos con el axón gigante del calamar. Su formulación matemática permitía adaptar los parámetros según los resultados de los experimentos y conseguía predecir la forma y velocidad del potencial de acción que transmite la señal. El éxito del modelo de Hodgkin-Huxley propició que los neurocientíficos valoraran positivamente el uso de herramientas matemáticas en la exploración del sistema nervioso y desde entonces son numerosos los trabajos en los que se han utilizado.

Así el intento de responder al *qué*, el *cómo* y el *porqué* del modo en el que se transmiten las señales en el sistema nervioso ha dado lugar a tres tipos de modelos matemáticos: descriptivo, mecanicista e interpretativo (Dayan y

Abbott, 2001). El objetivo de los modelos descriptivos -o estadísticos- es resumir los datos experimentales de forma compacta, pero con precisión, caracterizando lo que hacen las neuronas y los circuitos neuronales. A pesar de que estos modelos pueden estar motivados por el conocimiento del circuito neuronal subyacente, su objetivo es dar cuenta de un fenómeno matemáticamente, no pretenden explicarlo. En los modelos mecanicistas se explica la actividad del sistema nervioso sobre la base de la morfología neuronal, la fisiología y la circuitería. Se sigue el tradicional enfoque de la física aplicada a la modelización de sistemas naturales. Por último, los modelos interpretativos utilizan principios computacionales y de teoría de la información para explorar varios aspectos de las funciones del sistema nervioso, intentando en definitiva entender por qué el sistema nervioso funciona como lo hace.

En los métodos matemáticos mostrados en los artículos que conforman esta memoria de tesis la aproximación es menos definida, pero al mismo tiempo más ambiciosa ya que se pueden encontrar características de los tres tipos de modelos, sin habernos limitado específicamente a ninguno de ellos. Como hemos dicho, han surgido como fruto de la colaboración con el laboratorio del Dr. E. Fernández y, por lo tanto, con un enfoque interdisciplinar variable en el que la intención ha estado más dirigida a dar respuesta a las preguntas y necesidades que surgían en los trabajos que en él se realizaban que al intento de desarrollar un único modelo teórico encuadrable en uno de dichos tipos.

Debido a esta intención una de las principales características de nuestra aproximación desde las matemáticas al estudio de la retina ha sido trabajar

directamente con los datos obtenidos en los experimentos. Las herramientas matemáticas usadas han buscado el análisis de los datos experimentales y los métodos que hemos desarrollado han surgido principalmente del deseo de estudiarlos y el intento de explicarlos, buscando por tanto su utilidad para ello y, además, se han validado especialmente a partir de dichos datos.

Neuroprótesis visuales corticales.

Uno de los principales retos del laboratorio a lo largo de estos años ha sido el desarrollo de una neuroprótesis visual, basada en microelectrodos intracorticales, que pueda ayudar a personas ciegas o con baja visión residual a percibir el entorno que les rodea y orientarse en él.

Una neuroprótesis visual es básicamente un dispositivo capaz de crear o inducir percepciones visuales mediante la estimulación de cualquier parte de la vía visual, desde la retina al cerebro.

Actualmente ya existen algunos dispositivos diseñados para implantarse en la retina: ARGUS II®, IRIS® o Retina Implant AG®. Pero al situarlos ahí solo pueden llegar a ser útiles para alteraciones que afecten exclusivamente a las capas más externas de la retina (Figura 1.2A). Estas patologías representan menos de un 2,5% de todos los casos de ceguera, por lo tanto existen muchas personas que ya tienen degeneraciones muy avanzadas de la retina o que son ciegas a consecuencia de otras patologías -como por ejemplo la retinopatía diabética, el glaucoma o la lesión de los nervios ópticos- para las que no existen tratamientos médicos o dispositivos de ayuda válidos. Por ello la alternativa elegida en nuestro laboratorio es estimular directamente

la parte del cerebro que procesa la información visual, es decir la corteza visual (Figura 1.2D).

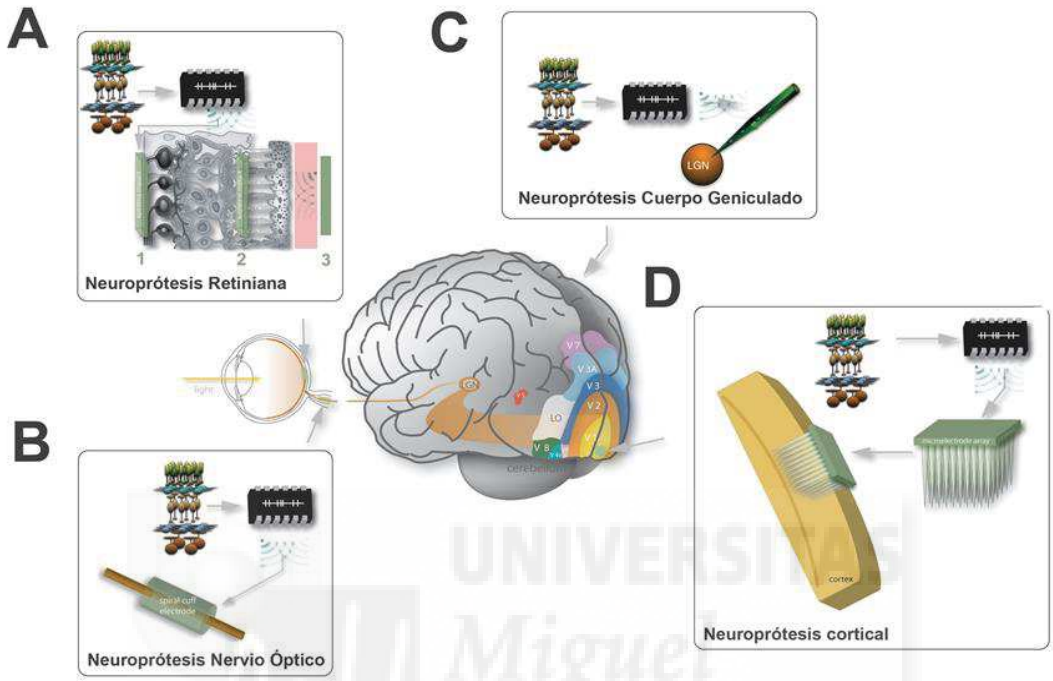

Figura 1.2. Esquema de los principales tipos de neuroprótesis visuales que se están desarrollando en la actualidad. En general el campo visual situado enfrente del sujeto es codificado por un pequeño dispositivo electrónico bioinspirado que se sitúa a nivel de unas gafas, más o menos convencionales. Las señales procedentes de este dispositivo son procesadas externamente y transformadas en impulsos eléctricos optimizados para estimular las neuronas de la retina (A), el nervio óptico (B), el cuerpo geniculado lateral (C) o la corteza visual primaria (D) mediante matrices de microelectrodos.

Uno de los problemas que se nos presentan no es tanto ser capaces de transmitir una imagen con una alta resolución como transmitir al sitio estimulado información que resulte útil (para tareas tales como orientación y movilidad, lectura, etc.). Para ello es fundamental comprender como se codifica la información visual en la retina y como se transmite esta información a la corteza visual, por lo que esta es una de las principales líneas de investigación del laboratorio y la que hemos abordado a lo largo de esta tesis doctoral.

Esta opción de nuestro grupo se basa en el hallazgo de que la estimulación eléctrica de la corteza occipital desencadena la percepción subjetiva de destellos de luz denominados técnicamente fosfenos. El primer trabajo sobre la aparición de fosfenos tras la estimulación eléctrica del córtex visual se debe a Lowënstein y Borchart en 1918, pero fueron los estudios del neurocirujano canadiense Wilder Penfield (Penfield y Rasmussen, 1950; Penfield y Jaspers, 1974), los que confirmaron estos hallazgos. Más tarde Brindley y Lewin (1968), (Brindley, Donaldson *et al*. 1972; Brindley, 1982) en la Universidad de Cambridge y el grupo del Dr. Dobelle (Dobelle y Mladejovsky, 1974; Dobelle, Mladejovsky *et al*. 1974, 1976) en la Universidad de Utah hicieron prolongadas observaciones sobre los fosfenos y los estímulos eléctricos que los desencadenaban, sentando las bases de una neuroprótesis visual a nivel cortical. Hay que destacar los trabajos del último grupo en los que sujetos que habían permanecido ciegos durante mucho tiempo, fueron capaces de leer caracteres Braille utilizando un sistema de electrodos más rápido incluso de lo que lo hacían a través del tacto. Sin embargo los resultados de sus estudios pusieron de manifiesto que una neuroprótesis basada en la estimulación cortical mediante electrodos superficiales como los que ellos utilizaron (Dobelle, 2000), puede tener una utilidad limitada. Esto es debido fundamentalmente a varios factores: la gran cantidad de corriente necesaria para producir los fosfenos, interacciones entre electrodos adyacentes, la producción ocasional de episodios dolorosos -debidos probablemente a irritación meníngea- y la posibilidad de desencadenar crisis epilépticas.

Una aproximación más eficaz, que permite la activación de neuronas con un mayor grado de especificidad espacial y menores niveles de corriente, es la

utilización de electrodos intracorticales (Normann, Maynard, *et al*., 1999; Rousche y Normann, 1999; Maynard, 2001). Se utilizaron por Schmidt, Bak *et al*. (1996) que implantaron 38 microelectrodos intracorticales en el córtex visual derecho de una mujer de 42 años, ciega desde hacía 22. De esos electrodos 34 fueron capaces de producir fosfenos durante un periodo de 4 meses con niveles de corriente inferiores a 25 μA. Desafortunadamente los electrodos no fueron diseñados para su uso crónico por lo que algunas de sus conexiones se rompieron en los primeros días del experimento.

En cualquier caso, todas estas investigaciones sugieren que un sistema de electrodos múltiples, insertado en los lugares apropiados del sistema visual, es capaz de inducir la percepción subjetiva de fosfenos, y podría ser utilizado para proporcionar una visión limitada pero útil a un gran número de personas ciegas (Fernández, Pelayo, *et al.* 2005; Fernández, 2008; Normann, Greger, *et al.* 2009).

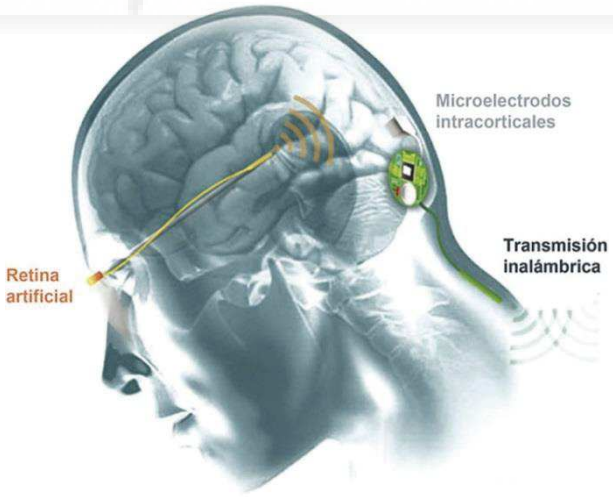

Figura 1.3: Esquema del funcionamiento de la neuroprótesis cortical propuesta, basada en múltiples microelectrodos intracorticales.

Un esquema del sistema completo en el que está trabajando nuestro grupo se presenta en la Figura 1.3. El campo visual situado enfrente del sujeto será codificado por una retina artificial bioinspirada, capaz de captar y procesar la información visual de una forma similar a como lo hace la retina humana. Las señales procedentes de este dispositivo serán procesadas externamente y transformadas en trenes de impulsos eléctricos optimizados para estimular las neuronas de la corteza visual.

El sistema se basa en que esta retina artificial bioinspirada, situada en unas gafas convencionales, capte el campo visual situado enfrente del sujeto, codifique y procese la imagen capturada. Las señales procedentes de ese dispositivo se transforman en trenes de impulsos eléctricos con los que estimular las neuronas de la corteza visual a través de microelectrodos intracorticales.

Como ya hemos comentado previamente, para que sea eficaz no se necesita transmitir una imagen con alta definición; hay que transmitir la información que sea útil para la zona del cerebro que se va a estimular. Pero es necesario saber cuál es dicha información, por eso es imprescindible un mayor conocimiento sobre cómo se codifica la visión en la retina y cómo se transmite hacia los centros visuales superiores. Simular las señales eléctricas generadas por el procesamiento visual biológico es mucho más difícil en las prótesis corticales que en las subretinianas porque en éstas sólo se reemplazan los fotorreceptores y no todas las células y circuitos de la retina.

Este planteamiento representa la base de la presente tesis doctoral, es decir, conocer y entender mejor la arquitectura funcional de la retina de los vertebrados. Necesitábamos saber más sobre los diversos tipos celulares, sus

relaciones topológicas, sus conexiones y sus características funcionales; entender cómo los circuitos en el interior de la retina gestionan la información sobre el color y la luminosidad de los objetos visuales, especialmente durante la visión activa.

Otro de nuestros objetivos ha sido contribuir al desarrollo de un modelo de la actividad de las células ganglionares -la salida que la retina transmite al cerebro- capaz de ser reproducido de una manera eficaz y fiable y de funcionar en tiempo real. Esto último implica intentar minimizar el número de canales necesarios para transferir la información. Para ello es importante poder caracterizar subpoblaciones de células ganglionares semejantes respecto a sus características funcionales. Conseguirlo supone obtener un tamaño más reducido de la población neuronal que se quiere simular, pero de un modo que maximice la información de los aspectos más relevantes del estímulo visual.

En una fase posterior nos hemos planteado qué simulaciones son más realistas y permiten una transferencia adecuada de la imagen natural. Para ello, es necesario tener un criterio para cuantificar qué valores de los parámetros usados en las funciones de la simulación proporcionan las mejores aproximaciones.

Clasificación morfológica. Tipos celulares.

Las técnicas de preparación de retinas aplanadas o enteras significaron un avance en el estudio de las células de la retina al permitir un estudio detallado de los árboles dendríticos que anteriormente tenían que ser

seccionados en experimentos clásicos como los de finales del siglo XIX de D. Santiago Ramón y Cajal o los recogidos en la famosa obra de Polyak (1941).

Posteriormente la introducción de la microscopía electrónica o de técnicas de inmunocitoquímica ha facilitado un mejor conocimiento de la morfología de las neuronas retinianas. La Figura 1.4 muestra un ejemplo de una misma célula amacrina de la retina humana vista en diferentes planos de foco.

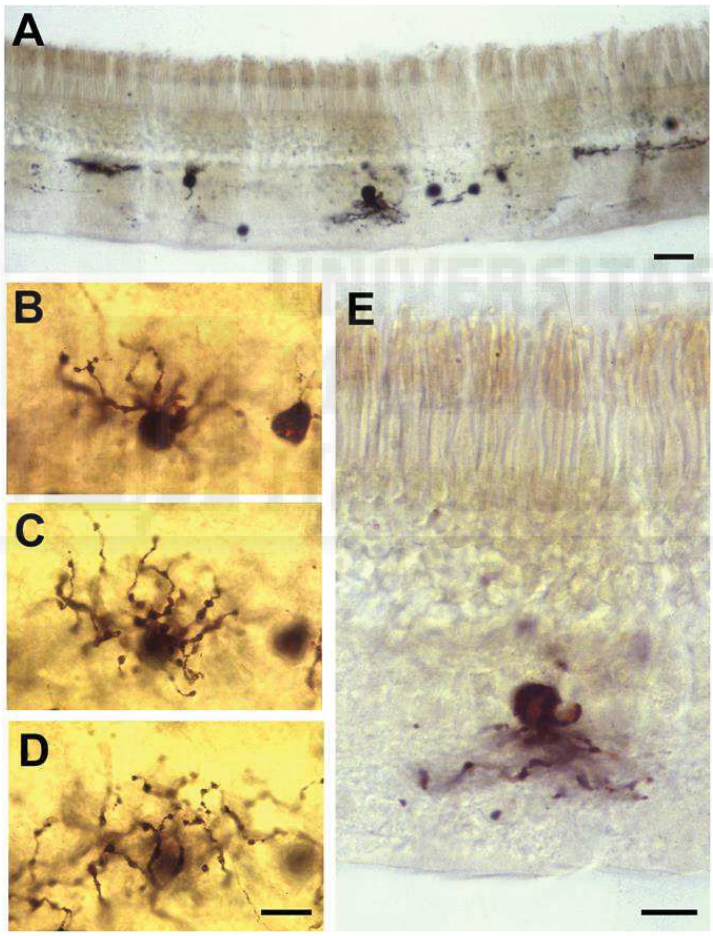

Figura 1.4. Célula amacrina AII de la retina humana.
A: Sección transversal de 25 μm de espesor para localizar la célula de interés. Barra de escala = 25 μm.
B-D: Microfotografías tomadas en diferentes planos de foco. Barra de escala = 10 μm.
E: Detalle de la célula. Barra de escala = 10 μm.

Así se han podido encontrar un mayor número de clases celulares distintas y describir de un modo más detallado y correcto los caminos visuales que parten de la retina. En general es necesario establecer una correcta clasificación basada en la forma porque resulta de gran utilidad como ayuda para dilucidar las posibles diferencias funcionales entre tipos celulares.

Por ejemplo, en el caso de las células ganglionares, tras la exitosa clasificación inicial en los tipos morfológicos alfa, beta, gamma y delta (Boycott y Wassle, 1974) se fueron proponiendo nuevos subtipos -con esta idea de relacionarlos con sus características funcionales- hasta llegar a la propuesta de 20 tipos recogida en Kolb et al. (1981). Esta última clasificación se basa en el tamaño del cuerpo celular y en la forma del árbol dendrítico, pero en ocasiones la caracterización de estas clases presenta dificultades, especialmente en las células con una menor presencia en la retina. Para distinguirlas correctamente y estudiar su relevancia es importante poder dar un valor de las irregularidades en distintas partes de la célula. Buscando parámetros que ayuden en esta tarea hemos recurrido a la geometría fractal.

La geometría fractal es una herramienta que permite describir matemáticamente, y de manera sencilla, objetos considerados extremadamente complejos o desordenados. Básicamente los objetos fractales son aquellos que reúnen algunas de las siguientes características (Falconer, 2003): tienen una estructura fina, que presenta peculiaridades en escalas arbitrariamente pequeñas; son irregulares; presentan algún tipo de autosemejanza; su dimensión fractal, calculada a partir de cualquiera de las diversas definiciones propuestas en la literatura, es mayor que su dimensión

topológica; en muchos casos los objetos fractales se obtienen a partir de un proceso recursivo que se define de un modo sencillo.

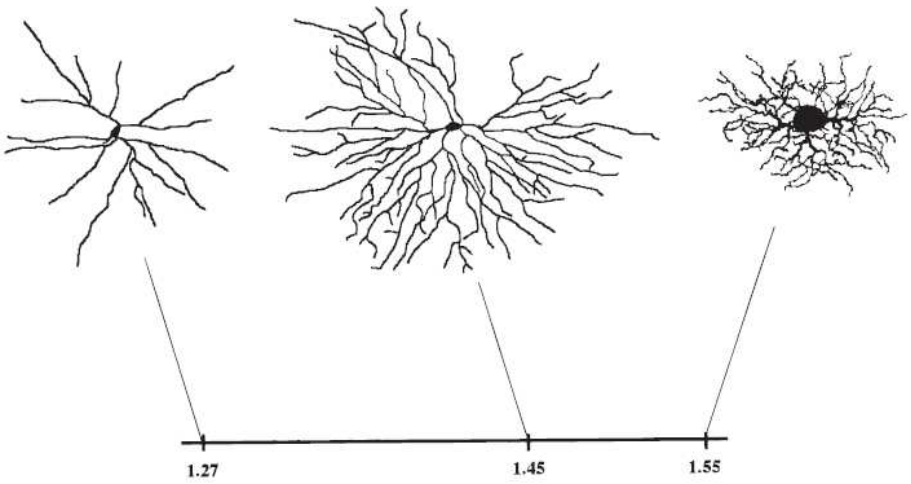

Figura 1.5: Ejemplos de diferentes células ganglionares de gato con sus respectivas dimensiones fractales como medida de irregularidad.

Los diferentes valores obtenidos según el tipo de célula -gamma, alfa y beta, de izquierda a derecha- sugieren la utilidad de las dimensiones fractales para distinguir tipos celulares. (Tomado de Jelinek y Fernández, 2001)

Algunas de estas características aparecen, en cierta medida, en la mayoría de las neuronas, debido principalmente a la presencia de las ramificaciones dendríticas. Esto es lo que induce al uso de la geometría fractal para analizar su forma, intentando discriminar e identificar tipos y clases celulares.

Los mosaicos celulares de la retina

En la retina las neuronas están distribuidas en capas siguiendo ciertos patrones regulares, formando varios circuitos locales que trabajan en paralelo para procesar la información de los distintos aspectos (luminosidad, contraste, color, movimiento,...) de la imagen que se analiza.

Durante el proceso de desarrollo y crecimiento de los mamíferos las neuronas tienden a situarse en las distintas capas de la retina siguiendo ciertos patrones regulares que evitan normalmente un excesivo solapamiento de sus campos dendríticos y que están relacionados con la función que realizan. Como consecuencia, las neuronas parecen teselar la superficie retiniana y por ello se habla de *mosaicos neuronales* al estudiar su disposición en ella.

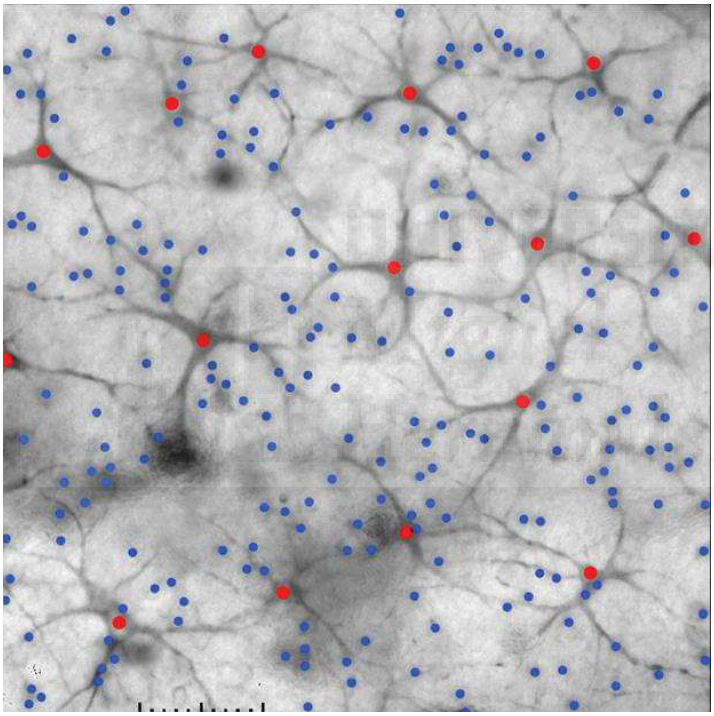

Figura 1.6. Mosaico de conos azules (puntos azules) y células horizontales (puntos rojos) en retina humana.

El estudio de estos mosaicos es de gran ayuda para conocer como realiza la retina la labor de procesamiento y transmisión de la información. Esto se produce con diferentes niveles de resolución espacial y además hay neuronas funcionales de determinadas clases que aparecen repetidas en

diferentes lugares de la retina. Las que se encargan de informar de los detalles más finos de la imagen suelen ser más pequeñas de tamaño y están situadas muy cerca unas de otras. Por el contrario, las encargadas de informar de movimiento o cambios de luminosidad suelen ser de tamaño más grande y están más alejadas entre sí (Cook, 2003). De ahí la importancia de disponer de distintos métodos cuantitativos que permitan evaluar las características (regularidad, densidad,...) de los distintos mosaicos neuronales, así como de las posibles interacciones entre ellos que, si existen, nos pueden indicar cuales son las vías de comunicación entre los mencionados circuitos. La figura 1.6 presenta un ejemplo de dichos mosaicos.

Los primeros estudios en los que se describen cuantitativamente los mosaicos retinianos usan una aproximación basada en una medida conocida en estadística espacial: la distancia al vecino más próximo, normalmente acompañada por el cálculo del índice de regularidad (Wässle y Riemann, 1978; Wässle *et al.*, 1983). Con esto los neurocientíficos ya disponían de una herramienta para evaluar la distribución espacial y la regularidad de un determinado mosaico.

Posteriormente se utilizó el correlograma espacial, especialmente en un método que se hizo muy popular llamado DRP *(density recovery profile)*, que permite también analizar las posibles relaciones entre los mosaicos (Rodieck, 1991).

Más recientemente se han comenzado a usar métodos basados en el diagrama de Voronoi porque permiten evaluar más características de la geometría de los mosaicos, como por ejemplo la distribución del número de

vecinas alrededor de cada neurona (ver Figura 1.7). Además, técnicamente es difícil dibujar exactamente los mosaicos retinianos y delimitar qué tesela corresponde a cada neurona individual, debido a la profusa e irregular ramificación del árbol dendrítico.

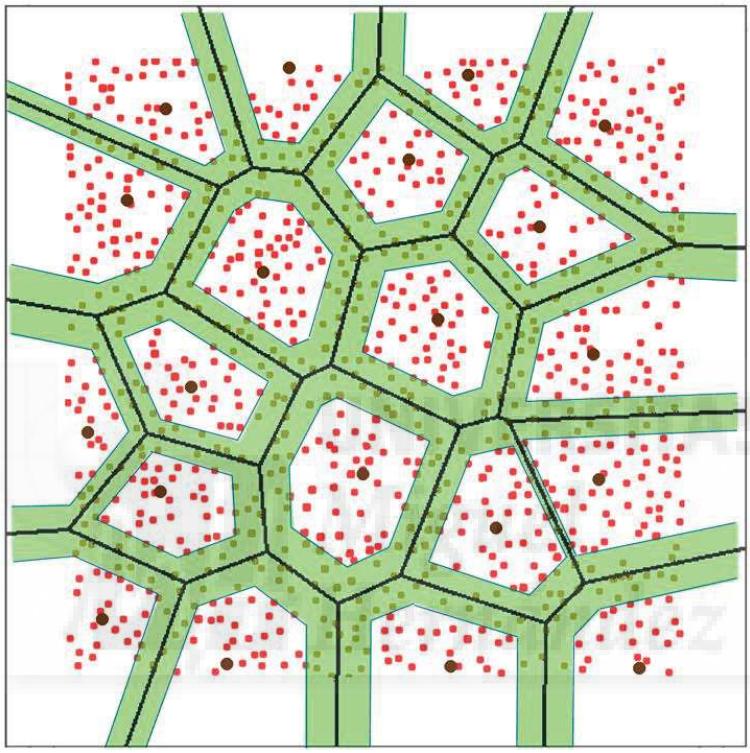

Figura 1.7. Diagrama de Voronoi mostrando conos rojos (puntos rojos) y células horizontales (puntos negros) en retina humana. En verde las bandas construídas para aplicar el método de la V-proporción desarrollado en Martínez, Bolea *et al.* (2010).

Los polígonos del diagrama de Voronoi proporcionan un ajuste más adecuado del campo dendrítico de cada neurona por lo que su uso mejora los anteriores métodos en los que tan sólo se considera la localización del soma. Por ello, utilizar esta estructura fue la opción elegida por nosotros como punto de partida para abordar el problema.

Codificación de la información

¿Qué código utilizan las neuronas para transmitir la información? Actualmente no hay un acuerdo total entre la comunidad científica sobre la respuesta a esta pregunta. Unos piensan que la clave es la frecuencia de descarga, lo más fácilmente reproducible al observar la respuesta de una neurona ante un estímulo dado. La neurona integra temporalmente eventos sinápticos aleatorios y produce una descarga eléctrica cuando el contador alcanza un cierto valor. Bajo este enfoque la descarga de las neuronas puede ser descrita como un modelo de Poisson, el más sencillo de los procesos estocásticos puntuales, en el que el número de eventos, en nuestro caso el disparo de potenciales de acción, en un intervalo de tiempo dado es una variable aleatoria y los números de eventos en dos intervalos disjuntos son independientes.

Otros neurocientíficos, contemplan por contra que lo relevante es la temporalidad relativa de los potenciales de acción ya que, entre otras razones, puede ocurrir que distribuciones completamente distintas de potenciales de acción tengan una misma frecuencia de disparo. Con esta premisa se considera que las neuronas funcionan más como detectoras de coincidencias o correlaciones que como integradoras. Para percibir correctamente los objetos del mundo real el sistema nervioso debe ser capaz de poner en relación distintas características de un mismo objeto sin mezclarlas con las de otro distinto. Si se describe la actividad neuronal únicamente por la frecuencia de descarga no es posible distinguir entre dos conjuntos de neuronas que codifican las características de dos objetos distintos y un gran conjunto neuronal que codifica el conjunto de todas esa

características; es decir, no se permite la representación de información estructurada.

Pero también subsiste otra importante polémica entre los investigadores: ¿la codificación neuronal que se realiza en la retina se basa en un código de células aisladas o más bien en un código poblacional? Este último enfoque surgió y se ha visto favorecido por la introducción de tecnología de registro poblacional utilizando múltiples multielectrodos, que permite analizar la codificación distribuida del conjunto de células registradas.

En un artículo muy influyente Nirenberg *et al.* (2001) sugirieron que las células ganglionares actúan como codificadores independientes. Los autores analizaban cómo pares de células ganglionares de la retina codifican el estímulo visual por sus patrones de disparo. En trabajos previos se había concluido que las células ganglionares cercanas tienen una fuerte tendencia a disparar en sincronía. Sn embargo estos autores afirman que estas correlaciones son irrelevantes para la codificación visual realizada por las células ganglionares, porque "*más de 90% de la información sobre los estímulos se pueden obtener de las células cuando se ignora su correlación*". Escriben como conclusión que "*las células ganglionares actúan en gran medida de forma independiente para codificar la información, lo que simplifica en gran medida el problema de la decodificación de su actividad*", porque "*la actividad de cualquier célula dada puede evaluarse por separado de otras células*". Estas afirmaciones provocaron la reacción crítica de varios de los investigadores citados por ellos, especialmente de M. Meister, autor de varios de los primeros trabajos en los que se usaron multielectrodos (Meister *et al.*, 1994) y en los que se afirmaba que el disparo concertado de células ganglionares es crítico para el

procesamiento del código neuronal (Meister *et al.*, 1995). Su réplica fue: "*Desafortunadamente, el artículo no contiene ninguna evidencia de estas proposiciones. Las afirmaciones se basan en dos métodos de análisis, ambos defectuosos*". (Meister y Hosoya, 2001)

En el momento de realizar nuestras investigaciones el tema seguía candente y buscamos utilizar diversas herramientas matemáticas que aplicadas a los registros obtenidos en nuestros experimentos permitieran apoyar una hipótesis u otra.

Por otra parte, en el caso de que se considere más relevante para codificar una escena visual la actividad poblacional, hay que estudiar -también matemáticamente- las correlaciones que se observen en los registros de grupos neuronales y cómo deben interpretarse.

Grupos de neuronas sincrónicas

Actualmente es posible obtener la respuesta de una población de neuronas gracias al uso en fisiología de las matrices de multielectrodos. En los experimentos realizados en nuestro laboratorio hemos usado la desarrollada por investigadores de la Universidad de Utah (Figura 1.8). Consiste en 100 microelectrodos de 1,5 mm de longitud, aislados eléctricamente unos de otros y situados en un substrato de silicona de 4 mm x 4 mm. Con esta arquitectura, al insertarlos en retinas activas o en otro tipo de tejido neuronal, se pueden registrar los potenciales de acción de decenas de neuronas simultáneamente. Además, con la tecnología adecuada, también pueden ser utilizados para estimular, incluso en intervenciones terapéuticas (Normann y Fernández, 2016).

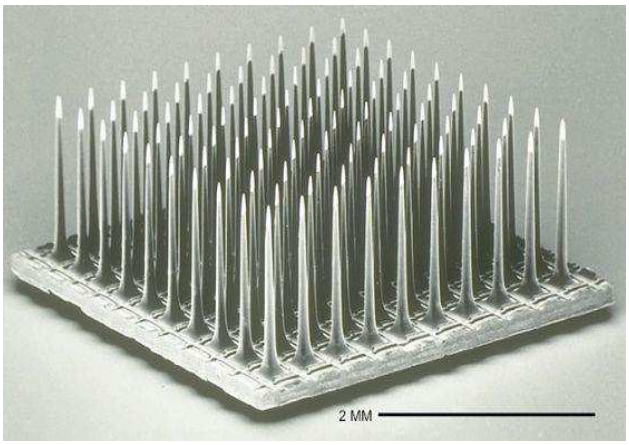

Figura 1.8: Matriz de multielectrodos de Utah.

El uso de este tipo de matrices de multielectrodos en los experimentos ha hecho necesario el desarrollo de nuevas herramientas para analizar adecuadamente todos los datos que con ellos se obtienen. Un primer problema cuando se trabaja con registros extracelulares multineuronales es discriminar e identificar los potenciales de acción, denominados espigas, de cada neurona individual. Esto ha sido muy estudiado y se conocen diversos algoritmos para realizar esta clasificación (Lewicki, 1998, Rey *et al.* 2015).

En nuestro laboratorio se desarrolló para ello *Nev2lkit*, un programa libre de código abierto (Bongard *et al*., 2014), que es el que hemos utilizado para el análisis de nuestros registros electrofisiológicos.

Una vez obtenidos los trenes de espigas correspondientes a cada célula de la población es interesante poder detectar grupos de células que disparan sincrónicamente. Con ello conseguimos reducir los datos con vistas a simularlos en retinas artificiales y, además, estos grupos pueden tener un papel relevante en la transmisión de la información. En este orden de ideas, cuando hablamos de sincronía estamos considerando aquellas situaciones en que dos o más neuronas disparan simultáneamente potenciales de acción

con más frecuencia de la que se produce asumiendo un modelo de probabilidad de disparo independiente. Normalmente en la retina la sincronía viene inducida por el estímulo.

Se han observado disparos sincrónicos en todas las etapas del procesamiento visual (Usrey y Reid, 1999) aunque la causa de que aparezcan puede ser distinta en cada una de ellas. Por ejemplo, una sola célula ganglionar de la retina inerva más de una célula del cuerpo geniculado lateral, eso provoca que en éste se registre una mayor sincronía.

El método más sencillo, y por tanto más usado, para detectar sincronía se basa en los correlogramas, pero estos solo permiten analizar pares de células. Schnitzer y Meister (2003), registrando con multielectrodos en retinas de salamandra, encontraron con frecuencia grupos numerosos de células disparando sincrónicamente, pero no llegaron a describir metodologías para su análisis. Partiendo de estos resultados hemos intentado desarrollar métodos que permitan estudiar y detectar la presencia de grupos de células que disparan de forma sincrónica. De manera resumida: si un grupo grande de células (por ejemplo 10) disparan sincrónicamente -algo muy poco probable-, el evento proporciona mucha información. Sin embargo, que dos células disparen casi simultáneamente en instantes temporales muy cercanos es mucho más probable, por lo que la información que esto nos aporta es escasa.

Decodificación de las respuestas

Una vez que se han estudiado algunas de las características principales de la codificación de la información que se produce en la retina se pueden

desarrollar técnicas y algoritmos que simulen la transmisión de dicha información.

El siguiente paso consiste en validar dichas simulaciones. Serán mejores aquellas que mejor transmitan el estímulo; por lo tanto, es preciso estudiar el modo en que se puede reproducir este a partir de las respuestas neuronales. Este es el denominado *problema de la decodificación*. Esto no debe estudiarse solo a partir de estímulos simples, como los que habitualmente se utilizan en los experimentos cuyo objetivo es conocer mejor la codificación, sino que deben usarse escenas naturales semejantes a las que ven los animales, ya que lo que se busca es simular verazmente su comportamiento sensorial.

Un acercamiento al modo en que estas imágenes naturales se decodifican en las áreas visuales superiores se basa en desarrollar modelos probabilísticos de las mismas para explicar la codificación que se realiza en la retina en términos de los parámetros que los caracterizan. Los trabajos de Olshausen y Field (1996, 2005) muestran que las propiedades de los campos receptivos obtenidos con simulaciones basadas en esta aproximación coinciden con los encontrados para neuronas de la corteza visual primaria de los mamíferos, pareciendo indicar que esta decodifica la información de un modo similar al modelo propuesto.

En todo caso, finalmente hay que utilizar algún procedimiento para cuantificar la validez del resultado obtenido en la reconstrucción de la escena comparándola con la original. De ese modo podremos valorar si los parámetros considerados son suficientes, si son los más relevantes, etc.; en definitiva, evaluar nuestro modelo de decodificación.

1.2 Objetivos

El objetivo general de la presente tesis es conocer cómo se procesa la información visual dentro de la retina y analizar con que códigos se transmite al cerebro para contribuir así al desarrollo de un modelo bioinspirado de retina artificial que se aproxime a las características funcionales básicas de las retinas biológicas.

Esto se pretende conseguir mediante los siguientes objetivos específicos:

- Discriminar tipos celulares en la retina mediante la utilización del análisis fractal.
- Estudiar las interacciones espaciales entre mosaicos neuronales mediante el diagrama de Voronoi.
- Cuantificar cómo las respuestas neuronales varían frente a diferentes estímulos para determinar de qué modo están siendo codificados
- Desarrollar y usar procedimientos para analizar registros simultáneos de respuestas de poblaciones celulares de la retina obtenidos experimentalmente con multielectrodos.
- Caracterizar, mediante diversos métodos, las células (o subgrupos de células) de una población que mejor discriminan un determinado estímulo y con qué parámetros lo hacen.
- Proponer nuevos modelos de estímulo-repuesta para poblaciones celulares a partir de los experimentos con multielectrodos.
- Diseñar, implementar y analizar algoritmos que permitan evaluar la fiabilidad de dichos modelos al ser aplicados a los datos empíricos.

UNIVERSITAS
Miguel
Hernández

2. Publicaciones

Aspectos morfológicos:

1. Fernández, E., Bolea, J.A., Ortega, G. y Louis, E. (1999). "Are neurons multifractals?" *Journal of Neuroscience Methods*, 89, pp. 151-157. **Factor de impacto:** 1.362

2. Ahnelt, P., Fernández, E., Martínez, O., Bolea, J.A. y Kubber-Heiss, A. (2000) "Irregular S-cone mosaics in non-primate retinas. Spatial interaction with axonless horizontal cells revealed by Voronoi based cross correlation." *Journal of the Optical Society of America A*, 17(3), pp. 580–588. **Factor de impacto:** 1.481

3. Martínez Mozos, O., Bolea, J.A., Ferrández, J.M., Ahnelt, P.K. y Fernández, E. (2010) "V-Proportion: A method based on the Voronoi diagram to study spatial relations in neuronal mosaics on the retina." *Neurocomputing*, 74 - 1-3, pp. 418- 427. **Factor de impacto:** 1.442

Codificación y decodificación:

4. Ferrández, J.M., Bolea, J.A, Ammermüller, J., Normann, R.A. y Fernández, E. (1999) "A Neural Network Approach for the Analysis of Multineural Recordings in Retinal Ganglion Cells" *Engineering Applications of Bio-Inspired Artificial Neural Networks*. Lecture Notes in

Computer Science, Vol. 1607, pg. 289-298. Berlin/Heidelberg: Springer. **Factor de impacto:** 0.872

5. Ferrández, J.M., Bongard, M., García-de-Quirós, F., Bolea, J.A. y Fernández, E. (2002) "Neural Coding Analysis in Retinal Ganglion Cells Using Information Theory" *Artificial Neural Networks - ICANN 2002.* Lecture Notes in Computer Science. Vol 2415, pg. 174-179. London: Springer-Verlag. **Factor de impacto**: 0.515

6. Bonomini M.P., Ferrández J.M., Bolea J.A. y Fernández E. (2005a) "Formulation and Validation of a method for classifying Neurons from multielectrode recordings" *Mechanisms, Symbols and Models Underlying Cognition*. Lecture Notes in Computer Science. Vol 3561, pp. 68-76. Berlin/Heidelberg: Springer. **Factor de impacto:** 0.402

7. Bonomini, M.P., Ferrández, J.M., Bolea, J.A. y Fernández E. (2005b) "DATAMeans: An open source tool for the classification and management of neural ensemble recordings" *Journal of Neuroscience Methods*, 148(2), pp. 137-46. **Factor de impacto:** 1.784

8. Díaz-Tahoces, A., Martínez-Álvarez, A., García-Moll, A., Humphreys, L., Bolea, J.A. y Fernández, E. (2015) "Towards the Reconstruction of Moving Images by Populations of Retinal Ganglion Cells" *Artificial Computation in Biology and Medicine*, Lecture Notes in Computer Science, Volume 9107, pp 220-227. **Factor de impacto**: (no evaluado)

ELSEVIER

Journal of Neuroscience Methods 89 (1999) 151–157

JOURNAL OF NEUROSCIENCE METHODS

Are neurons multifractals?

E. Fernández [a,*], J.A. Bolea [a], G. Ortega [b], E. Louis [b]

[a] *Instituto de Bioingeniería, Universidad Miguel Hernández, Campus de San Juan, Apartado 18, E-03580 San Juan, Spain*
[b] *Departamento de Física Aplicada, Universidad de Alicante, Apartado 99, E-03080 Alicante, Spain*

Received 3 November 1998; received in revised form 16 April 1999; accepted 9 May 1999

Abstract

In the last few years, fractal analysis has found widespread application in the field of neuroscience and some investigators are starting to use multifractals as a methodology that may provide information about the distribution of fractal dimensions in biological structures. This is so, despite of the technical difficulties of multifractal analysis. In this paper, we investigate the theoretical and practical aspects of studying and measuring the multifractal dimensions of neurons. Patterns were analysed by means of the standard box-counting method and a generalised sand-box method. Our results show that odd behaviours of D_q reported in the literature are a consequence of numerical deficiencies of the box-counting method and cannot be associated to peculiar geometrical characteristics of neurons. Instead the sand-box method gives a D_q which monotonically decreases with q. Although this result may indicate that neurons are multifractals, it is argued that size effects may in fact be the origin of this apparent multifractality.

Keywords: DLA aggregates; Fractal dimension; Multifractals; Neurons

1. Introduction

Over the past 20 years, fractal analysis has been widely used to characterise biological systems (Mandelbrot, 1982; Feder 1988; Bassingthwaighte et al., 1994; Cross 1994; Mandelbrot, 1994; Iannaccone and Khokha, 1996). In particular, it has been shown that fractal analysis is a useful tool for improving image description of neurons, and that, although the fractal dimension alone does not completely specify a cell's morphology, and indeed it should not be expected to, it is a statistically significant parameter for identifying and differentiating neuronal cell classes (Fernández et al., 1994; Fernández and Jelinek, 1999). On the other hand, the concept of fractal dimension (D) has been dampened by some severe limitations. First of all, the mathematically rigorous determination of D is almost impossible for a fractal point set obtained from digitised photos, drawings or other experimental data, although a very good estimate of D can be achieved by different methods of fractal analysis. Furthermore, there are several different dimensions, and several methods to calculate the fractal dimension, that may give slightly different numerical values of D for the same experimental data set (Jelinek and Fernández, 1998). An even more basic consideration is that most measurements cover only a relatively few decades (Russ, 1994; Avnir et al., 1998), so that some authors have suggested that most biological patterns are not fractals but space filling objects (Panico and Sterling, 1995). In spite of these problems, fractal analysis has already found widespread application in the field of neuroscience (see Fernández and Jelinek, 1999 for a review) and is being used in many other areas (Bundle and Havling, 1994; Nonnenmacher et al., 1994; Iannaccone and Khokha, 1996).

A criticism that could be levelled at almost all methods used to measure D, is that it is not always and adequate descriptor of a determined profile. For example, two neurons may appear visually very different from one to another, yet having the same fractal dimension (Smith et al., 1989, 1996; Fernández et al., 1994; Smith and Lange, 1996). Furthermore, we can imagine that a complex structure such as a neuron, can be a mixture of different fractals, each one with a different

* Corresponding author. Tel.: +34-6-5919439; fax: +34-6-5919434.
E-mail address: e.fernandez@umh.es (E. Fernández)

fractal dimension. In such a case, the whole structure will have a dimension which is simply the dimension of the component(s) with the largest density (Peitgen et al., 1992). This means that the resulting number may not characterise the mixture. Thus some investigators are starting to use multifractals as a more comprehensive methodology that may provide information about the distribution of fractal dimensions in biological structures (Smith et al., 1996; Smith and Lange, 1998). This is so despite of the fact that the technical difficulties of multifractal analysis are far more serious than those related to the analysis of the fractality itself. As an example we note that whereas even the most extensive numerical analysis carried out up to now (Vicsek et al., 1990) indicate that clusters generated through the diffusion-limited aggregation model (DLA) may be multifractals, widely accepted arguments show that they are in fact not (Lam, 1995).

In this work we discuss the theoretical and practical aspects of studying and measuring the multifractal dimensions of neurons, emphasising the serious difficulties encountered in multifractal analysis of experimental objects. We test our methods on DLA clusters having a number of pixels similar to that used in the analysis of neurons. Our results show that if the box-counting method is used, not only neurons but also standard DLA aggregates show an odd behaviour of the generalised dimension D_q, which is characterised by a non-monotic dependence on q. In particular, $D_{-\infty} < D_{\infty}$, a result clearly incompatible with the very basic properties of multifractals. Instead, if the sand-box method is used, the generalised fractal dimensions of both neurons and DLA aggregates behave as expected. We conclude that previously published abnormal results are a consequence of deficiencies of the box-counting method, rather than of unusual geometrical characteristics of neurons. On the other hand, comparison with present and previously published results for DLA aggregates, suggest that size effects are likely the origin of much of the apparent multifractality of neurons.

2. Methods

2.1. Retinal neurons

A random sample of retinal neurons from cat and turtle, whose fractality had been previously investigated (Fernández et al., 1994; Jelinek and Fernández, 1998) were examined in this study. Most of the cells were previously published images of retinal neurons that were characterised morphologically either using Golgi-impregnation techniques or intracellular injection of horseradish peroxidase or lucifer yellow after physiological recordings. All cells were drawn using camera lucida projection as seen in wholemount preparations (Fig. 1).

To determine the fractal dimension of the cells, the drawings were digitised by a scanner with a resolution of 300 dpi to produce black and white binary images. All the drawings were analysed in three ways: as binary or real drawings (black-on-white), as one-pixel-border images and as skeletonised tracings. The transformations were performed using the NIH-Image processing software (developed at the US National Institutes of Health and available on the Internet at http://rsb.info.nih.gov/nih-image/).

2.2. DLA clusters

To test our methods we calculated the D_q spectrum for several DLA clusters having a number of pixels similar to that of the neurons here investigated (both around 100 000). DLA (Witten and Sander, 1983) and the equivalent dielectric breakdown (DB) model (Niemeyer et al., 1984) are examples of growth in scalar fields. Those two models, together with their vectorial counterpart, the so called mechanical breakdown (MB) model devised to investigate crack propagation (Louis and Guinea, 1987) are the most intensively investigated growth models. Computer generated DLA aggregates having around 100 000 particles, were obtained in a two-dimensional grid, by implementing the enhanced diffusion algorithm which has been shown to be equivalent to the ordinary DLA process (Vicsek et al., 1990). Briefly, the procedure starts by fixing a single particle or seed point at the origen of a two-dimensional coordinate system. This particle is not allowed to move. Next we select a region of interest centred around the initial sticky or seed particle. The computer injects then a free particle at the boundary of the region and lets it to

Fig. 1. Line drawing of a retinal ganglion cell as seen in a whole-mount projection.

Fig. 2. Typical diffusion-limited aggregation (DLA) cluster containing around 100 000 particles generated on a triangular lattice.

move about randomly. Two things may happen in the course of this motion. Either the particle leaves the region of interest, in which case the computer forgets about it, or the particle stays in this region until it attaches to the first sticky particle and also becomes a sticky particle (we used a sticking probability of 100%). The procedure is then repeated until the growing cluster of connected sticky particles gets around 100 000 particles. For practical purposes, the computation was based on a triangular lattice of pixels and the free particle was allowed to move to one of its six neighbouring pixels in one time step. Fig. 2 shows an example of a simulated DLA cluster. All computations were performed using 16 decimal digits of precision on a Unix DEC3000 workstation, or on a Pentium II computer running Linux.

To determine the fractal dimension of the DLA aggregates in a similar way to that of retinal neurons, the computer-generated images were printed out and digitised by a scanner with a resolution of 300 dpi to produce black and white binary images. We also analysed DLA aggregates by using directly the simulated coordinates of each aggregated particle stored on the computer.

2.3. Multifractal analysis: box-counting method

In general, there are several basic approaches for measuring the fractal dimension of an object (Smith et al., 1989, 1996; Fernández and Jelinek, 1999; Jelinek and Fernández, 1998). Two of the most commonly used techniques, that can be also used for a multifractal analysis, are the box-counting and the so called sand-box or cumulative mass method.

To estimate D using the box-counting method, the Euclidean space containing the image is covered with d-dimensional boxes of linear size l. If we consider the finite size L of the object, we can use $\varepsilon = l/L$, which is the size of covering boxes normalised by the linear size of the structure, and write

$$N(\varepsilon) \propto \varepsilon^{-D} \tag{1}$$

where $N(\varepsilon)$ is the number of boxes needed to cover entirely the object and D is the fractal dimension. ε is made progressively smaller and the corresponding number of non-empty boxes, $N(\varepsilon)$ are counted. The logarithm of $N(\varepsilon)$ versus the logarithm of ε, gives a line whose gradient corresponds to D.

Clearly this is the crudest measure of the object, because no consideration is given to the fact that different numbers of object elements (e.g. pixels) can contact a box. Thus, this measure contains no information about the fine structure of the object. The next step toward the multifractal analysis is counting the pixels in each box $M_i(l)$. Using the mass distribution, and its q-th moments, the generalised dimensions are defined by

$$\sum_i \left(\frac{M_i(l)}{M_0}\right)^q \propto \left(\frac{l}{L}\right)^{(q-1)D_q} \tag{2}$$

where M_0 is the total number of pixels in the image.

In the analysis of multifractality, it is particularly important the use of sizes l be at least two orders of magnitude smaller than L and two orders of magnitude greater than the pixel size. This implies that the images must be as large as possible (Vicsek et al. 1990).

2.4. Multifractal analysis: sand-box method

The calculation of D_q for $q<0$ by means of the box-counting method is hindered by the fact that the boxes which contain a small number of particles give an excessively large contribution to the sum in the left-hand side of (Eq. (1)) and, as a consequence, the results are not reliable. To overcome this problem we have used the generalised sand-box method proposed by Vicsek et al. (1990). This method consists of calculating the average of masses $M(R)$ and their q-th moments within circles of radius R that are always centred on the cluster. The procedure reduces the undesired effect of almost empty boxes. The circles are randomly dis-

tributed on the aggregate. Commonly a number of circles smaller than 10% of the total number of particles or pixels in the aggregate is enough. Note also that non overlapping of the circles is not required. Then the analysis proceeds as above, namely, the scaling of $\langle M^q(R)\rangle$ with R is investigated, where (...) denotes the average over the centres. Accordingly, (Eq. (2)) takes the form,

$$\left\langle \left(\frac{M(R)}{M_0}\right)^q \right\rangle \propto \left(\frac{R}{L}\right)^{(q-1)D_q} \quad (3)$$

In implementing this method we have calculated the average in (Eq. (3)) on a set of circles centred on 5% of the total number of pixels. We have checked that increasing this number does not change the results.

3. Results

3.1. Retinal cells

According to fractal theory, if neurons are just simple fractals, what we should expect is a uniform measure or constant D. Thus, the graphical representation of D_q versus q should give more or less a straight line, because all the D_q values are approximately the same. However, it could happen that such a simple fractal picture cannot be sufficient to characterise neurons. In this case, what we would really have is something like a spectrum of numbers providing information about the distribution of fractal dimensions in these structures, and we should interpret these structures in terms of multifractal scaling (Vicsek, 1992).

Fig. 3 shows the results for two retinal ganglion cells using either the box-counting (empty symbols) or the generalised sand-box (filled symbols) methods. Clearly we did not get a uniform distribution of D_q versus q, so it seems that a single D value could not be enough for the characterisation of these cells. At this point, we can imagine that these retinal cells, have different areas with locally different D, which could reflect different branching patterns, different synaptic conectivity or different processing capabilities. If we assume that these neurons are multifractals, then an infinite hierarchy of exponents is needed to account for their complicated structure and the D_q distribution should decrease monotonically in value as q increases (Vicsek et al., 1990; Vicsek, 1992). Our results (Fig. 3) show important differences depending on the procedure used for the analysis. Specifically, whereas the generalised sand-box method gives a monotonically declining curve for D_q versus q for all q, the box-counting method gives, for $q<0$, what has been called by some authors (Bos et al., 1996; Smith and Lange, 1998) an anomalous D_q curve, in the sense that D_q is an increasing function of q for negative q.

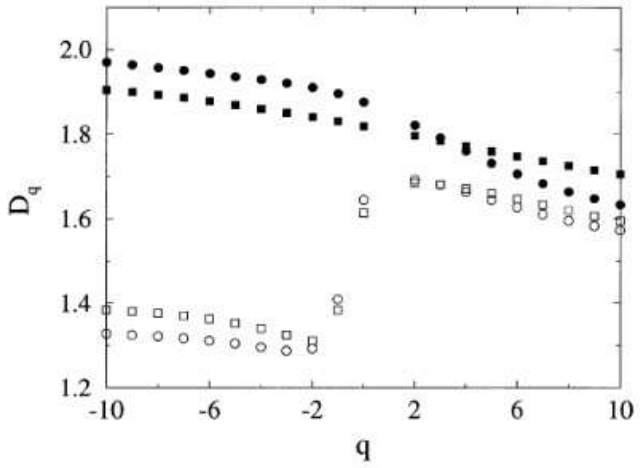

Fig. 3. Dependence of the generalised dimensions D_q on q for two neuronal cells of the turtle retina (circles and squares). The results were obtained by using either the box-counting (empty symbols) or a generalised sand-box (filled symbols) method (see text). The digitalised pictures of the cells contained around 20 000 pixels.

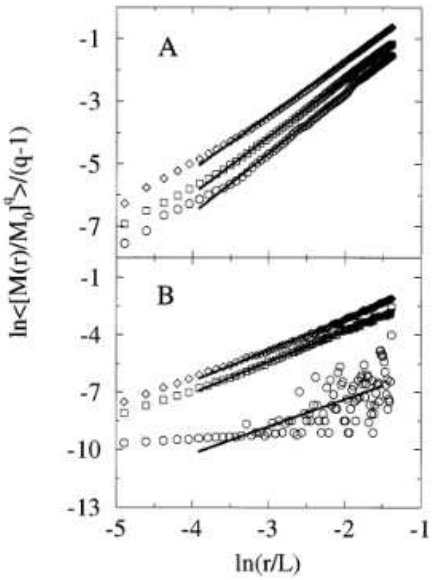

Fig. 4. Calculation of the generalised dimension D_q associated to the mass distribution in a neuronal cell of the turtle retina. The digitalised picture of the cell contained around 20 000 pixels. Calculations were carried out by means of either the generalised sand-box (A) or the box-counting (B) methods (see text). The results correspond to $q=-10$ (circles), $q=0$ (squares) and $q=10$ (diamonds). Straight lines were fitted for $\ln(r/L)$ in the range $[-4, -1.5]$. The generalised fractal dimensions which result from these fittings are: sand-box method, 1.92, 1.83 and 1.72, and box-counting method, 1.43, 1.62 and 1.60, for $q=-10$, 0 and 10, respectively.

Fig. 4 shows a typical set of results for a retinal cell, where the scaling of the moments of the box masses is demonstrated for $q=-10$, 0, 10. It is clear from this figure that the various moments scale differently and that the results obtained by means of the generalised sand-box method (Fig. 4A) are quite different of the

results given by the box-counting method (Fig. 4B). The strong dispersion of the data points observed in the box-counting results for $q = -10$ (circles) could be explained by the dominant contribution of boxes with too few pixels on the negative q's range (Vicsek, 1992). This illustrates the unsuitability of the box-counting method for $q < 0$.

The results of the generalised sand-box method (Figs. 3 and 4A) suggest that retinal neurons are not homogeneous fractals in the sense that the local scaling of the mass is described by a set of exponents. The overall dependence of D_q on q is consistent with the expected behaviour for a multifractal geometry because it shows a monotonic decay with increasing q.

3.2. DLA aggregates

Although the distribution of growth probabilities of DLA aggregates has been shown to be multifractal (Nittmann et al., 1987; Ohta and Honjo, 1988), the DLA cluster itsef, was originally suggested to be a self-similar fractal, characterised solely by the fractal dimension D. Subsequent extensive simulations have suggested that DLA clusters do in fact have a multifractal geometry (Vicsek et al., 1990). This result is, however, in contradiction with the analysis of Lam (1995) which indicates that finite-size effects may in fact be the origin of the apparent multifractal behaviour reported in previous numerical studies. Thus Lam (1995) concludes that DLA aggregates can be specified by the fractal dimension alone.

When we determined the D_q spectrum of DLA aggregates using the box-counting procedure, we found that for $q > 0$ they decrease monotonically with increasing q, as expected. However, our results show an anomalous behaviour for $q < 0$ (Fig. 5). The results do not depend on whether the coordinates of the pixels in the generated DLA clusters or those in the scanned version of these clusters were used in the multifractal analysis. Instead, the generalised sand-box technique, the D_q spectrum associated with the mass distribution gives a D_q spectrum that decreases monotonically with increasing q (Fig. 5).

The scaling of the moments of the box masses was similar to that for retinal neurons (Fig. 6), showing significant differences between the generalised dimensions. We carried out the above analysis for 10 DLA clusters and found similar scaling of the moments of the box masses, suggesting that the geometry of DLA might have a multifractal behaviour. Consequently, the numerical results suggest that the local density of DLA scales like a multifractal measure and, thus, has to be described by an infinite set of mass exponents. Note, however, that the difference $D_{-10} - D_{10}$ is in our case larger than that found by Vicsek et al. (1990), approximately 0.23 and 0.14, respectively, indicating that the apparent multifractal behaviour of Fig. 5 may in fact be a finite-size effect, as the clusters used by Vicsek et al. (1990) are an order of magnitude larger than those analysed here. This is in agreement with Lam's suggestion (Lam, 1995). This author pointed out that there does not seem to be any reason for the existence of any multiplicative cascade process for the distribution of mass inside the DLA and that the apparent multifractality obtained by means of numerical analyses should be a finite-size effect.

4. Discussion

Although some biological patterns can be adequately characterised with a single exponent, the fractal dimension, this measure is a global or average measure of an object, and says nothing about the spatial distribution of the measured property (Peitgen et al., 1992). In fact, some biological structures that look different and are structurally different, may have the same value of D (Smith et al., 1989; Fernández et al., 1994; Smith and Lange, 1996). Furthermore, it is common to find in the literature that observed data depart from the ideal fractal relationship defined by a straight-line log–log plot, and it has been suggested that this departure could be described by a multifractal behaviour (Russ, 1994). These recognised limitations of fractal dimension has

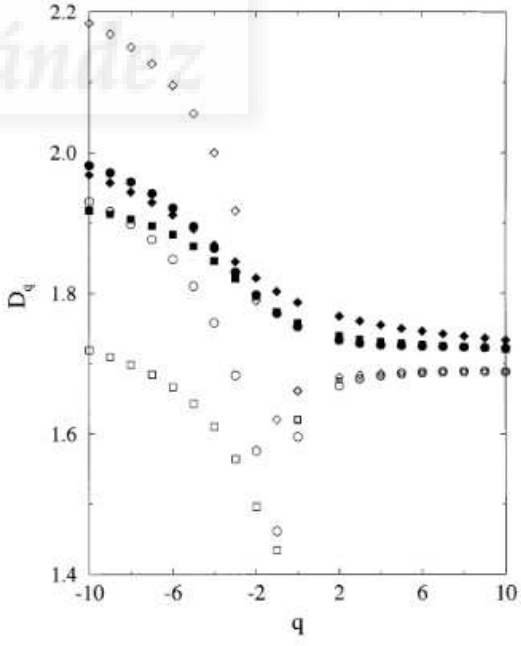

Fig. 5. Dependence of the generalised dimensions D_q on q for three diffusion-limited aggregation (DLA) clusters (circles, squares and diamonds) grown on a triangular lattice and having around 100 000 particles each. The results were obtained by using either the box-counting (empty symbols) or a generalised sand-box (filled symbols) method (see text).

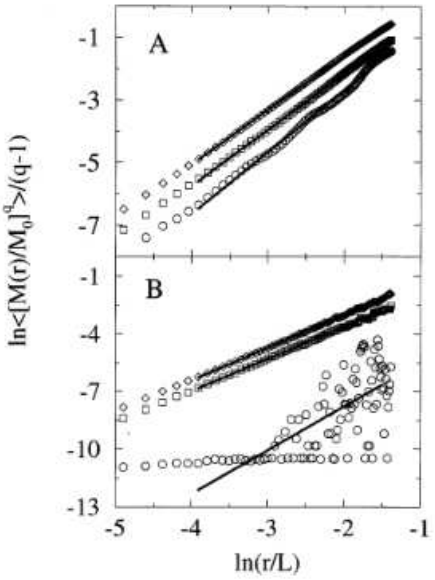

Fig. 6. Calculation of the generalised dimension D_q associated to the mass distribution in a diffusion-limited aggregation (DLA) cluster grown on a triangular lattice and containing around 100 000 particles. Calculations were carried out by means of either the generalised sand-box (A) or the box-counting (B) methods (see text). The results correspond to $q=-10$ (circles), $q=0$ (squares) and $q=10$ (diamonds). Straight lines were fitted for $\ln(r/L)$ in the range $[-4, -1.5]$. The generalised fractal dimensions which result from these fittings are: sand-box method, 1.98, 1.79 and 1.73, and box-counting method, 2.27, 1.66 and 1.69, for $q=-10$, 0 and 10, respectively.

lead to the search for other distinguishing measures such as the lacunarity and the multifractal distribution of fractal dimensions. In this context, recent studies (Smith et al., 1996; Smith and Lange, 1998) have suggested that certain individual nerve and glial cells may have a multifractal structure, although the behaviour of their generalised dimensions is rather odd. More specifically, the above mentioned studies reported what they call an anomalous D_q curve (Bos et al., 1996; Smith and Lange, 1998), in the sense that D_q is an increasing function of q for all q, a result clearly incompatible with the very basic properties of multifractality (Vicsek, 1992).

The present study was undertaken to elucidate whether retinal neurons are or not multifractals and to investigate the multifractal properties of these neuron cells. Our results show that if the box-counting method is used not only neurons but also standard DLA aggregates show the anomalous behaviour mentioned above. It has been shown by several authors that this problem is because of the fact that boxes which contain a small number of particles or pixels give an anomalously large contribution to the relative weight of each box. As a consequence, the box-counting method does not allow to get reliable results for negative q. A solution to this problem (Vicsek et al., 1990; Vicsek 1992; Smith and Lange, 1998) is to use the generalised sand-box method. Since the generalised sand-box method is based on studying the average of masses of circles centred on the object, there are no circles with too few pixels in them and so it is possible to get more reliable results for negative moments. Our results show that if the sand-box method is used, the generalised fractal dimensions of neurons do in fact behave as expected. We conclude that previous abnormal results should be a consequence of deficiencies of the box-counting method, rather than of unusual characteristics of neurons.

Apparently, our numerical results indicate that retinal neurons are true multifractals, and that the distribution of fractal dimensions in a neuron could be related with different growing probabilities, geometrical characteristics, synaptic connectivity or physiological responses. Unfortunately our results on DLA aggregates did not allow us to support this idea and we are forced to examine carefully this hypothesis. Thus although the distribution of growth probabilities of DLA aggregates has been shown to be multifractal (Amitrano et al., 1986; Ohta and Honjo, 1988) and there are some reports that suggest that these DLA aggregates might have multifractal geometry (Vicsek et al., 1990), the recent study of Lam (1995) shows that DLA follows simple scaling with strong finite-size effects. Our results are in agreement with the study of Lam (1995) and support the view that finite-size effects can account for the deviations observed from simple scaling. This interpretation provides a plausible description for all numerical results on neurons and DLA, and is already sufficient to explain the apparent multifractality of finite DLA aggregates and retinal neurons. Consequently the interpretation of complex scaling instead of finite-size effects is not well founded and have been shown to lead, at least for the case of DLA, to trivially wrong predictions, (see Lam, 1995 for a review). To this end we can not conclude that neurons are multifractals.

In this context it is interesting to comment on recent large scale simulations of DLA carried out by Mandelbrot (1992). This author showed that when the number of aggregate particles is very large (clusters having up to 40 millions particles were investigated) DLA clusters are no longer fractal but rather space filling objects having the same dimension than the underlying Euclidean space. If this result is confirmed the conclusion may be that DLA would only have a fractional dimension at a medium scale (through a more or less large number of decades). The change from a fractal to a non-fractal object may be a crossover effect. This may also be of relevance as far as the eventual multifractal character of the clusters is concerned. In fact, if that was the case, the present and previous results (Vicsek et al., 1990) indicate that medium size DLA clusters could be considered multifractal up to the same extent they are considered fractals. Something similar could be assessed in relation to neurons.

Finally although several studies of measures defined on fractal substrates, indicate that many distributions in nature should be interpreted in terms of multifractal scaling (Halsey et al., 1986; Peitgen et al., 1992; Mandelbrot, 1994; Lam, 1995) little is known about geometrical multifractality (Vicsek et al., 1990) and more studies are necessary to know the relevance and practical applications of these measurements in biological structures.

Acknowledgements

This work was supported by the Spanish 'Direccion General de Investigacion Cientifica y Tecnica' through grant PB94-1509 and the 'Comision Interministerial de Ciencia y Tecnologia' through grants PB96-0085 and SAF98 0098C02-02. EL acknowledges partial support from the European TMR NetworkFractals c.n.FMRXCT980183, and GO is grateful to the 'Ministerio de Educacion y Cultura' for a postdoctoral grant.

References

Amitrano C, Coniglio A, Di Lilerto F. Growth probability distribution in kinetic aggregation processes. Phys Rev Lett 1986;57:1016–19.

Avnir D, Biham O, Lidar D, Malcai O. Is the geometry of nature fractal? Science 1998;279:39–40.

Bassingthwaighte JB, Liebovitch LS, West BJ. Fractal physiology. Oxford: Oxford University Press, 1994.

Bos MTA, Opheusden JHH, van der Kaaden G. Anomalous multifractal spectrum of aggregating Lennard–Jones particles with Brownian dynamics. Physica A 1996;227:183–96.

Bundle A, Havling S. Fractals in Science. Berlin: Springer, 1994.

Cross SS. The application of fractal geometric analysis to microscopic images. Micron 1994;25:101–13.

Feder J. Fractals. New York: Plenum Press, 1988.

Fernández E, Eldred WD, Ammermder J, Block A, von Bloh W, Kolb H. Complexity and scaling properties of amacrine, ganglion, horizontal and bipolar cells in the turtle retina. J Comp Neurol 1994;347:397–408.

Fernández E, Jelinek H. Use of fractal theory in neuroscience: methods, advantages and potential problems. Methods: A companion to methods in I Enzymology. 1999. In press.

Halsey T, Meakin P, Procaccia I. Scaling structure of the surface layer of diffusion-limited aggregates. Phys Rev Lett 1986;56:854–7.

Iannaccone PM, Khokha M. Fractal Geometry in Biological Systems: An Analytical Approach. Boca Raton, Florida: CRC Press, 1996.

Jelinek H, Fernández E. Neurons and fractals: how reliable and useful are calculations of fractal dimensions. J Neurosci Meth 1998;81:9–18.

Lam CH. Finite-size effects in diffusion-limited aggregation. Phys Rev B 1995;52:2841–7.

Louis E, Guinea F. The fractal nature of fracture. Europhys Lett 1987;3:871–7.

Mandelbrot BB. The Fractal Geometry of Nature. NY: W.H. Freeman, 1982.

Mandelbrot BB. Plane DLA is not self-similar; is it a fractal that becomes increasingly compact as it grows? Physica A 1992;191:95–107.

Mandelbrot BB. Fractals lacunarity, and how it can be tuned and measured. In: Nonnenmacher TF, Lose GA, Weibel ER, editors. Fractals in Biology and Medicine. Boston: Birkhauser Verlag, 1994:21.

Niemeyer L, Pietronero L, Wiesmann HJ. Fractal dimension of dielectric breakdown. Phys Rev Lett 1984;52:1033–6.

Nittmann J, Stanley HE, Touboul E, Daccord G. Experimental evidence: for multifractality. Phys Rev Lett 1987;58:619–22.

Nonnenmacher TF, Losa GA, Weibel ER. Fractals in Biology and Medicine. Basel: Birkauser, 1994.

Ohta S, Honjo H. Growth probability distribution in irregular fractal-like crystal growth of ammonium chloride. Phys Rev Lett 1988;60:611–4.

Panico J, Sterling P. Retinal neurons and vessels are not fractal but spacefilling. J Comp Neurol 1995;361:479–90.

Peitgen H-O, Jürgens H, Saupe D. Fractals for the Classroom. Part One. New York: Springer-Verlag, 1992.

Russ J. Fractal Surfaces. NY: Plenum Press, 1994.

Smith TG, Behar TN, Lange GD, Sheriff Jr WH, Neale EA. A fractal analysis of cell images. J Neurosci Meth 1989;27:173–80.

Smith TG, Lange GD. Biological cellular morphometry-fractal dimensions, lacunarity and multifractals. In: Nonnenmacher TF, Losa GA, Weibel ER, editors. Fractals in Biology and Medicine. Basel: Birkauser, 1998.

Smith TG, Lange GD. Fractal studies on neuronal and glial morphology. In: Iannaccone PM, editor. Fractal Geometry in Biological Systems: An Analytical Approach. Boca Raton, FL: CRC Press, 1996:173.

Smith TG, Lange GD, Marks WB. Fractal methods in cellular morphologyn-dimensions, lacunarity and multifractals. J Neurosci Meth 1996;69:123–36.

Vicsek F, Family F, Meakin P. Multifractal geometry of diffusion-limited aggregates. Europhys Lett 1990;12:217–22.

Vicsek T. Fractal Growth Phenomena. Singapore: World Scientific, 1992.

Witten TA, Sander LM. Diffusion-limited aggregation. Phys Rev B 1983;27:5686–97.

UNIVERSITAS
Miguel
Hernández

Irregular S-cone mosaics in felid retinas. Spatial interaction with axonless horizontal cells, revealed by cross correlation

Peter Kurt Ahnelt

Institut für Allgemeine und Vergleichende Physiologie, Universität Wien, Wien, Austria

Eduardo Fernández, Oscar Martinez, and Jose Angel Bolea

Bioengineering Institute, Universidad Miguel Hernández, Alicante, Spain

Anna Kübber-Heiss

Institut für Pathologie und Gerichtsmedizin, Veterinärmedizinische Universität, Wien, Austria

Received September 8, 1999; revised manuscript received November 23, 1999; accepted November 24, 1999

In most mammals short-wavelength-sensitive (S) cones are arranged in irregular patterns with widely variable intercell distances. Consequently, mosaics of connected interneurons either may show some type of correlation to photoreceptor placement or may establish an independent lattice with compensatory dendritic organization. Since axonless horizontal cells (A-HC's) are supposed to direct all dendrites to overlying cones, we studied their spatial interaction with chromatic cone subclasses. In the cheetah, the bobcat, and the leopard, anti-S-opsin antibodies have consistently colabeled the A-HC's in addition to the S cones. We investigated the interaction between the two cell mosaics, using autocorrelation and cross-correlation procedures, including a Voronoi-based density probe. Comparisons with simulations of random mosaics show significantly lower densities of S cones above the cell bodies and primary dendrites of A-HC's. The pattern results in different long-wavelength-sensitive-L- and S-cone ratios in the central versus the peripheral zones of A-HC dendritic fields. The existence of a related pattern at the synaptic level and its potential significance for color processing may be investigated in further studies. [S0740-3232(00)02203-1]

OCIS codes: 330.7310, 330.1720, 330.5310, 330.6180, 330.6130, 330.5000.

1. INTRODUCTION

It is generally assumed that variations of retinal photoreceptor mosaics found among species with differing lifestyles reflect the design of the eye's optics and neuronal grain.[1] Basically, the retinal sensory layer serves as a testing ground for evolution.

A. Mammalian S-Cone Mosaics: Generally Irregular

The possibilities of identifying short-wavelength-sensitive (S) cones in primates[2–5] have initiated studies of their S-cone mosaic properties and of the consequences for spatial and chromatic processing.[6,7] The fact that in most diurnal species S cones constitute only a minor subpopulation has been attributed to the defocusing effects of S image components. Application of antiopsin antibody to other mammalian species provides a more balanced view on S-cone mosaics. Irregular rather than regular patterns appears to be the rule among most mammals with S-cone mosaics (Fig. 1). This group includes marsupials such as the opossum,[8] as well as rabbits, cats, horses, rats, and guinea pigs,[2,9–11] but the irregularity has been also found in *Tarsius*, a nocturnal prosimian,[12] and in both the dichromatic and the trichromatic marmoset (*Callithrix*), a diurnal platyrrhine monkey.[13] Although not crystalline, the peripheral S-cone mosaic of humans and Old World monkeys is clearly nonrandom.[5,14,15] S-cone submosaics of similar regularity have also evolved in two other mammalian groups. In both groups, the ground squirrels and their relatives[16,17] and the tree shrews,[18] the regular S-cone mosaics are associated with cone-dominant retinas.

B. S-Cone Patterns and Connectivity to Interneurons

Over the years it has been established that most placental mammals have two types of horizontal cell (HC).[19,20] The specific role of these cell types' dendritic trees, both connecting to cones,[21,22] has remained an enigma. For primate HC's, it has been shown[23–26] that a weighting of connectivity exists with respect to the two major classes of cones. H2-HC's (possibly a modified axonless type[20]) have elevated connection densities to S cones within their dendritic field but also connect to long-wavelength-sensitive (L) and middle-wavelength-sensitive (M) cones. For other mammalian species, no conclusive evidence for the existence of chromatic connection patterns has been reported.

An important approach toward probing for mutual interdependence of mosaics such as S cones and HC's is cross correlation.[27,28] Recently, the method of autocorrelation by establishment of a density recovery profile has

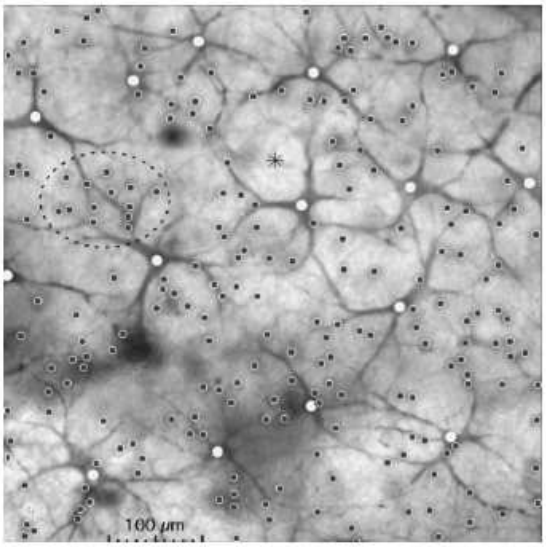

Fig. 1. Cheetah retina, superior periphery: JH455 labeling. S-cone position plotted on composite image of horizontal cell (HC) level merged from focused portions within a series of optical sections. S cones (dark spots) are irregularly arranged. Clustering preferentially appears above areas in which peripheral dendrites from HC's overlap (enclosed within dashed circle). A-HC bodies (white circle indicates nucleus position) and primary dendrites remain largely free of S cones as well as zones with few or no dendrites (asterisk).

been extended to correlate the positions of S cones with the positions of underlying S-cone specific bipolar cells (blue bipolars) in the primate retina.[29] The result suggests that there is direct dependence between the two mosaics, whereby the blue bipolar cell positions have more degrees of freedom by virtue of the lateral range of their dendrites. Extending this concept to interneuron types with even larger dendritic range and considerable overlap such as axonless horizontal cells (A-HC's[30,31]) would imply that the two mosaics should become practically independent. If there is still correlation, it may then point to other constraints.

The present paper takes a new approach, based on the individual shapes of Voronoi domains, to probe for specific spatial correlations between HC's and spectral cone types in nonprimate mammals. It discusses possible approaches toward verification of the properties of irregular mosaics.

2. MATERIALS AND METHODS

A. Specimens and Data Acquisition

Eyes from three cheetahs, two European lynxes, one leopard, and two mandrills (zoo animals delivered to veterinary pathology for autopsy) were removed 20 min to 20 h after death and were fixed in 4% paraformaldehyde in phosphate buffered saline solution. Isolated retinas were prepared as whole mounts and were then labeled with one or two antibodies [we used peanut agglutinin, antiopsin JH492, and antiopsin JH455 (the last two were kindly provided by J. Nathans)], as described elsewhere.[8] JH455 labeled not only the S-cone outer segments but also occasionally the complete cones, and, more importantly, it consistently led to colabeling of cell bodies and major dendrites of A-HC's (Fig. 1).

Positions of cells were mapped with an on-line videomicroscopy system (Hamamatsu 2400 camera; Apple Power Mac with Video-Monitor-Genlock software). Through-focus series were captured digitally (Photometrix) from outer segments to HC's to create Adobe Photoshop multilayer files. Point pattern graphs were created in CANVAS or Photoshop overlay planes. For pattern analysis, x and y coordinates were identified with NIH Image software.

B. Data Analysis

The spatial organization of the S-cone and the A-HC mosaics was analyzed with the Spatial Point Pattern software[32] by means of the distribution of nearest-neighbor distances.[33] Furthermore, we also used analysis of cross correlation between different arrays.[27–29,34,35] We introduce what is, to our knowledge, a new procedure that is based on the Voronoi (or Dirichlet) tessellation to adapt to the frequently noncircular dendritic fields (DF's) of many A-HC's.

The diagram obtained by the method is illustrated in Fig. 2. First, a population is chosen as a reference (in our case, the A-HC's). Then the Voronoi tessellation for these cells is computed.[36–38] Each Voronoi polygon consists of all the points in the plane that are closer to one

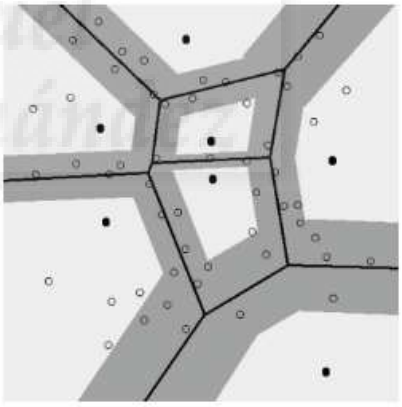

Fig. 2. Diagram obtained by the Voronoi-based cross-correlation procedure. Each Voronoi domain defines the area in the plane of the A-HC population that is closer to one A-HC than to any other A-HC of the array. The areas are uniform, indicating that A-HC's tile the retina evenly. The next step is the construction of bands around the edges of the Voronoi polygons and the computation of the number of points belonging to the upper population (S cones) inside these bands. The basic idea is that, if both populations are independent, then the occurrence of an A-HC should not alter the probability of the occurrence of S cones, and the average density of S cones should be the same inside and outside the bands. The width of each band is calculated specifically for each point and each edge of the Voronoi diagram (see Section 2). In this illustration the gray bands represent a bandwidth of 0.29 (=29% to the distance between a given A-HC and its closer Voronoi edges). For this bandwidth, the areas inside (white) and outside (gray) the polygons are equivalent, so the same number of S cones is expected (V proportion is equal to 0.5) inside and outside the bands. Since there are more S cones inside the bands, the V proportion (=0.82) is higher than expected and indicates a negative correlation between both mosaics.

Table 1. Nearest-Neighbor Histograms of Cones Shown in Fig. 3

Cell Type	n	Mdist[a] (μm)	SD	P[b]
Cheetah A-HC	38	112.7	23.7	*R*[c]: 0.000
Cheetah SC[d]	353	25.7	11.9	*I*[e]: 0.037
Mandrill SC	244	37.9	8.5	*R*: 0.000
Mandrill LC[f]	2074	14.2	1.9	*R*: 0.000

[a] Mdist, nearest-neighbor distance.
[b] P, probability value found by the Clark–Evans method.[41]
[c] R, regular distribution.
[d] SC, short-wavelength-sensitive cone.
[e] I, irregular distribution.
[f] LC, long-wavelength-sensitive cone.

cell than to any other cell in the mosaic. The next step is the construction of bands around the edges of the Voronoi polygons and the computation of the number of points belonging to the distal population (S cones) inside these bands. The basic idea is to study the pattern of interdependence among the two component patterns. Thus, if both populations are independent, then the occurrence of a reference cell should not alter the probability of the occurrence of the sample cells, and the average density of sample cells should be the same inside and outside the bands. However, it could happen that the sample cells (e.g., S cones) show either a positive or a negative correlation with the reference cells (e.g., A-HC's). In a two-dimensional array this may simply reflect the physical size of the cells; in layered samples it may be a manifestation of more-subtle effects. If reference cells inhibit sample cells, then the latter will be near the edges of the Voronoi diagram, and the number of sample cells inside the bands will be significantly higher than expected. If the number of sample cells inside the bands is decreased, it means that reference cells are positively correlated with them.

The expected proportion of cells inside the bands, provided that both populations are independent, is easily calculated. Let Δr be the width of each band (it is not fixed for the entire area being studied but is proportional to the distance between a given point and its closer Voronoi edges, being $0 < \Delta r < 1$). Thus Δr could be 10% of the distance from the edge to the point ($\Delta r = 0.1$), 20% of the distance from the edge to the point ($\Delta r = 0.2$), etc.

$|V(p_i)|$, area of the Voronoi polygon;

$N_{V(p_i)}$, number of points in $|V(p_i)|$;

$|V(p_i, \Delta r)|$, area of the Voronoi region after reduction of the Voronoi domain by a factor of Δr (white region in Fig. 2);

$|V(p_i, B)| = |V(p_i) - |V(p_i, \Delta r)|$ (shaded region in Fig. 2);

$N_{V(p_i, \Delta r)}$, number of points in $|V(p_i, \Delta r)|$;

$N_{V(p_i, B)}$, number of points in $|V(p_i, B)|$. Then the proportion between $|V(p_i)|$ and $|V(p_i, \Delta r)|$ in a closed Voronoi polygon for every Δr is

$$|V(p_i, \Delta r)| = (1 - \Delta r)^2 |V(p_i)|, \quad (1)$$

$$|V(p_i, B)| = |V(p_i)|[1-(1 - \Delta r)^2]. \quad (2)$$

Assuming a random distribution of points, the expected number of points inside the bands is related to the bandwidth; hence that number of points inside the bands $[N_{V(p_i, B)}]$ for a determined Δr is

$$N_{V(p_i, B)} = N_{V(p_i)}[1-(1 - \Delta r)^2], \quad (3)$$

and the V proportion between the number of points inside the bands and the total number of points is written as

$$N_{V(p_i, B)}/N_{V(p_i)} = 1-(1 - \Delta r)^2. \quad (4)$$

This V proportion varies depending on Δr, as is shown in Table 2 below. If the measured V proportion is higher than expected, it means that there are more points inside the bands, which suggests a negative correlation. If the measured V proportion is smaller than expected, it indicates a positive correlation.

Voronoi domains and nearest-neighbor distances were computed by use of the incremental algorithm first described in Ref. 36. To avoid the consequences of edge effects we considered only those polygons inside the convex hull of the reference points. A specific program was developed in C++ and was compiled in a Linux station to permit performance of all the statistical and graphical techniques. The program is available on request.[39] To test the significance of this measure we calculated the V proportion for several Δr values. Furthermore, we also used a Monte Carlo test procedure. This involves generating a set of two random and independent patterns, each with the same number of points as the empirical reference and upper points, in a study area identical to that of the real pattern. We did this 100 times for each field, and then the mean and the standard deviation (SD) of the V proportion for each Δr were calculated.

C. Computer Simulations

To simulate a negative correlation process, random x- and y-coordinate values were generated independently for every reference and upper point by use of a Strauss-type simple inhibition process.[37] Distributions were randomly generated by positioning of one cell at a time in the sampling field (identical to that of the empirical pattern) and by determination of its distance to its closest neighbor. Whenever the cell's nearest-neighbor distance was smaller than the value of the effective radius, which was determined by use of the density recovery profile on the real sample,[27] the cell was eliminated. The minimum distance allowed between reference and upper points was given by the effective radius of the cross correlogram of the real sample.[27,29] This process was continued until the simulated distribution reached the same cell density as that of the real mosaics. To test the statistical significance of this model's fit of the data, we used the refined nearest-neighbor analysis.[32,37,40] (See Table 1 and Fig. 3.)

3. RESULTS

A. Histology and General Topography

Application of JH455 antibody results in consistent and intense labeling of outer segments in a minor population of cones in mammalian retinas. In the cheetah, S-cone proportions varied from 8% to 15%, with a maximum of ~7000/mm^2 in the temporal retina and ~1000/mm^2 in the

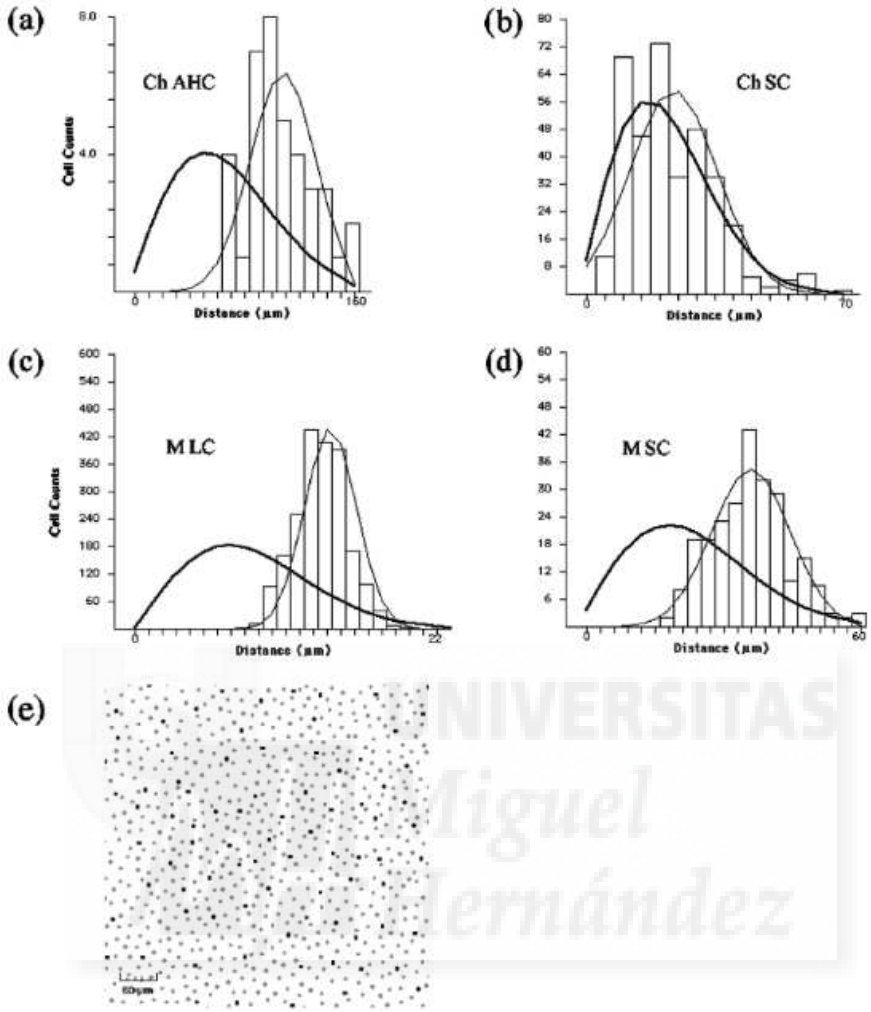

Fig. 3. Nearest-neighbor analysis of cheetah [(a), (b)] and mandrill [(c)–(e)] cell mosaics (see Table 1 for data). (a) Cheetah A-HC's (Ch AHC) show a near-Gaussian (regular) histogram. (b) The histogram of cheetah S cones (Ch SC) is close to a Rayleigh distribution, while (c) mandrill L and M cones (M LC) and (d) mandrill S cones (M SC) have regular patterns. (e) Sample of peripheral cone mosaic from mandrill retina (black, S cones; gray, putative L and M cones). Scale bar, 50 μm.

far periphery. At any location the mosaic of S cones appeared irregular [Fig. 3(b)], leading to local clustering as well as to major areas lacking labeled S cones (Fig. 1). This is in contrast to samples of L and M cones [Fig. 3(c)] and of S cones [Fig. 3(d)] in the peripheral retina of the mandrill, which—at different scales—have regular (Gaussian) intercone distributions. Local mosaic properties of lynx and leopard retinas were qualitatively similar to the findings in the cheetah retina. The following data refer to samples from cheetah retinas unless otherwise noted.

Occasionally, complete cones were labeled, allowing identification of pedicles linking to first-order interneurons [Fig. 4(b)]. In addition to the S-cone population, a plexus of cells having the typical characteristics of felid A-HC's[42] was labeled. When judged from the position of their cell bodies, the A-HC's are regularly spaced [Fig. 3(a)], except for a few occasions in which single cells appear to be missing within the plexus. In contrast to the smooth concentric DF's of short-axon HC's, the DF outline of A-HC's is often polygonal or extremely elongated. A few major dendrites originate at irregular angles (Fig. 1) from the cell bodies, which are often ill defined and situated between their broad bases. Thus the spatial tiling derived from the cell bodies often represents a more regular pattern than is found in the patterns at the level of their eccentric dendrites. Labeling of A-HC elements was most intense and extensive close to the ora serrata. It remained visible across approximately two thirds of the retina but faded toward the central areas, presumably because the reagents did not diffuse completely where the retina is thicker.

Overlays of mapped cones [Fig. 1] onto the HC plexus allow direct inspection of possible spatial interactions. Sometimes clustering of cones is associated with sites in which only peripheral dendrites of A-HC's overlap (Fig. 4). Conversely, in areas above A-HC bodies and primary dendrites, few or no S cones are situated at the photoreceptor level (Fig. 1, asterisk), but these observations require specific statistical analysis.

B. Statistical Analysis of S-Cone A-HC Mosaic Interactions

Assignment of individual S cones to HC's dendrites is hardly possible solely by comparison of the overlays. Nonetheless, it may be assumed that unspecific connections to underlying mosaics will result, on average, in either regular or random distribution. Specific interactions, however, may be revealed by cross-correlation procedures.

In a first run we mapped the major part of a meridian in 18 overlapping samples and applied circular density recovery procedures. Although our results showed the presence of a minimum above A-HC centers, we found that this cross-correlation method is not well suited for noncircular fields. The shape of Voronoi domains is derived from individual intercell distances and therefore may represent a better representation of DF's. Thus we designed a two-step tessellation procedure to produce such polygonal reference areas instead (Figs. 2 and 5, 6).

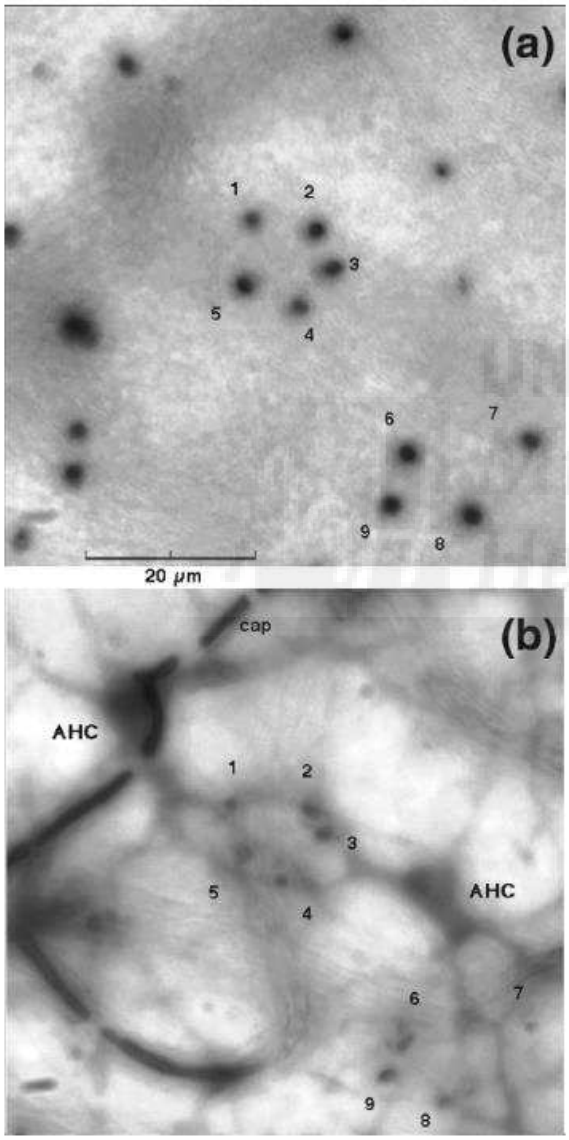

Fig. 4. Leopard retina: JH455 labeling. (a) Composite of focused portions at the level of the inner outer segment. Two clusters of S cones are numbered (1–5, 6–9). (b) Same location at the level of the outer plexiform layer. Labeled pedicles of S cones are located above overlapping dendrites from two HC's (AHC's). A third HC is located beyond the lower right-hand corner. Peroxidase reaction also labels erythrocytes in two capillaries (cap).

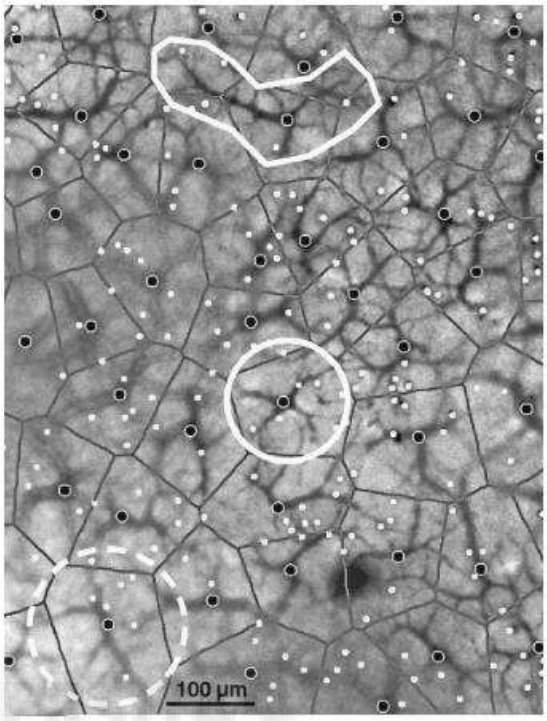

Fig. 5. Lynx retina: circular domains versus Voronoi domains. Comparison of actual A-HC branching with overlays, indicating that only in some cases are circular samplings (solid white circle) adequate approximations. Voronoi domains (polygonal grid) generally provide more-adequate spatial approximations of DF's than do circles (dashed white circle). However, since the Voronoi procedure is based solely on the locations of cell bodies and does not produce concave corners, it may also fail for cells with extreme (bipolar or angular) dendritic domains (white polygon).

C. Triple-Labeling Analysis

Fluorescein isothiocyanate labeling of L-cone outer segments with JH492 reveals the population of cones [fluorescent: white spots in Fig. 6(a)], in addition to JH455–DAB-labeled S cones (black spots) and A-HC's [Fig. 6(b)]. This allows one to plot comparative cross-correlation analysis for both cone subpopulations. As is evident from the mappings [Fig. 6(c)], L-cone positions are regularly spaced. Their density does not change significantly between positions above A-HC bodies versus the bands above peripheral dendrites [Fig. 7(a)]. S cones [DAB labeled: black spots in Fig. 6(d)], however, aggregate above eccentric areas [Fig. 6(d)], resulting in significant overrepresentation in Voronoi bands [Fig. 7(b), see Table 2]. Maximum deviation (~6.5%) occurs at bandwidths of 30%, which covers ~50% of all the Voronoi areas.

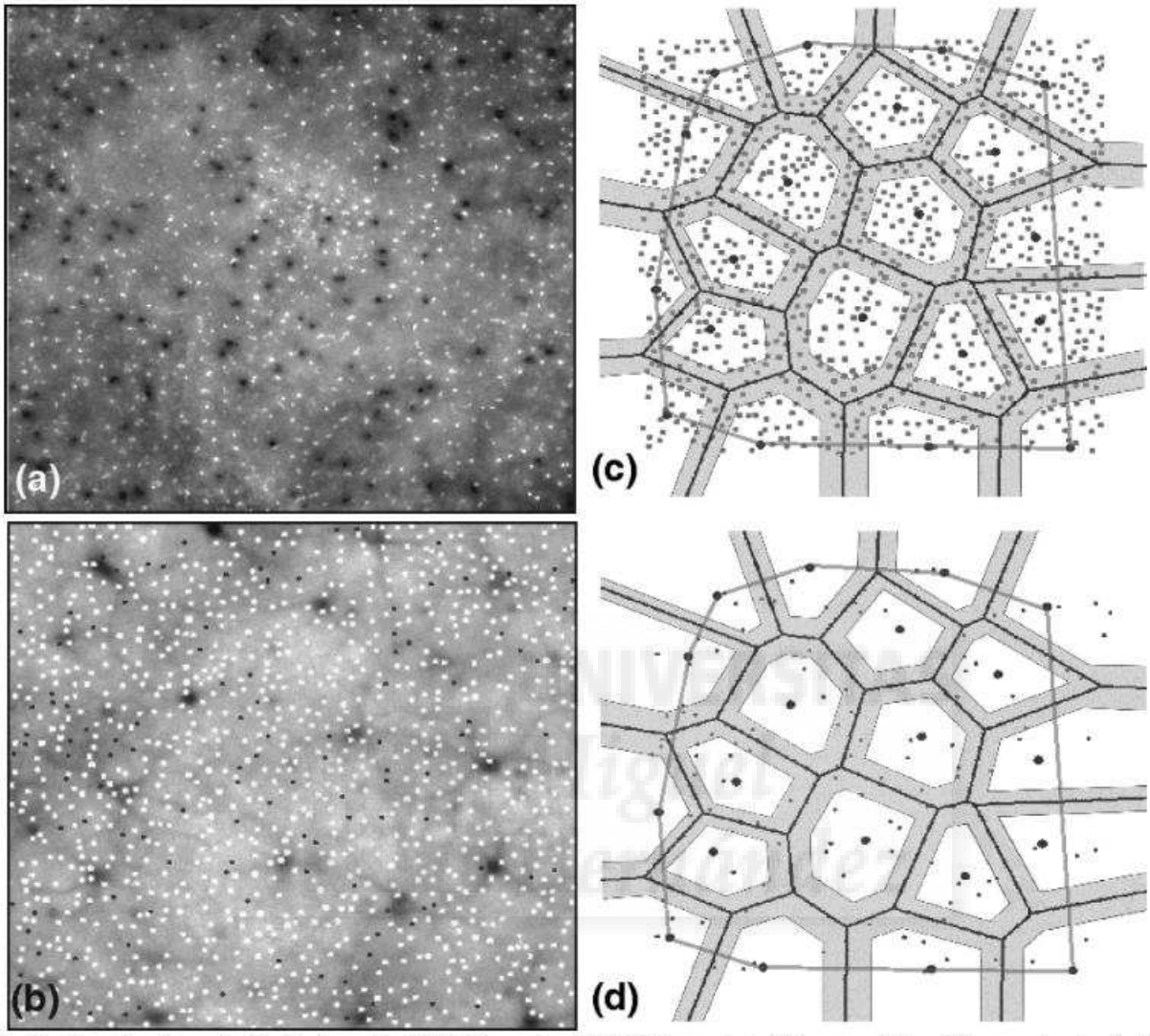

Fig. 6. Cheetah retina: double labeling with JH455 (S cones) and JH492 (L cones). (a) Minor population of S cones visualized with DAB (black spots) is interspersed between fluorescent outer segments of L cones visualized with fluorescein isothiocyanate (white spots). (b) Plane of labeled A-HC's with overlay of mapped cones. (c) Voronoi analysis of L-cone mosaic. Local L-cone density is not influenced by the underlying A-type HC organization. (d) Voronoi analysis of S-cone mosaic. S cones are preferentially located in and near the Voronoi bands. Solid lines connecting filled points in (c) and (d) demarcate measurement area (convex hull).

Table 2. Expected and Actual Percentages of L and S Cones in A-HC Voronoi Bands of Increasing Thickness[a]

Percentage of L Cones in Band			Percentage of S Cones in Band		
Bandwidth (%)	Simulation (%)	L cones	Bandwidth (%)	Simulation (%)	S cones
10	17.90 ± 1.79	18.96	10	18.15 ± 1.95	20.86
20	34.10 ± 2.16	35.67	20	34.09 ± 2.57	38.74
30	48.55 ± 2.21	50.26	30	48.60 ± 2.60	55.30
40	61.65 ± 2.01	63.13	40	61.49 ± 2.62	64.24
50	72.73 ± 2.19	73.34	50	72.49 ± 2.52	74.83

[a] See Fig. 7.

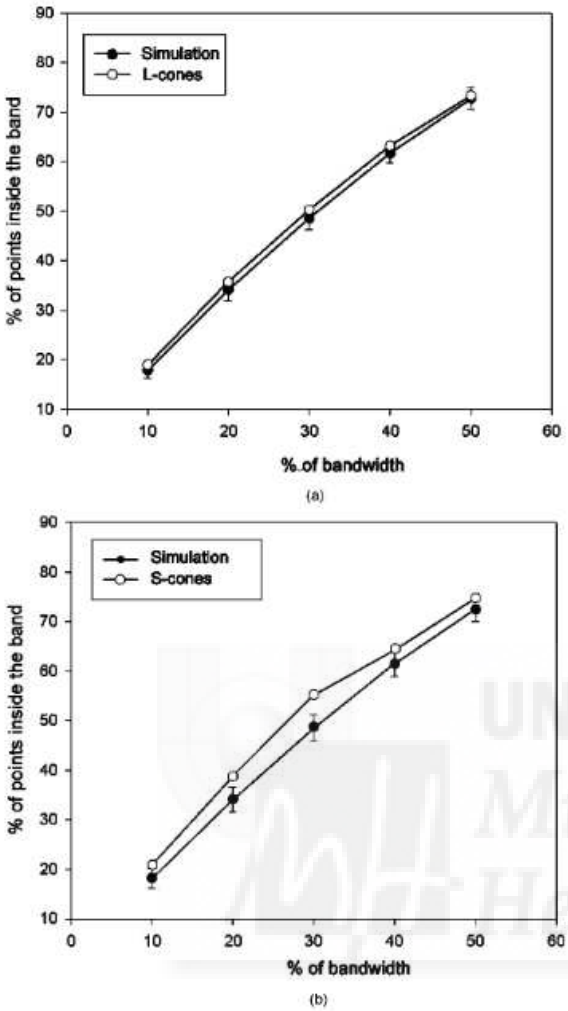

Fig. 7. Cones expected from simulation and cones actually found inside A-HC Voronoi bands from cheetah retina. (a) Plots of L cones and simulations. The filled circles show the results (mean ± SD) of 100 simulated random fields with the same number of L cones located in a study area identical to that of the real pattern. The relative proportions of L cones do not differ from those derived from the simulation at any bandwidth (10–50%). (b) Plot of S cones (open circles). Although the S-cone mosaic is close to random arrangement, it shows consistent and significant ($P > 0.01$) overrepresentation in bands including 10–50% of the Voronoi domain. Maximum deviation is at 30% bandwidth, equivalent to ~50% portions of the Voronoi areas (Table 2).

4. DISCUSSION

The findings of the present study support the view that the seemingly random mosaic of S cones is in fact biased in relation to an underlying matrix of attractors or repellers coincident with the A-HC dendrites and cell bodies.

The reason for the colabeling of A-HC's by the anti-S-opsin antibody JH455 is still unclear. Labeling did not occur in the domestic cat (two trials; see also Ref. 43) and has not yet been observed in retinas of other species. This may imply that the phenomenon is limited to a few species or that it is related to our specimen acquisition procedures, which allow, for example, for better transretinal diffusion of antibodies. It could also be that we were labeling nonphotoreceptoral opsins[44–46] or that felid HC's share some transcriptional segments with S cones, such as has recently been reported for bipolar cells in mice.[47] In any case, the double labeling of all S cones and major portions of the A-HC plexus allowed us to analyze the interaction of the two mosaics by cross correlation.

A. Regular versus Irregular S-Cone Mosaics

It seems that, among mammals, regular mosaics of S cones are present only in some species with partially or totally cone-dominant retinas such as diurnal Old World primates, Scandentia (*Tupaia*) and Sciurids. These groups are likely to have evolved independently from nocturnal or crepuscular ancestors. Thus a regular S-cone mosaic may provide a particular advantage for diurnal (arboreal) habitats. The existence and the nature of such a potential benefit remain obscure and seem dispensable for most mammals, including other primates (see Subsection 1.A above).

B. Connectivity Patterns for Irregular S-Cone Mosaics

It is important to emphasize that the methodology of the present study shows statistical correlation but does not provide direct evidence for related connectivity patterns of S-cone mosaics and of A-HC's. Detailed reconstructions of synaptic circuitry at the cone–HC interface and intracellular labeling of HC's, combined with S-cone labeling, are necessary to clarify the chromatic microtopography. Taking into consideration this important restriction, we may discuss implications rendered possible by this spatial interaction.

In primates the S-cone and the blue-bipolar mosaics appear to adapt to each other in both regular[29] and irregular[48] patterns. For equids, an A-HC connecting specifically to S cones has been described,[9] and a similar HC type seems to be present in a marsupial.[49] Both these examples suggest that, in spite of the apparent irregularity of S-cone mosaics, specific connection patterns and even cell types may exist by means of adaptive dendritic branching of interneurons.[50]

Comparing A-HC intercell distances with DF dimensions in the cat[31] and the rabbit[30] implies that each retinal location may be covered by dendrites of at least three to four A-HC's. This implies that for (S) cones no specific spatial arrangement should be necessary to establish A-HC contacts. Still, for felid retinas, the present study demonstrates partial decomposition of the cone subtypes above A-HC DF's (Figs. 1, 6, and 7). The overall increase of the percentage of S cones in the peripheral bands of A-HC Voronoi domains [Fig. 6(b) and Table 2] versus the portions around the cell bodies is significant but may not seem substantial for functional consequences. Several factors, such as specific synaptic affinity and position within the DF's, may magnify the effect, as has been shown for primate HC's.[24]

For rabbit HC's, a recent study[51] based on combining opsin antibody labeling with intracellular single-cell labeling (Procion Yellow) suggests that A-HC's connect to both L- and S-cone types. In principle, this statement does not interfere with the possibility, set forth here, of spatial segregation. Indeed, the figures presented in this

paper suggest that a similar correlation of S cones and A-HC's may prevail in the dorsal retina (in the rabbit, chromatic interactions seem regionally restricted[52] owing to the dorsoventral gradient of photopigment coexpresion). In addition, an electron microscopic reconstruction of a rabbit A-HC[53] shows connections to the majority of overlying pedicles. It was noted, however, that a few pedicles in the center of the DF were found to lack invaginating dendrites from this cell.[53] In accordance with the implications of the present study, it seems possible that those pedicles are S-cone pedicles avoided by the reconstructed cell and that they are possibly connected to overlapping peripheral dendrites of neighboring A-HC's.

C. Functional Implications

The spatial anticlustering of S cones above A-HC's may have consequences for postreceptoral pathways, provided that there are related connectivity patterns. In this case the periphery of A-HC dendrites and associated bipolars would receive mixed input from both S and L cones, whereas around the soma primary dendrites and bipolars may connect mainly to L cones. The resolution of this chromatic landscape may be coarse but could suffice for the requirements of S-cone-related channels (lower spatial and temporal resolution). Whether this will actually lead to local inhomogeneities with respect to spatial grain and sensitivity will depend on the quality of the image itself and on the actual preservation or integration of positional information in the subsequent pathways.

D. Developmental Aspects

The ontogenetic events leading to such correlated mosaic patterns are still not clear. In primates[54] and rats[55] a set of cones—possibly with S-opsin expression—may precede further differentiation. Should relatively fixed S-cone positions be implemented first, establishing connectivity sites would require increased flexibility from elements in the underlying mosaics, such as blue bipolars.[13,29]

Also, S-opsin expression in a first set of cones might be influenced by establishment of primary connections with dendrites of postmitotic HC's. After further growth of the dendrites, as well as of the overall retina, these positions might end up being displaced from the HC body, while other cones might follow a default (green) course of expression or might be transdifferentiated.[55]

Such interaction could be driven by spatially restricted inhibitory factors in A-HC's during differentiation. In this sense, it is notable that different isoforms of glutamic acid decarboxylase (GAD), the enzyme that synthesizes γ-aminubutyric acid, have spatially distinct expression in rabbit HC's.[56] GAD67 is expressed throughout the A-HC's and short-axon HC's, while GAD65 is restricted to A-HC somata and primary dendrites.

5. CONCLUSION

We have examined examples of the seemingly random organization of S cones that appears to be prevalent in most mammals. In the retinas of three felid species additional labeling of axonless horizontal cells (A-CH's) has enabled us to test whether the arrangement of these cells exerts a positional influence on the cone submosaics.

By the introduction of concentric Voronoi domains derived from A-HC nuclei positions as locally adaptive elements for cross correlation, a concentrical gradient was revealed above A-HC dendritic fields for S but not for L cones. Detailed structural, developmental, and physiological analyses are necessary to clarify whether this spatial correlation also manifests itself in complementary patterns of chromatic connectivity. At present, a gap between knowledge and synthetic concepts exists, particularly for the retinal mosaics of mammals other than primates. Discovering further details of the cone–HC interfaces in these and other species will help us to achieve a more unified view of mammalian photoreceptor circuitry.

ACKNOWLEDGMENTS

Part of this work was supported by a bilateral travel grant from Austria and Spain. The authors are grateful to J. Nathans for providing the antibodies and to N. Kouyama for supplying information on the density recovery profile procedure. C. Schubert provided expert technical assistance with specimen preparation and data acquisition.

P. Ahnelt can be reached by e-mail at peter.ahnelt@univie.ac.at.

REFERENCES

1. A. Hughes, "The topography of vision in mammals of contrasting life style: comparative optics and retinal organization," in *Visual System of Vertebrates*, F. Crescitelli, ed. (Springer, Berlin, 1972), Vol. 7, pp. 613–756.
2. A. Szél, T. Diamantstein, and P. Röhlich, "Identification of the blue-sensitive cones in the mammalian retina by anti-visual pigment antibody," J. Comp. Neurol. **273**, 593–602 (1988).
3. P. K. Ahnelt, H. Kolb, and R. Pflug, "Identification of a subtype of cone photoreceptor, likely to be blue sensitive, in the human retina," J. Comp. Neurol. **255**, 18–34 (1987).
4. F. M. de Monasterio, S. J. Schein, and E. P. McCrane, "Staining of blue-sensitive cones of the macaque retina by a fluorescent dye," Science **213**, 1278–1281 (1981).
5. C. A. Curcio, K. A. Allen, K. R. Sloan, C. L. Lerea, J. B. Hurley, I. B. Klock, and A. H. Milam, "Distribution and morphology of human cone photoreceptors stained with anti-blue opsin," J. Comp. Neurol. **312**, 610–624 (1991).
6. D. R. Williams, "Seeing through the photoreceptor mosaic," Trends Neurosci. **9**, 193–198 (1986).
7. D. R. Williams and R. Collier, "Consequences of spatial sampling by a human photoreceptor mosaic," Science **221**, 385–387 (1983).
8. P. K. Ahnelt, J. N. Hokoç, and P. Röhlich, "Photoreceptors in a primitive mammal, the South American opossum, *Didelphis marsupialis aurita*: characterization with anti-opsin immunolabeling," Visual Neurosci. **12**, 793–804 (1995).
9. D. Sandmann, B. B. Boycott, and L. Peichl, "Blue-cone horizontal cells in the retinae of horses and other equidae," J. Neurosci. **16**, 3381–3396 (1996).
10. A. Szél, P. Röhlich, A. R. Caffe, B. Juliusson, G. Aguirre, and T. van Veen, "Unique topographic separation of two spectral classes of cones in the mouse retina," J. Comp. Neurol. **325**, 327–342 (1992).
11. A. Szél and P. Röhlich, "Two cone types in rat retina detected by anti-visual pigment antibodies," Exp. Eye Res. **55**, 47–52 (1992).
12. A. Hendrickson, H. Djajad, and D. Sajuthi, "The nocturnal

simian *Tarsius* has short wavelength cones in an unusual topography," Invest. Ophthalmol. Visual Sci. Suppl. **40**, 238 (1999).
13. P. M. Martin and U. Grünert, "Analysis of the short wavelength-sensitive ('blue') cone mosaic in the primate retina: comparison of New World and Old World monkeys," J. Comp. Neurol. **406**, 1–14 (1999).
14. M. B. Shapiro, S. J. Schein, and F. M. de Monasterio, "Regularity and structure of the spatial pattern of blue cones of macaque retina," J. Am. Stat. Assoc. **80**, 803–812 (1985).
15. C. A. Curcio and K. R. Sloan, "Packing geometry of human cone photoreceptors: variation with eccentricity and evidence for local anisotropy," Visual Neurosci. **9**, 169–180 (1992).
16. K. O. Long and S. K. Fisher, "The distributions of photoreceptors and ganglion cells in the California ground squirrel, *Spermophilus beecheyi*," J. Comp. Neurol. **221**, 329–340 (1983).
17. P. K. Ahnelt, "Characterization of the color related receptor mosaic in the ground squirrel retina," Vision Res. **25**, 1557–1567 (1985).
18. B. Müller and L. Peichl, "Topography of cones and rods in the tree shrew retina," J. Comp. Neurol. **282**, 581–594 (1989).
19. A. Gallego, "Horizontal cells of the Tetrapoda retina," Prog. Clin. Biol. Res. **113**, 9–29 (1982).
20. L. Peichl, D. Sandmann, and B. B. Boycott, "Comparative anatomy and function of mammalian horizontal cells," in *Development and Organization of the Retina*, L. M. Chalupa and B. L. Finlay, eds. (Plenum, New York, 1998).
21. B. B. Boycott and H. Kolb, "The horizontal cells of the rhesus monkey retina," J. Comp. Neurol. **148**, 115–139 (1973).
22. H. Kolb, A. Mariani, and A. Gallego, "A second type of horizontal cell in the monkey retina," J. Comp. Neurol. **189**, 31–44 (1980).
23. P. K. Ahnelt and H. Kolb, "Horizontal cells and cone photoreceptors in primate retina: a Golgi-light microscopic study of spectral connectivity," J. Comp. Neurol. **343**, 387–405 (1994).
24. P. K. Ahnelt and H. Kolb, "Horizontal cells and cone photoreceptors in human retina: a Golgi-electron microscopic study of spectral connectivity," J. Comp. Neurol. **343**, 406–427 (1994).
25. D. M. Dacey, B. B. Lee, D. K. Stafford, J. Pokorny, and V. C. Smith, "Horizontal cells of the primate retina: cone specificity without spectral opponency," Science **271**, 656–659 (1996).
26. T. L. Chan and U. Grünert, "Horizontal cell connections with short wavelength sensitive cones in the retina: a comparison between New World and Old World primates," J. Comp. Neurol. **393**, 196–209 (1998).
27. R. W. Rodieck, "The density recovery profile: a method for the analysis of points in the plane applicable to retinal studies," Visual Neurosci. **6**, 95–111 (1991).
28. R. W. Rodieck and D. W. Marshak, "Spatial density and distribution of choline acetyltransferase immunoreactive cells in human, macaque, and baboon retinas," J. Comp. Neurol. **321**, 46–64 (1992).
29. N. Kouyama and D. W. Marshak, "The topographical relationship between two neuronal mosaics in the short wavelength-sensitive system of the primate retina," Visual Neurosci. **14**, 159–167 (1997).
30. S. L. Mills and S. C. Massey, "Distribution and coverage of A- and B-type horizontal cells stained with neurobiotin in the rabbit retina," Visual Neurosci. **11**, 549–560 (1994).
31. H. Wässle, L. Peichl, and B. B. Boycott, "Topography of horizontal cells in the retina of the domestic cat," Proc. R. Soc. London Ser. B. **203**, 269–291 (1978).
32. E. Fernández, N. Cuenca, and J. De Juan, "A compiled BASIC program for analysis of spatial point patterns, application to retinal studies," J. Neurosci. Methods **50**, 1–15 (1993).
33. H. Wässle and H. J. Riemann, "The mosaic of nerve cells in the mammalian retina," Proc. R. Soc. London Ser. B **200**, 441–461 (1978).
34. J. Cook, "Getting to grips with neuronal diversity," in *Development and Organization of the Retina*, L. M. Chalupa and B. L. Finlay, eds. (Plenum, New York, 1998), pp. 91–120.
35. J. E. Cook, "Spatial properties of retinal mosaics: an empirical evaluation of some existing measures," Visual Neurosci. **13**, 15–30 (1996).
36. P. J. Green and R. Sibson, "Computing Dirichlet tessellations in the plane," Comput. J. (Cambridge) **21**, 68–173 (1978).
37. P. J. Diggle, *Statistical Analysis of Spatial Point Patterns* (Academic, New York, 1983).
38. L. Galli-Resta, E. Novelli, Z. Kryger, G. H. Jacobs, and B. E. Reese, "Modelling the mosaic organization of rod and cone photoreceptors with a minimal spacing rule," Eur. J. Neurosci. **11**, 1461–1469 (1999).
39. Requests for this program may be sent to O. Martinez at the address given on the title page.
40. B. N. Boots and A. Getis, *Point Pattern Analysis* (Sage, Beverly Hills, Calif., 1988).
41. P. J. Clark and F. C. Evans, "Distance to nearest neighbor as a measure of spatial relationship in populations," Ecology **34**, 445–453 (1954).
42. H. Wässle, B. B. Boycott, and L. Peichl, "Receptor contacts of horizontal cells in the retina of the domestic cat," Proc. R. Soc. London Ser. B **203**, 247–267 (1978).
43. L. Peichl, Max-Planck-Institut für Hirnforschung, 60528 Frankfurt a.M., Germany (personal communication, 1999).
44. B. G. Soni and R. G. Foster, "A novel and ancient vertebrate opsin," FEBS Lett. **406**, 279–283 (1998).
45. H. Sun, D. J. Gilbert, N. G. Copeland, N. A. Jenkins, and J. Nathans, "Peropsin, a novel visual pigment-like protein located in the apical microvilli of the retinal pigment epithelium," Proc. Natl. Acad. Sci. USA **94**, 9893–9898 (1997).
46. I. Provencio, G. Jiang, W. J. De Grip, W. P. Hayes, and M. D. Rollag, "Melanopsin: an opsin in melanophores, brain, and eye," Proc. Natl. Acad. Sci. USA **95**, 340–345 (1998).
47. M. I. Chiu and J. Nathans, "A sequence upstream of the mouse blue visual pigment gene directs blue cone-specific transgene expression in mouse retinas," Visual Neurosci. **11**, 773–780 (1994).
48. X. Luo, K. K. Gosh, P. R. Martin, and U. Grünert, "Analysis of two types of cone bipolar cells in the retina of a New World monkey, the marmoset, *Callithrix jacchus*," Visual Neurosci. **16**, 707–719 (1999).
49. S. J. N. Hokoç, M. Medeiros De Oliveira, and P. K. Ahnelt, "Three types of horizontal cells in a primitive mammal, the opossum (*Didelphis marsupialis aurita*)," Invest. Ophthalmol. Visual Sci. Suppl. **34**, 1152 (1993).
50. E. V. Famiglietti, Jr., "Functional architecture of cone bipolar cells in mammalian retina," Vision Res. **21**, 1559–1563 (1981).
51. I. Hack and L. Peichl, "Horizontal cells of the rabbit retina are non-selectively connected to the cones," Eur. J. Neurosci. **11**, 2261–2274 (1999).
52. R. Pflug and H. Reitsamer, "Topographic variation of cone–cone interaction in spectral sensitivities determined from small field ERGs of rabbit retina," Invest. Ophthalmol. Visual Sci. Suppl. **40**, 238 (1999).
53. E. Raviola and R. F. Dacheux, "Axonless horizontal cells of the rabbit retina: synaptic connections and origin of the rod aftereffect," J. Neurocytol. **19**, 731–736 (1990).
54. K. C. Wikler and P. Rakic, "An array of early-differentiating cones precedes the emergence of the photoreceptor mosaic in the fetal retina," Proc. Natl. Acad. Sci. USA **91**, 6534–6538 (1994).
55. A. Szél, B. Vigh, T. van Veen, and P. Röhlich, "Development of cone distribution patterns in mammals," in *Development and Organization of the Retina*, L. M. Chalupa and B. L. Finlay, eds. (Plenum, New York, 1998), pp. 43–59.
56. M. A. Johnson and N. Vardi, "Regional differences in GABA and GAD immunoreactivity in rabbit horizontal cells," Visual Neurosci. **15**, 743–753 (1998).

UNIVERSITAS
Miguel
Hernández

Neurocomputing 74 (2010) 418–427

Contents lists available at ScienceDirect

Neurocomputing

journal homepage: www.elsevier.com/locate/neucom

V-Proportion: A method based on the Voronoi diagram to study spatial relations in neuronal mosaics of the retina

Oscar Martinez Mozos [a,*], Jose A. Bolea [b], Jose M. Ferrandez [c], Peter K. Ahnelt [d], Eduardo Fernandez [b]

[a] Department of Computer Science and System Engineering (DIIS), University of Zaragoza, Edificio Ada Byron, C/Maria de Luna, 1, 50018 Zaragoza, Spain
[b] Bioengineering Institute, Miguel Hernandez University, Spain
[c] Department of Electronics and Computer Technology, Technical University of Cartagena, Spain
[d] Department of Physiology, Medical University of Vienna, Austria

ARTICLE INFO

Article history:
Received 4 March 2010
Received in revised form
2 July 2010
Accepted 24 July 2010
Communicated by J.-M. Ferrández
Available online 16 October 2010

Keywords:
Voronoi diagram
Spatial relations
Neuronal mosaics
Retina

ABSTRACT

The visual system plays a predominant role in the human perception. Although all components of the eye are important to perceive visual information, the retina is a fundamental part of the visual system. In this work we study the spatial relations between neuronal mosaics in the retina. These relations have shown its importance to investigate possible constraints or connectivities between different spatially colocalized populations of neurons, and to explain how visual information spreads along the layers before being sent to the brain. We introduce the V-Proportion, a method based on the Voronoi diagram to study possible spatial interactions between two neuronal mosaics. Results in simulations as well as in real data demonstrate the effectiveness of this method to detect spatial relations between neurons in different layers.

1. Introduction

In the last decades, the development of technological advances has been largely inspired by nature and specially by biological systems. This is even more relevant in the fields of artificial intelligence and cognition, where computer scientists are often looking for models that mimic the characteristics of perception and information processing performed by the human brain and by the different sensory systems attached to it.

One of the most important sensory systems in humans is the visual system. In the human brain, 30% of the sensory neurons belong to this system [1]. This fact corroborates the predominant role of the visual sense in the human perception. Although all components of the eye are important to perceive visual information, the retina is a fundamental part of the visual system. The retina is basically a piece of brain tissue that gets direct stimulations from the outside world's lights and images [2]. A relatively easy access to the retina, together with the possibility of studying the information processing in an intact portion of the nervous system make this part of the eye a unique model to study the nervous system in general [3] and the visual system in particular [4].

There exist several attempts to develop bio-inspired artificial retinas with the purpose of replacing or partially recovering damaged functionalities in perception [5,6]. Moreover, retinal-inspired models have been used to improve the vision system in robots [7,8]. However, the complete information process inside the retina is not fully understood yet. A central challenge is therefore to understand how the retina is designed to solve the image processing task.

The retina is organized into layers formed by many local neuronal circuits which work in parallel with each other to asses the different aspects of an image. In each layer, neurons of the same type are spatially distributed into regular or irregular patterns known as *retinal mosaics*. The neurons often have dendrites that extend in a competitive manner reducing the overlap of their dendritic fields and resulting in a tessellation across the retina [9,10]. As a result, an assembly of efficiently connected functional circuits between the mosaics of different neuronal subtypes is created. The study of the spatial relations between these mosaics is highly relevant to understand how the visual information spreads along the different layers, and how it is finally processed before being sent to the brain.

The study of the spatial relations between neural populations has also shown its importance to investigate possible constrains or

* Corresponding author. Tel.: +34 97 676 2472; fax: +34 976 761 914.
E-mail addresses: omozos@gmail.com, ommozos@unizar.es (O. Martinez Mozos), joseangel.bolea@educa.madrid.org (J.A. Bolea), jm.ferrandez@upct.es (J.M. Ferrandez), peter.ahnelt@univie.ac.at (P.K. Ahnelt), e.fernandez@umh.es (E. Fernandez).

0925-2312/$ - see front matter © 2010 Elsevier B.V. All rights reserved.
doi:10.1016/j.neucom.2010.07.020

connectivities between different cell types. A positive spatial dependency between two different populations of neurons may be an indicator of some connection patterns between them [11–14]. The spatial information is moreover helpful to study dependencies during development [15].

This paper introduces a method to study spatial relations between two neuronal mosaics in the retina. The key idea of this work is to calculate the Voronoi diagram in one of the populations, and then study the distribution of neurons from the second population inside the polygons of the diagram. Using polygonal areas around neuronal cells is a realistic approximation, since neurons present different irregularities in their structure [16].

The remaining part of the paper is organized as follows. After introducing some related work in Section 2, we describe the Voronoi diagram in Section 3. The V-Proportion measurement is presented in Section 4. We validate this method with simulated populations in Section 5. Several real neuronal mosaics from the retina are analyzed in Section 6. Finally, we conclude in Section 7.

2. Related work

Different methods to study spatial relations between two cell populations have been proposed in the past. An extension of the density recovery profile (DRP) [17] for two populations is used in the work by Kouyama and Marshak [18] to study interdependences between two types of S-cone cells. This extension is called cross-correlational density recovery profile (cDRP). Opposite to the conventional DRP, which is based on autocorrelations of the same population, the cDRP uses one of the populations as reference and calculates the correlation of the second population.

The different DRP methods are based on circular domains around the reference cells. In contrast to this technique, the V-Proportion measurement is based on polygonal domains around the cells, which generally provide more adequate spatial approximations of dendritic fields than circles [14]. However, since our Voronoi procedure is based solely on the locations of cell bodies and does not produce concave corners, it may also fail for cells with extreme dendritic domains.

Another measurement used to study spatial dependencies is the K-function [19], which uses second order analysis of stationary point processes. The K-function is used by Diggle [20] to analyze the spatial relation between on- and off-cells in the retina. A multivariate counterpart of the J-function [21] is introduced by Lieshout and Baddeley [22] to study possible interdependences between two population of points. The authors applied this metric to study spatial dependencies of beta cells in the cat retina [22].

K-nearest neighbor histograms have been also applied to study possible spatial correlations between neuronal mosaics. For example, Wässle et al. [23] apply this method to study Beta cells in the cat retina.

In the work by Diggle et al. [24], the authors use Monte Carlo methods for conducting likelihood-based analysis of point process models in neuronal data. In particular, they fit a bivariate pairwise interaction model in point data corresponding to retinal amacrine cells.

In the previous methods, only the coordinates of the center of the cells are used. Our V-Proportion method, however, applies a domain around the reference cells to study possible spatial relations between the different populations. This domains adapt better to the dendritic fields of neurons.

Finally, Ahnelt et al. [14] apply a first version of the V-Proportion to analyze interactions between irregular S-cone mosaics and axonless horizontal cells. In comparison to [14], this paper presents several improvements. First, we solve the edge problem by ignoring points lying on open Voronoi polygons. This approximation reduces the number of points used in the statistics, however, it increases the confidence of the final results. Second, in this paper we introduce a method to determine the level of spatial correlation between two populations. In addition, we apply the V-Proportion to real populations whose possible spatial correlations have not been studied before.

3. The Voronoi diagram

The Voronoi diagram is one of the most useful geometrical constructions to study point patterns, since it provides all the information needed to study proximity relations between points [25].

A Voronoi diagram can be defined as follows. Let $S=\{s_1,s_2,\ldots,s_n\}$ be a limited set of points in the two-dimensional Euclidean plane. These points are also called *Voronoi sites*. Now each site s_i is assigned the rest of points in the plane $p\notin S$ which are nearest to it

$$V(s_i)=\{p|d(p,s_i)\leq d(p,s_j);\ p\notin S,\ \forall s_j\neq s_i\}, \quad (1)$$

with $d(.,.)$ representing the Euclidean distance function.

This process creates a tessellation of the plane into (sometimes unbounded) convex polytopes, also called *Voronoi polygons*. Let $V(s_i)$ be the Voronoi polygon corresponding to the site s_i, then all the points inside this polygon are at least as close to s_i as to any other site s_j.

The edges of the Voronoi polygons form the Voronoi diagram $V(S)$ of the sites S. Note that a point lying on one edge of the Voronoi diagram has two nearest neighbors sites, and each vertex has at least three. An example of a Voronoi diagram is shown in Fig. 1.

4. The V-Proportion measurement

The main idea of this work is to study spatial interdependences between two neuronal populations. Each neuron is represented by a point in the two-dimensional Euclidean plane. Usually these points correspond to the cell bodies of the neurons.

Our method consists of two main steps. In the first one, we select a population as the set of sites from which we calculate the Voronoi diagram. This diagram is extended with a set of bands around the edges of the Voronoi polygons. In the second step, the remaining population is superimposed on the Voronoi diagram and a set of

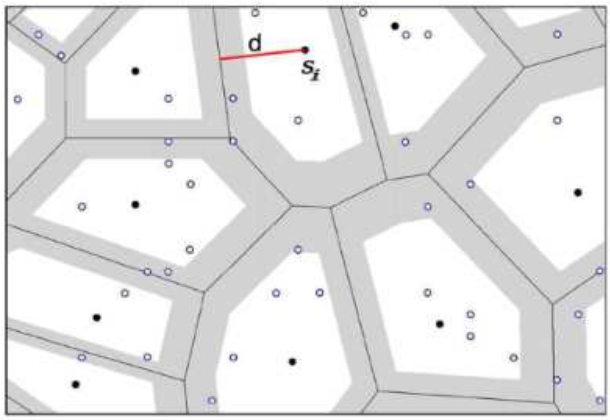

Fig. 1. Part of a Voronoi diagram (black lines) for a set of sites (filled circles). Bands around the edges of the Voronoi diagram are shown in grey. In this particular case $\delta=0.29$, indicating the 29% of the distance d between a Voronoi edge and its closest site s_i. The P population is shown in open circles.

statistics are calculated, which represent the spatial relations between both populations.

First, the Voronoi diagram of the sites S is calculated using the criterion in (1). After obtaining the Voronoi diagram we establish a set of bands around the edges of the resulting Voronoi polygons. These bands are shown as grey areas in Fig. 1. The width of each band is not fixed but is proportional to the distance between a given edge and its closest site. This proportion is represented by the parameter δ with $0 < \delta < 1$. We then superimpose the set of points P, which corresponds to the second population of cells, on the extended Voronoi diagram containing the bands.

The basic idea behind this configuration is the following. If both populations S and P are spatially independent, then the occurrence of a site point should not alter the probability of the occurrence of P points, and the average density of P points should be the same inside and outside the bands. However, it could happen that P points show either a positive or negative spatial correlation with the sites. If the sites inhibit the P points, then the latter will appear near the edges of the Voronoi diagram, and the number of P points inside the bands will be significantly higher than expected. On the contrary, when the number of P points inside the band is decreased, it will mean that the sites are positively correlated to them.

Using the previous concepts, we define the V-Proportion value as the relation between the number of points inside the bands and the total number of points

$$\mathrm{V-Proportion} = \frac{|P_B|}{|P|}, \tag{2}$$

with the set $P_B \subseteq P$ defined as

$$P_B = \{p_j \in P | d(p_j, e_j) \leq \delta \cdot d(s_i, e_j), \text{ if } p_j \in V(s_i)\}, \tag{3}$$

where e_j is the nearest $V(s_i)$ edge to the point p_j. The set P_B thus represents the subset of P points lying inside the bands of the extended Voronoi diagram. The V-Proportion value varies depending on the width of the bands, which is indicated by the parameter δ.

The interpretation of the V-Proportion measurement is as follows. If the V-Proportion is higher than expected, that would suggest a negative correlation between S and P. On the contrary, if the measured V-Proportion is smaller than expected, that would indicate a positive correlation.

An example of this process is shown in Fig. 1. This figure shows two populations of points representing two different types of cells. Each cell is represented by the 2D coordinates of its center. The point population depicted in filled circles is used as sites for the Voronoi diagram. The resulting edges of the Voronoi diagram are shown in black lines. Following the previous approach, the edges were extended with bands whose sizes are dependent on the distance of each edge in the direction to its closest site (grey bands). In this particular case $\delta = 0.29$, indicating that the band width is 29% of the distance d to its closest site s_i. In a next step, the second point population P (marked as open circles) was superimposed to the obtained geometrical construction.

To test the significance of the V-Proportion, we use a Monte Carlo test procedure. This involves generating a set of two random and independent patterns, each with the same number of points as the two empirical populations S and P, and in a study area identical to that of these patterns. We repeat the generation T times for different values of δ, and then the mean and the standard deviation of each simulated V-Proportion are calculated. The resulting plot is compared with the V-Proportion obtained with the two real S and P populations. Whenever the real V-Proportion raises above the random equivalent simulation, then we can assume a negative interaction between populations, that is, S inhibits P. If the real V-Proportion is below the simulated one, then a clustering process occurs in which S points attract P points. If the real V-Proportion is close to the simulated one, we cannot assume any significant spatial interaction between the two populations.

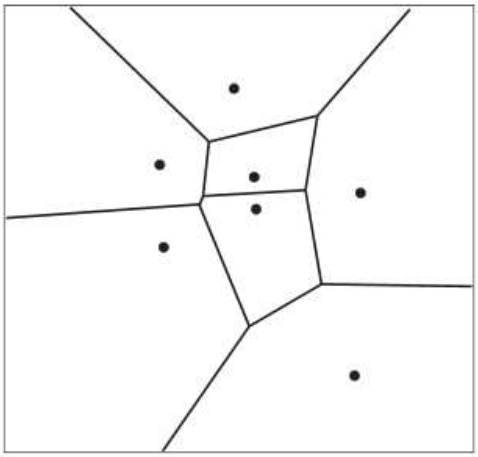

Fig. 2. Voronoi diagram (black lines) for a set of sites (filled circles). The polygons close to the borders of the sampling window remain open since there are no neighboring points in those directions.

Finally, an important problem when working with point populations is the edge effect. Typically, the observation of the two point patterns is restricted to a regular sampling window, while usually the patterns extend beyond it. Furthermore, the Voronoi polygons on the boundary of the window are open because they have no neighboring points in those directions as shown in Fig. 2. This edge effect affects the sense of bands in the Voronoi polygons adjacent to the edges. In our case, we solve this problem by removing the Voronoi polygons intersecting the edges of the sampling area (open polygons). Similar approaches have been applied in other works for studying cell mosaics [26,27]. Although this heuristic reduces the total number of points used for the study, we think the results represent the spatial relations in a more reliable manner.

5. Validation of the V-Proportion measurement

In this section we present a validation of the proposed V-Proportion measurement. We analyze several pairs of simulated populations following different spatial relations. In particular, we simulate pairs of populations showing a positive correlation, a negative correlation, and neither positive nor negative correlation. We then calculate the V-Proportion for each of the simulated pair of populations. The results indicate that we can clearly detect the three previous behaviors using the V-Proportion measurement. We finally present some guidelines to determine the level of positive/negative correlation using the V-Proportion plot.

5.1. Detection of a positive correlation

The first behavior we want to detect is a positive correlation between two point populations. A positive correlation means that the points in one population tend to form clusters around the points of the other population. To simulate this behavior we apply the Poisson cluster process introduced in [28,29]. We first generate the site points following a bi-dimensional Poisson process. For each site, a set of offspring points is generated (P population). The positions of the offspring points relative to their corresponding sites are independent and identically distributed according to a bi-dimensional normal distribution. More details on the implementation can be found in [30].

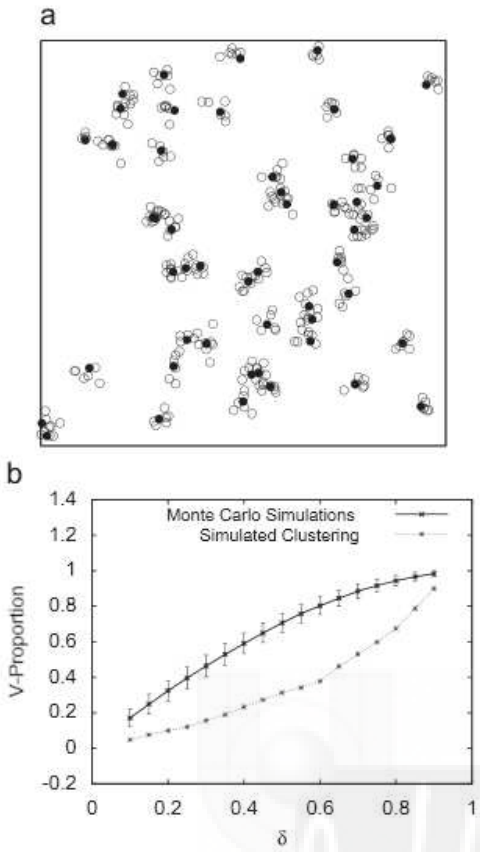

Fig. 3. (a) A Poisson cluster with $\sigma^2 = 25$ in pixel units. The area of the original image is 300 × 300 pixels. Sites are shown as filled circles, whereas *P* points are depicted as open circles. (b) Plot of the V-Proportion with error bars drawn at the 95% confidence interval. The clustering is clearly detected by the V-Proportion.

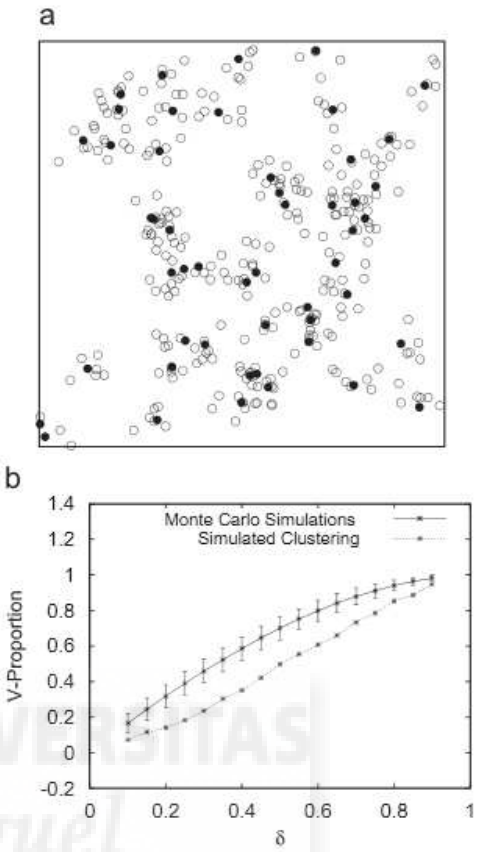

Fig. 4. (a) A Poisson cluster with $\sigma^2 = 100$ in pixel units. The area of the original image is 300 × 300 pixels. Sites are shown as filled circles, whereas *P* points are depicted as open circles. (b) Plot of the V-Proportion with error bars drawn at the 95% confidence interval. The clustering is detected within a confidence interval of 95%.

Different pairs of populations were generated following this approach. All pairs contained the same number of sites and *P* points: 50 and 300, respectively. The populations were contained in an image area of 300 × 300 pixels. For each pair of populations, a different variance σ^2 was used for the bi-dimensional normal distribution of the offspring points. Example simulations together with their corresponding V-Proportion plots are shown in Figs. 3 and 4. The clusters in Fig. 3(a) were simulated with a variance of $\sigma^2 = 25$ (in pixel units). In this case the clustering was detected within a confidence interval of 95% (Fig. 3(b)). The clusters in Fig. 4(a) have a variance of $\sigma^2 = 100$. This clustering was still detected within a confidence interval of 95% using the V-Proportion measurement (Fig. 4(b)).

5.2. Detection of a negative correlation

The second behavior we want to detect is a negative correlation between two point populations. A negative correlation means that points from one population tend to be far away from the points in the other population. A way to simulate this kind of behavior consists of generating offspring points that cannot be closer to any site point less than a certain distance. To generate pairs of populations with negative correlations we followed the method presented in [31]. This approach generates a site population in which the sites are separated each other by a certain distance. A second population is generated whose points are not allowed to be closer to a site point by a distance smaller than a certain threshold. Fig. 5(a) presents a pair of populations following the previous criteria. In this case the sites (filled circles) have a minimum distance of 60–80 pixels between them. The *P* points (open circles) are generated with a minimum distance of 70–80 pixels to the closest site. The V-Proportion plot in Fig. 5(b) clearly indicates a negative correlation between both populations within the 95% confidence interval.

5.3. Lack of spatial correlation

The third behavior we are interested in is the lack of spatial correlation between two populations. In our case this means that the populations does not present neither positive nor negative correlation. To simulate this behavior we randomly generate two populations in a certain area, each population following a bi-dimensional Poisson distribution. Example of such simulation can be shown in Fig. 6(a). In this case we generated 50 sites and 300 *P* points in an image area of 300 × 300 pixels. The resulting V-Proportion plot is presented in Fig. 6(b). The real V-Proportion maintains inside the confidence interval of the Monte Carlo simulated populations which indicates no spatial correlation at all.

5.4. Determining the level of correlation

As shown in the previous experiments, the V-Proportion is able to detect positive or negative correlations using different confidence

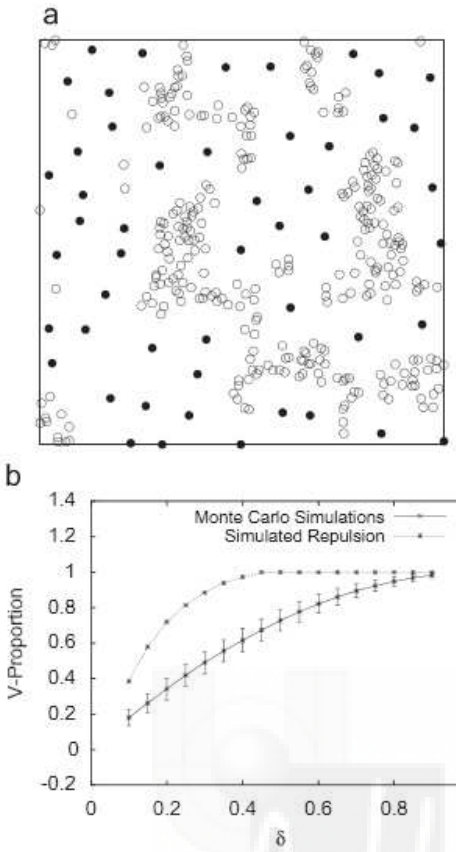

Fig. 5. (a) The image shows two populations with a negative correlation. Sites are shown in filled circles while P points are depicted as open circles. (b) The V-Proportion plot suggests a negative correlation. Error bars are drawn at the 95% confidence interval.

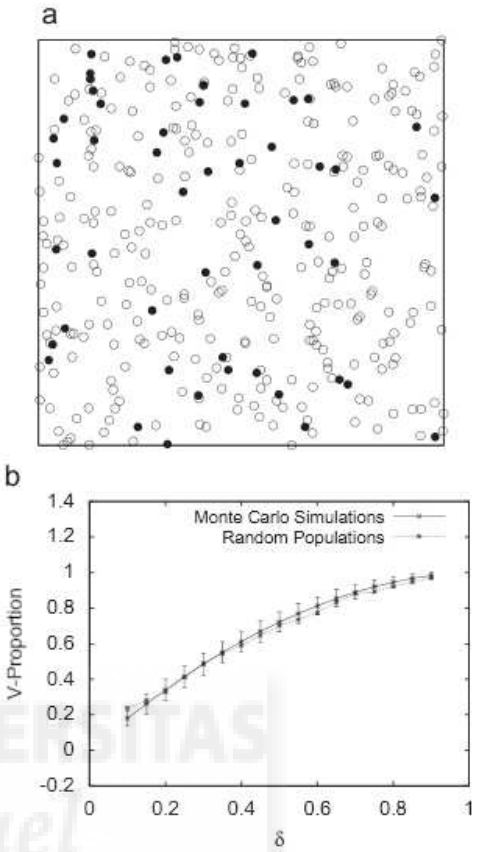

Fig. 6. (a) The image shows two random populations. Sites are shown in filled circles while P points are depicted as open circles. (b) According to the V-Proportion plot there is no evidence of a positive or negative correlation. Error bars are drawn at the 95% confidence interval.

intervals. Once the level of confidence is set, the V-Proportion of the population to be analyzed is compared with the simulated data. We can interpret the resulting plot is as follows. Whenever the V-Proportion of the analyzed population lies above (or below) the confidence intervals of the simulated population for any band width δ, we can assume a negative (or positive) correlation.

A way to measure the level of correlation is to calculate the area between the V-Proportion curves of the real patterns and the random simulations. Bigger areas would imply higher levels of correlation. An example is shown in the plot of Fig. 7(a). This plot corresponds to the negative correlation example of Fig. 5. The area between the real V-Proportion and the simulated one is depicted in grey color. Alternatively, it could be interesting to concentrate on some specific band width subinterval (Fig. 7(b)).

Using this method we can find the band width subinterval, which is directly related to the subinterval of distances to the central body of the neurons, that gives the best significance for the probability of containing the major part of the second population in the mosaic.

6. Experiments with real populations

In this section we analyze different pairs of neuronal mosaics in the retina of the eye. The objective is to extract possible spatial relations between them, and to explain their biological implications.

The procedure for obtaining the point patterns used in Sections 6.1, 6.2 and 6.3 are explained in their respective works [23,32,33]. For this paper we have used the point patterns supplied by the authors.

In the case of the data points of Section 6.4, we manually identified and demarcated the positions of cells on transparent planes from appropriately labeled micrographs or focus planes of overlying retinal layers. This process was carried out using the image processing software ImageJ or Photoshop. The 2d-coordinates of the points in the resulting calibrated mosaics were identified using the ImageJ software. All point patterns can be downloaded from [34].

When calculating the confidence intervals for the Monte Carlo simulations we chose a value of 95% since this is a standard value used in the literature. This value is, however, a free parameter that the user can determine depending on the specific situation in which the experiments are carried out.

Finally, the V-Proportion is based on statistical approximations and its results should be interpreted as the *likelihood* of the existence of a spatial correlation within a certain confidence interval.

6.1. On- and off-beta cells in the cat retina

We first study the spatial relations between beta ganglion cells in the retina of a cat (Fig. 8). Beta cells are associated with the

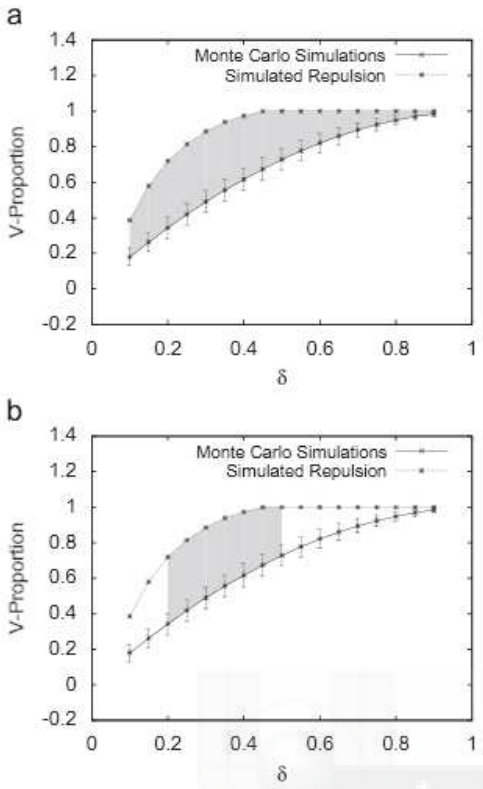

Fig. 7. (a) Total area between the V-Proportion curves of the real patterns and the random simulations in Fig. 5. (b) The area corresponding to a subinterval.

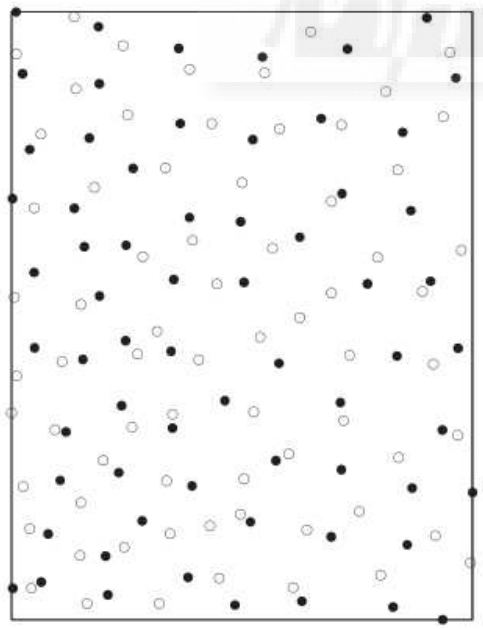

Fig. 8. On-cells (filled circles) and off-cells (open circles) from a cat's retina [23].

resolution of fine detail in the cat's visual system. They can be classified as on- or off-cells, depending on the branching level of their dendritic tree in the inner plexiform layer. Analysis of the spatial pattern provides information on the cat's visual discrimination. In particular, independence of the on- and off-components would strengthen the assumption that there are two separate channels for brightness and darkness [23].

The pattern shown in Fig. 8 was investigated in [23] using histograms of nearest-neighbor distances (ignoring edge effects). To test the independence of the on- and off-patterns, a random translation of the off-component was superimposed on the on-component, and the resulting nearest-neighbor histogram was compared with the original one by a sign reversal test. The authors in [23] concluded that both types of beta cells form a regular lattice, which are superimposed independently. This data was also analyzed in [22] using the J-function with a result greater than 1, which confirmed conclusions in [23]. Our results using the V-proportion are shown in both plots of Fig. 9. Using a confidence interval of 95% we cannot assume any significant spatial relation between on- and off-cells. This result is in accordance with [22,23].

6.2. Blue cones vs bipolar cells in the macaque retina

The second pair of mosaics we analyze is composed of two different types of neuronal cell populations found in the retina of macaque monkeys: blue bipolar cells and blue cones (Fig. 10). The mosaics used in this study were first presented in [32]. In that work, the authors suggested that blue cones tended to be close to blue bipolar cells and that nearly all blue bipolar cell dendrites terminated beneath the blue cones. The positive correlation of blue cones and blue bipolar cells was confirmed by the same authors in [18] using cross-correlational density recovery profile (cDRP). The finding that the blue cones and the blue bipolar cells

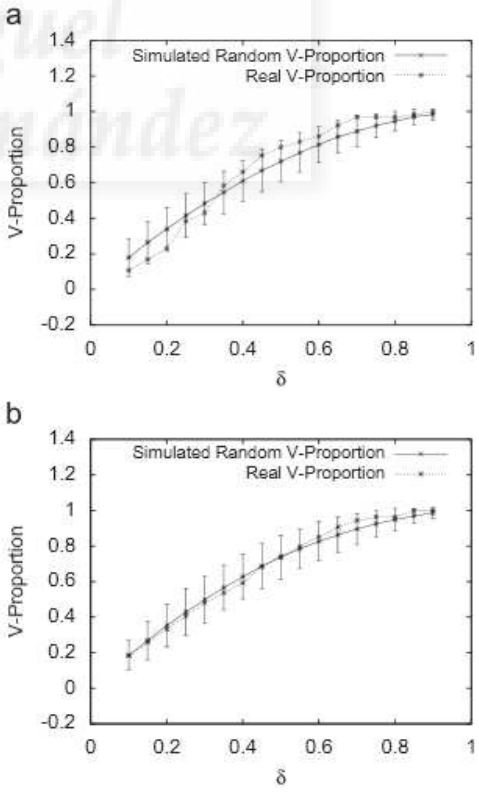

Fig. 9. Plots of the V-Proportion of the mosaics from Fig. 8. (a) When the on-cells are used as sites there is no significant spatial relation of off-cells. (b) The lack of spatial patterns between the two populations is even more evident when off-cells are used as sites. Error bars are drawn at the 95% confidence interval.

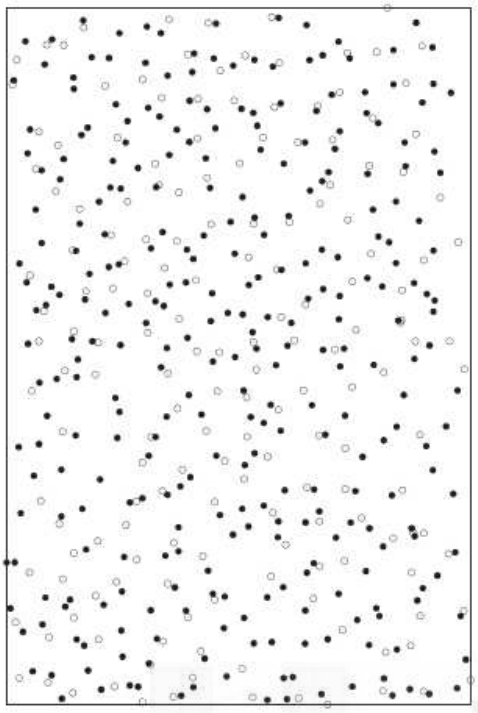

Fig. 10. Bipolar cells (filled circles) and blue cones (open circles) from the Macaque retina [32].

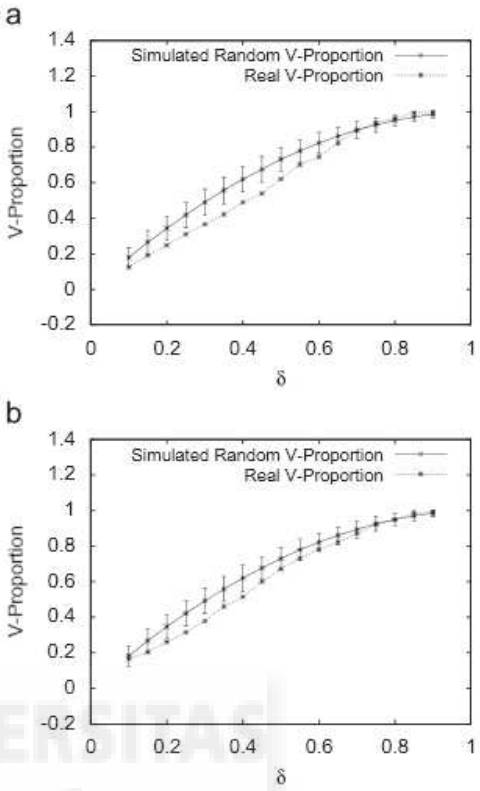

Fig. 11. Plots of the V-Proportion of the mosaics from Fig. 10. (a) When the bipolar cells are used as sites, the real V-Proportion lies under the simulated V-proportion and outside its error bars for a band width ranging from 0.2 to 0.6. The error bars of the Monte Carlo simulation are drawn within the 95% confidence interval. This result suggests a positive correlation between blue cones and blue bipolar cells. (b) The V-Proportion plot is calculated when the blue cones are used as sites. This plot also suggests a positive correlation of bipolar cells with respect to blue cones.

were closer together than expected suggests that the position of the perikarya of these neurons were influenced by their synaptic connections or other development interactions [18].

To analyze the mosaics from Fig. 10 we first set the bipolar cells as sites and the blue cones as *P* points. We then calculated the V-proportion following the approach presented in Section 4. As Fig. 11(a) shows, the V-Proportion lies under the simulated one for a band with ranging from 0.2 to 0.6, and within the 95% confidence interval. This result suggests that blue cones tend to be close to blue bipolar cells, and it confirms similar findings in [18]. In a second experiment, we set the blue cones as sites and calculated the V-Proportion of blue bipolar cells. The resulting plot in Fig. 11(b) suggests a positive correlation in this direction as well.

6.3. *Short-wavelength-sensitive cones vs blue cone bipolar cells in the marmoset monkey*

In a third experiment we analyzed the possible spatial relations between short-wavelength-sensitive (SWS) cones and blue cone bipolar cells in the retina of a marmoset monkey [33]. In this species the S-cone mosaic has an irregular characteristic. In [33], the authors compared the neuronal connectivity of Old World and New World primates, concluding that there exist similarities between them.

In this experiment we first used the blue bipolar cells as sites and analyzed the spatial distribution of the SWS cones. The initial distribution of points is shown in Fig. 12. The V-Proportion of Fig. 13(a) does not show any positive correlation within the 95% confidence interval. However, when swapping the populations (placing SWS as sites), the V-Proportion (Fig. 13(b)) shows a possible positive correlation of blue cone bipolar cells with respect to SWS cells. This last result is in accordance with the behavior of bipolar cells in the Macaque retina shown in Section 6.2.

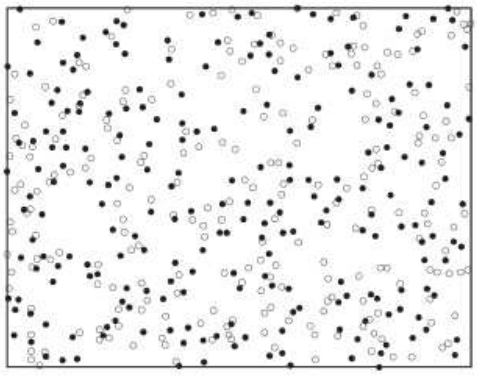

Fig. 12. Blue cone bipolar cells (filled circles) and SWS cones (open circles) from a marmoset's retina [33].

6.4. *S-cone positions vs irregular positions among the otherwise hexagonal lattice of M- and L-cones in a rhesus macaque fovea*

The foveas of human and primate retinas provide maximum acuity by having highly condensed cone mosaics. Such mosaics had

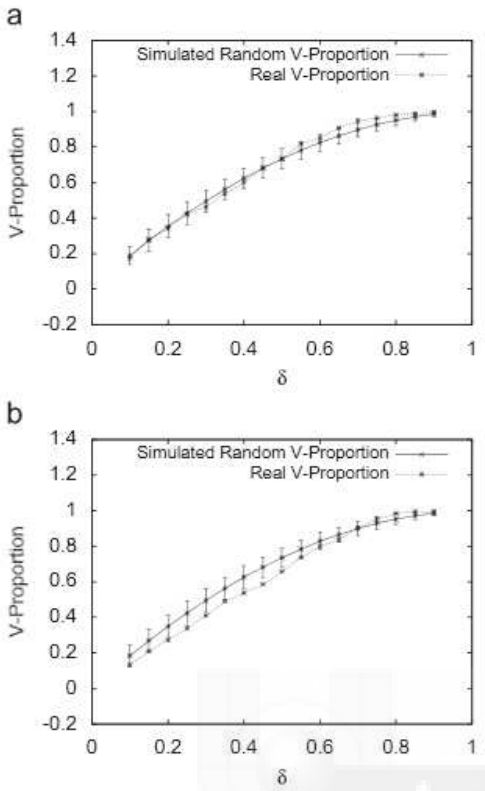

Fig. 13. Plots of the V-Proportion of the mosaics from Fig. 12. (a) When the bipolar cells are used as sites the real V-Proportion does not show any significant correlation within the 95% confidence interval. (b) The V-Proportion plot is calculated when the SWS cones are used as sites. This plot suggests a positive correlation of bipolar cells with respect SWS cones within the 95% confidence interval.

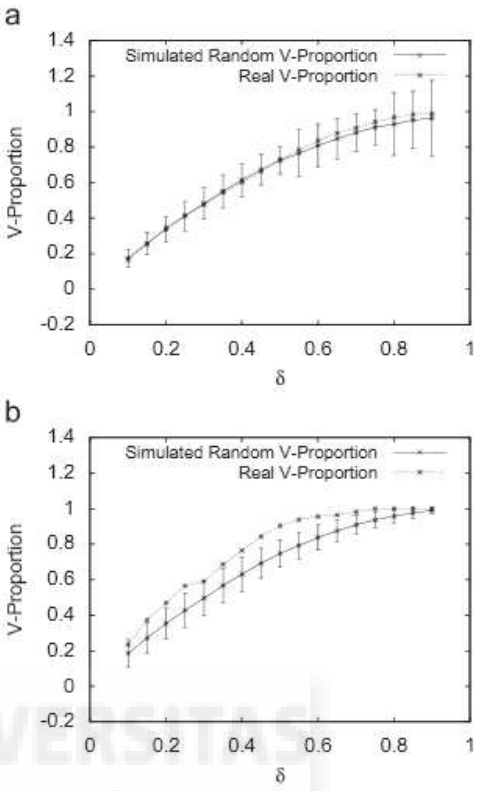

Fig. 15. V-Proportion plots of the mosaics from Fig. 14. (a) When the B cones used as sites, the real V-Proportion does not show any significant correlation within the 95% confidence interval. (b) When the M/L-cones with irregular (non-hexagonal) positions are used as sites, there exist a significant negative correlation within the 95% confidence interval.

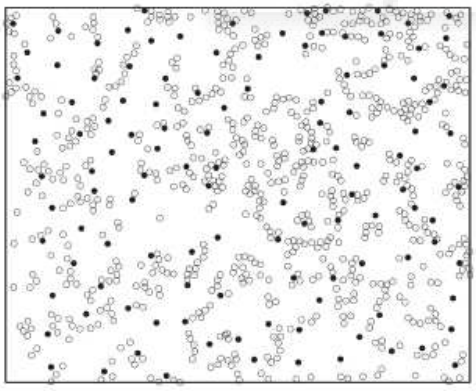

Fig. 14. Subpopulation with irregular mosaic positions (⟨6⟩ neighbors) among the otherwise hexagonal lattice of the dominant M/L-cones (open circles) and positions of S-Cones (filled circles) in a rhesus macaque fovea [35].

been previously analyzed with respect to lattice regularity [35–37] but there had been no approach to quantitatively study a possible relationship between S-cone positions and non-hexagonal *defects* of the M/L-cone lattice. In this last experiment we wanted to analyze the spatial relationships of S-cones with a specific feature of foveal microarchitecture.

The analyzed mosaic consists of a minor short wavelength sensitive S-cone and a dominant medium and long wavelength M/L-sensitive cone subpopulation as shown in Fig. 14. Overall, the foveal mosaic is a highly regular nearly crystalline lattice with predominant 1:6 (hexagonal) neighborship relations. However, previous detailed packing analyses [35–37] have revealed lattice discontinuities represented by cone positions with ⟨6⟩ cone neighbors subdividing the hexagonal mosaic in patchy. In a rhesus monkey foveal mosaic with labeled S-cones these positions with irregular number of neighbors have been identified in a previous study [35]. The current approach now allows us to evaluate the S-cone positions in relation to these mosaic distortions.

As revealed in the plot of Fig. 15(b) the foveal S-cones tend to be negatively correlated with the irregular positions suggesting that their location is prevalently associated with an undisturbed mosaic zone. This finding has interesting implications for understanding the processes underlying the developmental condensation of this mosaic.

7. Conclusion

This paper presented a method based on the Voronoi diagram to study possible spatial interactions between two cell mosaics. The new measurement, called V-Proportion, is able to detect different types of spatial interdependencies such as positive correlations, negative correlations, as well as lack of correlations. Additionally, the V-Proportion is calculated in a way that a confidence interval can be attached to the resulting behavior eventually revealing the significant range along the relative band widths. Results from

simulations as well as in real data sets demonstrate the effectiveness of the V-Proportion method to detect spatial relations between subpopulations of neurons or other (biological) entities.

Acknowledgments

We want to thank Stephen J. Eglen for making available the beta cells mosaics from [23]. This research has been supported in part by Grants SAF2008-303 03694 and CIBER BBN from the Spanish Government and by the Spanish ONCE.

References

[1] J. Jonas, J. Muller-Bergh, U. Schlotzer-Schrehardt, G. Naumann, Histomorphometry of human optic nerve, Investigative Ophthalmology and Visual Science 31 (1990) 736–744.
[2] H. Kolb, E. Fernandez, R. Nelson, Webvision: the neural organization of the vertebrate retina ⟨http://webvision.med.utah.edu/⟩, 2009.
[3] J. Dowling, The Retina: An Approachable Part of the Brain, Harvard University Press, Cambridge, MA, 1987.
[4] H. Kolb, The neural organization of the human retina, in: J. Heckenlively, G. Arden (Eds.), Principles and Practices of Clinical Electrophysiology of Vision, Mosby Year Book Inc.1991, pp. 25–52.
[5] C. Morillas, S. Romero, A. Martinez, F. Pelayo, E. Ros, E. Fernandez, A design framework to model retinas, Biosystems 87 (2007) 156–163.
[6] G.J. Chader, J. Weiland, M.S. Humayun, Artificial vision: needs, functioning, and testing of a retinal electronic prosthesis, in: J. Verhaagen, E.M. Hol, I. Huitenga, J. Wijnholds, A.B. Bergen, G.J. Boer, D.F. Swaab (Eds.), Neurotherapy: Progress in Restorative Neuroscience and Neurology, Progress in Brain Research, vol. 175, Elsevier2009, pp. 317–332.
[7] W. Fink, M. Tarbell, CYCLOPS: a mobile robotic platform for testing and validating image processing and autonomous navigation algorithms in support of artificial vision prostheses, Computer Methods and Programs in Biomedicine 96 (2009) 226–233.
[8] A.R. Hafiz, F. Alnajjar, K. Murase, A new dynamic edge detection toward better human–robot interaction, in: Lecture Notes in Computer Science, vol. 5744, 2009, pp. 44–52.
[9] J. Cook, L. Chalupa, Retinal mosaics: new insights into an old concept, Trends in Neuroscience 23 (2000) 26–34.
[10] J. Cook, Spatial regularity among retinal neurons, in: L. Chalupa, J. Werner (Eds.), The Visual Neurosciences, MIT Press2003, pp. 463–477.
[11] P. Ahnelt, H. Kolb, Horizontal cells and cone photoreceptors in primate retina: a Golgi-light microscopic study of spectral connectivity, The Journal of Comparative Neurology 343 (1994) 387–405.
[12] D. Dacey, B. Lee, D. Stafford, J. Pokorny, V. Smith, Horizontal cells of the primate retina: cone specificity without spectral opponency, Science 271 (1996) 656–659.
[13] T. Chan, U. Grünert, Horizontal cell connections with short wavelength-sensitive cones in the retina: a comparison between new world and old world primates, The Journal of Comparative Neurology 393 (1998) 196–209.
[14] P. Ahnelt, E. Fernandez, O. Martinez, J. Bolea, A. Küber-Heiss, Irregular S-cone mosaics in felid retinas. Spatial interaction with axonless horizontal revealed by cross-correlation, Journal of the Optical Society of America A 17 (2000) 580–588.
[15] S. Eglen, Development of regular cellular spacing in the retina: theoretical models, Mathematical Medicine and Biology 23 (2006) 79–99.
[16] E. Fernandez, J.A. Bolea, G. Ortega, E. Louis, Are neurons multifractals? Journal of Neuroscience Methods 89 (1999) 151–157.
[17] R. Rodieck, The density recovery profile: a method for the analysis of points in the plane applicable to retinal studies, Visual Neuroscience 6 (1991) 95–111.
[18] N. Kouyama, D. Marshak, The topographical relationship between two neuronal mosaics in the short wavelength-sensitive system of the primate retina, Visual Neuroscience 14 (1997) 159–167.
[19] B. Ripley, The second-order analysis of stationary point processes, Journal of Applied Probability 13 (1976) 255–266.
[20] P. Diggle, Displaced amacrine cells in the retina of a rabbit: analysis of a bivariate spatial point pattern, Journal of Neuroscience Methods 18 (1986) 115–125.
[21] M. van Lieshout, A. Baddeley, A nonparametric measure of spatial interaction in point patterns, Statistica Neerlandica 50 (1996) 344–361.
[22] M. van Lieshout, A. Baddeley, Indices of dependence between types in multivariate point patterns, Scandinavian Journal of Statistics 26 (1999) 511–532.
[23] H. Wässle, B.B. Boycott, R.-B. Illing, Morphology and mosaic of on- and off-beta cells in the cat retina and some functional considerations, Proceedings of the Royal Society of London, Series B (Biological Sciences) 212 (1981) 177–195.
[24] P. Diggle, S. Eglen, J. Troy, Case Studies in Spatial Point Process Modelling, Springer, pp. 215–233.
[25] M. de Berg, O. Cheong, M. van Kreveld, M. Overmars, Computational Geometry: Algorithms and Applications, third ed., Springer-Verlag, 2008.
[26] L. Galli-Resta, E. Novelli, Z. Kryger, G. Jacobs, B. Reese, Modelling the mosaic organization of rod and cone photoreceptors with a minimal-spacing rule, The European Journal of Neuroscience 11 (1999) 1461–1469.
[27] C. Duyckaerts, G. Godefroy, Voronoi tessellation to study the numerical density and the spatial distribution of neurones, Journal of Chemical Neuroanatomy 20 (2000) 83–92.
[28] J. Neyman, E. Scott, A statistical approach to problems of cosmology, Proceedings of the Royal Society of London, Series B (Methodological) 20 (1958) 1–43.
[29] P. Diggle, Statistical Analysis of Spatial Point Patterns, Academic Press, 1983.
[30] S.M. Ross, Simulation, Academic Press, 1997.
[31] E. Fernandez, N. Cuenca, J.D. Juan, A compiled basic program for analysis of spatial point patterns: application to retinal studies, Journal of Neuroscience Methods 50 (1993) 1–15.
[32] N. Kouyama, D. Marshak, Bipolar cells specific for blue cones in the macaque retina, Journal of Neuroscience 12 (1992) 1233–1252.
[33] X. Luo, K.K. Ghosh, P.R. Martin, U. Gruenert, Analysis of two types of cone bipolar cells in the retina of a New World monkey, the marmoset, *Callithrix jacchus*, Visual Neuroscience 16 (1999) 707–7191.
[34] ⟨http://www.informatik.uni-freiburg.de/~omartine/mosaics_data_sets.html⟩, 2010.
[35] D. Purn, P.K. Ahnelt, M. Grasl, Iso-orientation areas in the foveal cone mosaic, Visual Neuroscience 5 (1990) 511–523.
[36] C. Curcio, K. Sloan, Packing geometry of human cone photoreceptors: variation with eccentricity and evidence for local anisotropy, Visual Neuroscience 9 (1992) 169–180.
[37] D.H. Wojtas, B. Wu, P.K. Ahnelt, P.J. Bones, R. Millane, Automated analysis of differential interference contrast microscopy images of the foveal cone mosaic, Journal of the Optical Society of America A, Optics, Image Science, and Vision 25 (2008) 1181–1189.

Oscar Martinez Mozos received his Ph.D. degree ("Dr. rer. nat.") from the University of Freiburg (Germany) in 2008, and his M.Sc. degree in Applied Computer Science from the same university in 2005. In 1997 he completed a M.Eng. in Computer Science at the University of Alicante (Spain). He visited Japan as fellow of the Canon Foundation in Europe in 2008. He is interested in perception in robots and humans, and his research areas include machine learning, artificial intelligence, robotics, and neuroscience.

Jose A. Bolea was born in Zaragoza, Spain in 1961. He received the B.Sc. degree in Mathematics (program in Statistics and Operations Research) from the University of Valencia in 1984, and a M.Sc. degree in Bioengineering from the University Miguel Hernandez de Elche (Alicante) in 2000. In the last years he has been using mathematical tools in the field of computational neurosciences. His research interest include information theory, multivariate analysis, neural networks and fractal geometry. His work aims to be applied to know the interplay between neuronal shape and function and to understand information processing in the nervous system.

Jose M. Ferrandez was born in Elche, Spain in 1969. He received the M.Sc. degree in Computer Science in 1995, and the Ph.D. degree in 1998, all of them from the Universidad Politecnica de Madrid, Spain. He is currently Associate Professor at the Department of Electronics, Computer Technology and Projects at the Universidad Politecnica de Cartagena and Head of the Electronic Design and Signal Processing Research Group at the same University. He is also the coordinator of Spanish Thematic Network RTNAC (rtnac.org) and the iberoamerican network CANS (rcans.org), related to Natural and Artificial Computation. He is also the Chairman of the International Conference IWINAC, International Work Conference on the Interplay between Natural and Artificial Computation. His research interests include bioinspired processing, neuromorphic engineering and low vision prosthesis.

Peter K. Ahnelt is senior researcher in the Neurophysiology division of the Department of Physiology at the Medical University of Vienna. After his Ph.D. at the Department of Zoology at the University of Vienna he became assistant professor at the Department of General and Comparative Physiology at the Medical faculty. He had postdoctoral and associate positions at the Department of Physiology, University of Utah, Salt Lake City (USA) and exchange collaborations including labs in Alicante (Spain), Budapest (Hungary) and Rio de Janeiro (Brazil). His research interests focus on Retinal Neurobiology, in particular the identification of color specific photoreceptors and their synaptic connectivity patterns.

Eduardo Fernandez Jover received the M.D. degree from the University of Alicante, Spain, in 1986 and the Ph.D. degree in Neurosciences in 1990. He is currently Associate Professor at the University Miguel Hernandez, Spain, and Director of the Artificial Vision Laboratory at the Bioengineering Institute of the University Miguel Hernandez, Spain. In the last years he has been using histological as well as electrophysiological techniques to understand how mammalian retinal cells and the circuitry within the retina can manage and code visual information. He is actively working on the development of a visual neuroprosthesis for the profoundly blind.

A Neural Network Approach for the Analysis of Multineural Recordings in Retinal Ganglion Cells

Ferrández J.M.[1], Bolea J.A[1], Ammermüller J. [2], Normann R.A. [3], Fernández E.[1]

[1]Instituto de Bioingeniería, U. Miguel Hernández, Alicante,
[2]Dept. Neurobiologie, Univ. Oldenburg, Germany,
[3]Dept. Bioengineering, University Utah, Salt Lake City, USA,
Corresponding Author: jm.ferrandez@umh.es

Abstract. In this paper the coding capabilities of individual retinal ganglion cells are compared with respect to the coding capabilities of small population of cells using different neural networks. This approach allows not only the identification of the most discriminating cells, but also detection of the parameters that are more important for the discrimination task. Our results show that the spike rate together with the exact timing of the first spike at light-ON were the most important parameters for encoding stimulus features. Furthermore we found that whereas single ganglion cells are poor classifiers of visual stimuli, a population of only 15 cells can distinguish stimulus color and intensity reasonable well. This demonstrates that visual information is coded as the overall set of activity levels across neurons rather than by single cells.

1. Introduction

Our perception of the world, our sensations about light, color, music, speech, taste, smell are coded in raw data by the peripheral sensory systems, and sent, by the corresponding nerves, to the brain where this code is interpreted and colored with emotions. The raw or binary sensory data consists of sequences of identical voltage peaks, called action potentials. Seeing implies the decoding the patterns of spike trains that are sent to the brain, via the optic nerve, by the visual transduction element, the retina. Thus, the external world object features, as size, color, intensity... are transformed by the retina into a myriad of parallel spikes sequences, which must describe with precision and robustness all the characteristics perceived. Understanding this population code is, nowadays, a basic question for visual science.

Understanding the code means quantifying the amount of information each cell carries, and studying the possible parameters that are used by the cells for transmitting the data. The system has to assign meaning to this population code. Thus for a given pattern of action potentials, the brain has to estimate the stimulus that has produced it. The encoding has to be unequivocal and fast in order to ensure object recognition for any single stimulus presentation.

A considerable number of studies have focused on single ganglion cell responses [1][2]. Traditionally, the spiking rate, or even the spontaneous firing rate has been used as information carrier due to their close correlation with the stimulus intensity in all sensory systems [3] [4], however single neurons produce only a few spikes in response to different presentations and they must code a huge spectrum in their firings. The exact temporal sequence of action potentials in only one cell may also code the main stimulus features as it occurs in other systems (e.g. auditory coding [5]) however the response of a single cell to repetitions of the same stimuli often has a considerable variability for different presentations and cannot unequivocally describe the stimulus. Furthermore the timing sequence differs not only in the time events but also in the number of spikes, producing uncertainty in the decoding. Finally the same sequence of neural events may be obtained by different stimulus, introducing ambiguity in the neural response. So, it is a complex task to "understand" the neural coding just by analizing a single ganglion cell response.

New recording techniques and the emergence of new electrode array technologies, allow simultaneous recordings from populations of neuronal cells. However there are still many difficulties associated with collecting and analyzing activity from many individual cells simultaneously. FitzHugh [6] proposed a statistical analyzer that applied to the neural data estimates the characteristics of the stimulus. Different approaches have been used on the construction of such a decoder, including information theory [7], linear filters [8], discriminant analysis [9]...etc.

In this paper we used two different artificial neural networks, one trained by back-propagation and other implemented with auto-organizing maps to estimate how an ensemble of retinal ganglion cells can encode the characteristics of the light incident at the retina. Our results show that artificial neuronal networks are useful tools for analyzing multineuronal recordings and that visual information is coded as the overall set of activity levels across neurons rather than by single cells.

2. Methods

Experiments were performed on isolated turtle (*Trachemy scripta elegans*) retinas. Retina isolation has been described in detail before [9]. Briefly the turtle was sacrificed by decapitation conforming to ECC rules. The eye was then enucleated and hemisected under dim illumination, and the retina was removed under bubbled Ringer solution taking care to keep intact the photoreceptor outer segments. Then the retina was placed flat onto a beam splitter with the photoreceptor side facing down (Figure 1).

Light stimuli were produced from a tungsten lamp. Flashes with a duration of 0.2 seconds, followed by a 0.24 second period of darkness, were used as typical stimuli. Wavelength selection (400, 450, 488, 514, 546, 577, 600, 633 and 694 nm) was achieved with narrow band filters, and intensities were controlled with neutral density filters. Different spot sizes (ranging from 0.195 to 2.6 mm) were also used through

this study in order to learn how well recordings from a network of ganglion cells could be used to predict the shape, color and intensity of the visual stimulus. Each set of stimuli was presented 7 times. Responses were amplified with a differential amplifier and stored in a Pentium based computer. A custom analysis program sampled the incoming data at 20 kHz, plotted the waveforms on the screen, and stored the record for later analysis.

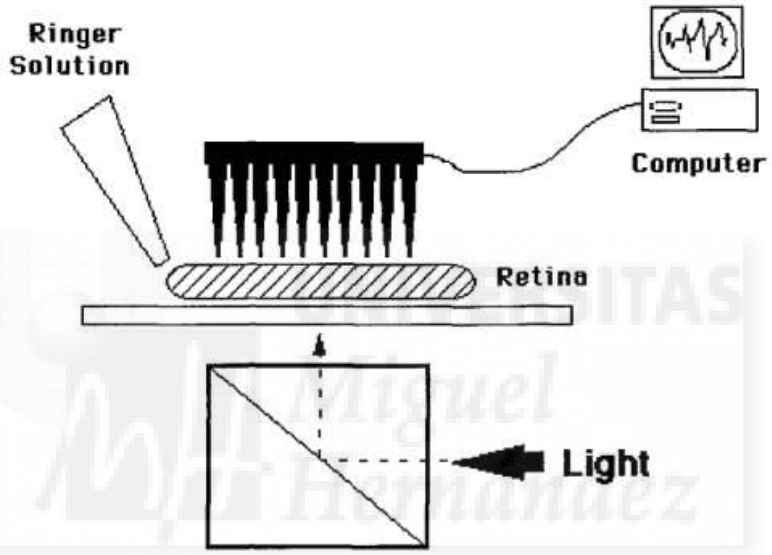

Fig 1. Recording method

Extracellular multielectrode recordings were performed using the Utah microelectrode array (UEA). It consists in an array of 100 isolated, 1.5 mm long silicon needles with platinized tips. Electrodes are arranged in a regular square pattern, spaced at 400 microns from each other. In each experiment we recorded neural activity from about 80-90 electrodes. We selected the electrodes with the highest signal to noise ratio and isolated 1 to 2 units from the multiunit responses by setting the thresholds to high levels [9]. For each electrode and presentation, the time of the first and second spike, the number of spikes, and the interspike interval during light-ON were stored for further analysis. Figure 2 shows an example of simultaneously recorded responses from 15 electrodes to 8 consecutive flashes of 546 nm, 2.6 mm diameter.

3. Analysis

In this study we selected the signals from those electrodes that had the highest signal to noise ratios. In general, multi-unit signals were obtained from most of the electrodes and often single unit separation was difficult so that we selected those 13-15 prototypes which were unequivocal in terms of both amplitude and shape. For each electrode, a 4-vector element was constructed using the number of spikes, the relative time of the first and second spike, and the interspike interval of these firings. A 60-element vector (4 variables x 15 cells) was used as the input matrix to our different neural network approaches.

Two different neural networks were used. The first one was a three layer backpropagation [10], with 20 nodes in the hidden layer. The output layer consisted of the same number of neurons as the classes to be recognized. Using this architecture, each neuron on the output layer only fires for a certain stimulus, and the rest of the neurons of the output layer have no activation (winner take all network). The activation function used for all neurons, including the output layer was the hyperbolic tangent sigmoid transfer function given by:

$$f(x) = \frac{2}{1+e^{-2x}} - 1 \qquad (1)$$

using as initial momentum and adaptive learning rate the values established by default by the Matlab Neural Network Toolbox. The initial weights were randomly initialized and the network was trained to minimize a sum squared error goal of 1, for providing more generality to the estimation stage.

The other network used was the Kohonen Supervised Learning Vector Quantization (LVQ) [11] with 16 neurons in the competitive map, and a learning rate 0.05. This network is a competitive network, where the neurons with weights more similar to the input, increase their strength in response to this input, decreasing the rest of the nodes except those in a close neighborhood. This establishes a topological relation in the map. The main advantage of using learning vector quantization is that it takes less time to reach the convergence criteria.

Once the network was trained, the estimation with extended data were used, and the correlation coefficients between the stimulus and their estimations were computed. Other studies use their own concepts as mutual information [8] in order to assess the overall quality of the reconstruction, but there does not exist a common agreement about the measure that best estimates the goodness of the prediction.

4. Results

For many stimulus conditions and many cells only a few spikes were produced in response to light-ON. Figure 2 shows a raster plot of the response time stamps of 15 cells to several identical presentations of a full field flash, using a wavelength of 546, log. relative intensity = -0.5. Stimulus is indicated in channel 1, so that 8 different flashes are shown. It can be seen that most of the cells are ON-OFF, and that they only fire a few spikes in response to the stimulus. Another characteristic is that for a given cell, different presentations of the same, identical stimuli, evoke different responses. These responses differ not only in the number of spikes but also in their relative timing, manifesting variability in their spiking behavior. This variability produces *uncertainty* for recognizing the right stimuli using only one individual cell, because there is no unequivocal function that associates the firing variables with the provided visual information.

Ambiguity is another aspect noticed. Thus a single cell can have exactly the same response to different stimuli, making the stimulus estimation task much more difficult. These aspects are presented in detail in Ammermüller et al. [9], and they point to population coding as the strategy used to represent information in the visual system.

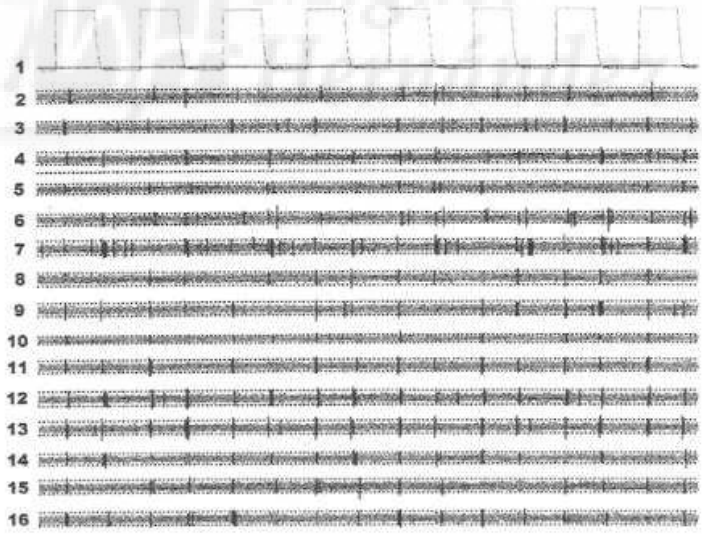

Fig. 2. Multielectrode response raster plot.

Figure 3 shows the correlation between the output of a trained backpropagation neural network and the correct stimuli, which in this case consisted in 8 different intensities. The three wavelenghts choosen were those where discrimination of the population was worst (633 nm), intermediate (546 nm) and best (450 nm). It can be seen that the

scores show variability depending on the cell and the wavelength studied. On average, all single cells were far below ideal discrimination, although to a varying degree. The cells with higher estimation scores were cells 8, 10, 11 and 12. On the other hand, the performance of all the cells taken together ("All" column) exceeded 0.95 for all wavelengths.

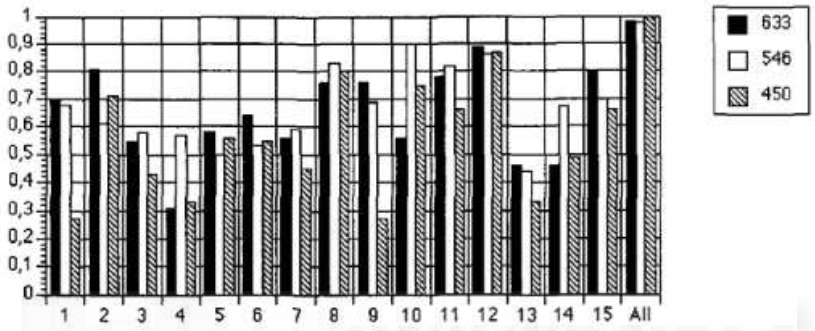

Fig. 3. Intensity estimation scores for individual cells and for all the cells taken together ("All" column) using a BP network

Color estimation is more complex, and the estimation rates for single cells were considerably lower (Figure 4). For these kind of studies the intensity was fixed and we asked the network to correctly classify nine different wavelengths. Again the population discrimination was fairly good, with correlation coefficients ranging from 0.95 to 0.97, values that clearly surpassed all the individual cell coefficients for all kinds of stimuli.

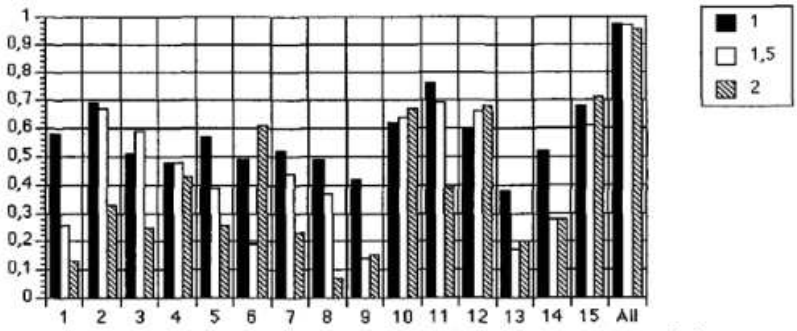

Fig. 4. Color estimation scores for individual cells and for all the cells taken together ("All" columns) using a BP network

For validating the above mentioned results, the same data was presented to another kind of neural network, a supervised learning vector quantization (LVQ) with 20 nodes in the competitive layer. This network converged faster than the back-propagation (BP) network, and again the cells with higher estimation scores were cells 8, 10, 11 and 12. The results obtained by using all the cells together was nearly the same as that obtained using the BP algorithms (Figure 5).

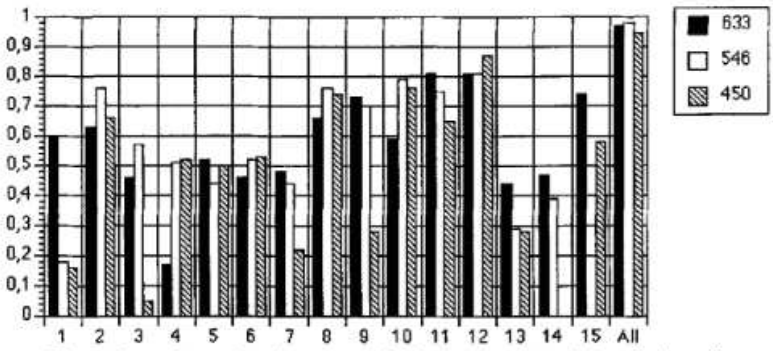

Fig. 5. Intensity estimation scores for isolated cells and for all the cells taken together ("All" column) using a LVQ network

The wavelength discrimination using competitive networks behaved similarly to the prior feedfoward network. Lower estimation scores were obtained, even for the whole population. This could be due to the difficulty of the network in fixing a decision border which divides the different clusters, however these values were clearly higher than the correlation rates obtained by using only individual cells (Figure 6).

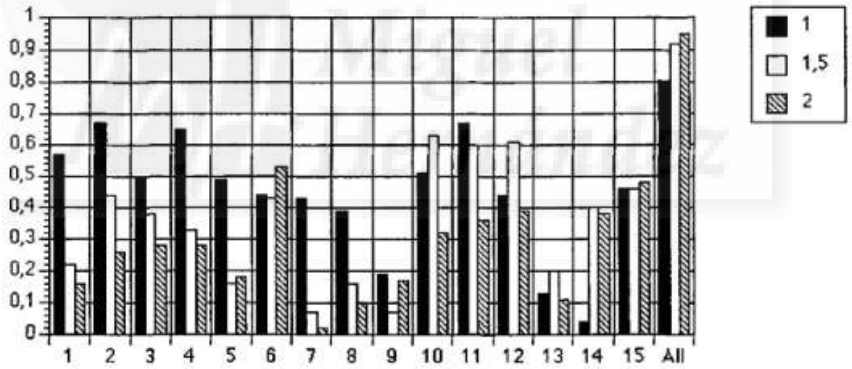

Fig. 6 Color estimation scores for individual cells and for all the cells taken together ("All" column) using a LVQ network

In order to get some insight into the relative importance of each one of the variables for the discrimination task, we used a BP network with 20 nodes in the hidden layer. The input to this layer was only the spike rate (N), only the timing of the first spike (T1), only the timing of the second spike (T2), or only the time difference between spike one and spike two (Interval) for the entire population of 15 cells. We also used all these parameters taken together. Figure 7 shows the correlation indexes between the real stimuli and the network estimations. Spike rate (N in figure 7) was the most important variable followed by the exact timing of the first spike (T1). The timing of the second spike (T2) and the interspike interval carried less information, and were

poor coding elements. When all the variables from the ensemble of cells were used the correlation coefficients were close to 1.

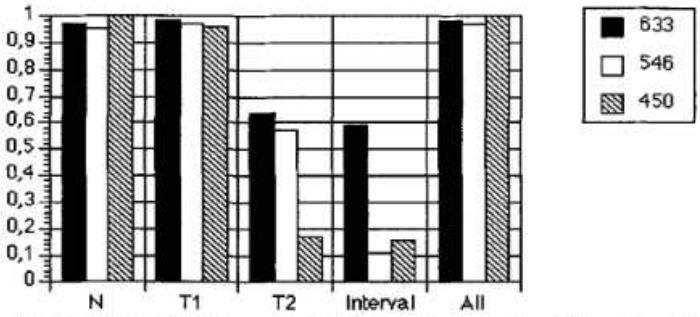

Fig. 7. Intensity estimation scores for the population using different variables

Basically the same results were obtained for color discrimination, although the overall performance was not as good as in the case of intensity discrimination (Figure 8).

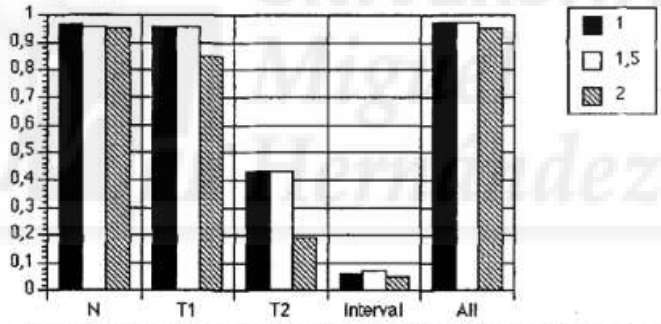

Fig. 8. Color estimation scores for the population using different variables

5. Conclusions

In this paper, a connectionist method has been used to investigate how color and intensity can be estimated from single cells and from populations of retinal ganglion cells. Two different neural networks, a feedfoward backpropagation and a competitive LVQ, have been used for determining the coding capabilities of individual cells versus a group of neurons. The correlation between the estimation of the networks and the real stimuli was used for quantifying the transmitted information. Both networks indicate that the brain could potentially deduce reliable information about stimulus features from the response patterns of ganglion cell populations but not from single ganglion cell responses.

The spike rate together with the exact timing of the first spike at light-ON were the most important parameters that encoded stimulus features as it has been shown for

different systems [4,5]. The fact that the number of spikes, or the first spike's relative timing, obtain the same estimation index as the overall parameters, approximately 0.95, could imply redundancy in the transmitted information, and could be related to the robustness in the data transference inherent to this system.

A more refined data set will help in providing more accuracy to our analysis. Thus, new physiological techniques which decrease the level of the background noise in the recorded responses, and an efficient separation of the action potential prototypes recorded with a single electrode [12], will help to isolate the firing parameters from artifacts which contaminate our present recordings.

Finally, while the quality of the different coding parameters could be assessed by using this neural network approach, we have no idea if indeed the brain also focuses on these variables. Once the visual code is understood, the construction of spiking retina models which reflects with accuracy the physiological recordings will be available.

Acknowledgements
This research is being funded by CICYT SAF98-0098-CO2-02, DFG SFB 517 and NSF grant #IBN 9424509.

References

1 Ammermuller J., Kolb H. "The Organization Of The Turtle Inner Retina. I. ON- and OFF-Center Pathways." J. Comp. Neurol. 358(1), pp. 1-34, 1995.

2 Ammermuller J., Weiler R., Perlman I.: "Short-term Effects Of Dopamine On Photoreceptors, Luminosity- And Chromaticity-Horizontal Cells In The Turtle Retina." Vis. Neurosci. 12(3), pp. 403-412, 1995.

3 Kuffler, S. W. "Discharge Patterns And Functional Organization Of Mammalian Retina". J. Neurophysiol. 16, pp 37-68, 1953.

4 Berry M. J., Warland D. K., Meister M.: "The Structure and Precision of Retinal Spike Trains" Proc. Natl. Acad. Sci USA 94(10), pp. 5411-5416, 1997.

5 Secker H. and Searle C.: "Time Domain Analysis of Auditory-Nerve Fibers Firing Rates". J. Acoust. Soc. Am. 88 (3) pp. 1427-1436, 1990.

6 Fitzhugh, R. A.: "A Statistical Analyzer for Optic Nerve Messages". J. Gen. Physiology 41, pp. 675-692, 1958.

7 Rieke F., Warland D., van Steveninck R., Bialek W.: "Spikes: Exploring the Neural Code". MIT Press. Cambridge, MA, 1997.

8 Warland D., Reinagel P., Meister M.: " Decoding Visual Information from a Population of Retinal Ganglion Cells". J. Neurophysiology 78, pp. 2336-2350, 1997.

9 Ammermüller J., Fernández E., Ferrández J.M., Normann R.A.: "Color and Intensity Discrimination of Retinal Ganglion Cells in the Turtle Retina". J. Physiology. (under revision).

10 McClelland J., Rumelhart D.: "Explorations in Parallel Distributed Processing", vol. 1 and 2. MIT Press, Cambridge MA, 1986.

11 Kohonen T.: "Self Organization and Associative Memory" vol. 8. Springer Series in Information Sciences, Springer-Verlag NY, 1984.

12 Ohberg F, Johansson H., Bergenheim M., Pedersen J., Djupsjobacka M. "A Neural Network Approach to Real-Time Spike Discrimination during Simultaneus Recordings from several Multi-Unit Filaments." Journal of Neuroscience Methods 64 (1996), pp. 181-187.

Neural Coding Analysis in Retinal Ganglion Cells Using Information Theory

J.M. Ferrández[1,2], M. Bongard[1,3], F. García de Quirós[1], J.A. Bolea[1], and E. Fernández[1]

[1]Instituto de Bioingeniería, U. Miguel Hernández, Alicante,
[2]Dept. Electrónica y Tecnología de Computadores, Univ. Politécnica de Cartagena,
[3]Dept. Neurobiologie, Univ. Oldenburg, Germany
Corresponding Author: jm.ferrandez@upct.es

Abstract. Information Theory is used for analyzing the neural code of retinal ganglion cells. This approximation may quantify the amount of information transmitted by the whole population, versus single cells. The redundancy inherent in the code may be determined by obtaining the information bits of increasing cells datasets and by analyzing the relation between the joint information compared with the addition the information achieved by aisle cells. The results support the view that redundancy may play a crucial feature in visual information processing.

1. Introduction

Information transmission and information coding in neural systems is one of the most interesting topics in neuroscience, nowadays. As technology grows new neural acquisition tools become available. They permit recording simultaneously tens, even hundreds of cells stimulated under different conditions. This process produces enormous data files, which need new tools for extracting the underlying organization of the neural principles, captured in the recordings.

First of all, it is necessary to determine if there exists an aisle cell coding, or a population coding. An aisle cell fires with limited action potentials, in a restricted interval, so it is difficult to code, numerically speaking, a broad spectrum of stimuli on its parameters. On the other hand a population of cells have more coding capabilities, and it can provide robustness to the representation of the stimuli by using redundancy on the population firing patterns. Adding more cells for coding the same stimuli will produce a fault tolerance system.

There have been published studies about auditory [1] and olfactory coding [2], however understanding visual coding is a more complex task due to and number and characteristics of the visual stimulation parameters, and the difficulty of achieving a filtered population ganglion cells firing pattern database with a considerable number of cells recorded simultaneously. New tools are also required for understanding this vast database. Initially it has been applied statistical analysis, [3][4][5] for obtaining insights about the parameters used in the visual system for coding and transmitting the

J.R. Dorronsoro (Ed.): ICANN 2002, LNCS 2415, pp. 174–179, 2002.

information to higher centers in the visual hierarchy. Artificial neural networks are also another tool, which can provide, supervised or autoorganizative, new insights about the way visual parameters are encoded and the inherent organization principles. [5][6]

Recent approaches use Information Theory for quantifying the code transmission. It can be used for comparing, also, the aisle cells coding capability versus the population code. It looks at the disorder, entropy, of a system, assuming that a system with more variability (disorder) will be able to transmit more symbols that a system with zero variance. Some studies [8] replace symbols with a list of action potential firing times for analyzing the neural data.

This paper uses information theory for quantifying the information transmitted by single retinal ganglion cells compared with the information conveyed by the whole population. The number of neurons in the datasets is also changed for determining if information grows linearly with number of neurons involved in the coding or it saturates, producing a redundancy phenomenon. Finally the redundancy effect will be observed for assuming if it is consequence of the saturation limit on the information, or if it exists for lower number of cells, aspect that will produce the desired robustness in the code. The results show that information is transmitted by the population code mainly, there exist some saturation on the information provided, determined by the stimuli dataset, and redundancy appears for all numbers of cells involved in the coding.

2. Methods

Registers were obtained on isolated turtle (Trachemy scripta elegans) retinas. The turtle was dark adapted for a few hours, before it was sacrificed and decapitated. Then the head was stored half an hour under 4° Celsius in order to ease the removing of the vitreous. The eye was enucleated and hemisected under dim illumination, and the retina was removed using bubbled Ringer solution taking care to keep intact the outer segment when removing the pigment epithelium. The retina was flatted in an agar plate, and fixed using a Millipore filter with a squared window where the electrodes will be placed. The agar plated with the retina was placed in a beam splitter with the ganglion cell on the upper side and bubbling Ringer solution flowed through the filter.

Light stimulation was applied using a halogen light lamp, selecting the wavelength by means of narrow band pass interference filters. Intensity was fixed by using neutral density filters, and a shutter provides flashes of the stimuli to the preparation. For each stimuli (the wavelength, the intensity, and the spot was varied) seven consecutive flashes, with 250 msec. length, were applied, using a lens to focus the stimulus on the photoreceptor layer of the whole retina.

The Utah microelectrode array was used for obtaining the extracellular recordings (Figure 1). It consists in an array of 100 (10x10); 1.5 mm long niddles with a platinized tip 50 microns long. The distance between each niddle is 400 mm, and the rest of the array is insulated with polyamide for providing biocompatibility. It was mounted on a micromanipulator, and each electrode was connected to a 25000 gain band pass (filtered from 250 to 7500 Hz) differential amplifier. The analog signal was digitized using a multiplexer and an A/D converter and stored in a computer.

The pre-processing consisted of fixing a threshold (based on an estimate of the noise of the electrode) in order to extract the kinetics of electrical activity above this threshold. Spike waveform prototypes were separated by template matching. For each stimulus and for each electrode, the time of the first and second spike, the number of spikes, and the interspike interval during the flash interval was also computed.

3. Information Theory

Information theory had its origins in 1929, Shannon published "The Mathematical Theory of Communication" [10] where thermodynamic entropy was used for computing different aspects about information transmission. Later it was applied for computing the capacity of channels for encoding, transmitting and decoding different messages, regardless of the associated meaning.

Information theory may be used as a tool for quantifying the reliability of the neural code just by analyzing the relationship between stimuli and responses. This approach allows one to answer questions about the relevant parameters that transmit information as well as addressing related issues such as the redundancy, the minimum number of neurons need for coding certain group of stimuli, the efficiency of the code, the maximum information that a given code is able to transmit, and the redundancy degree that exists in the population firing pattern.

In the present work, the population responses of the retina under several repetitions of flashes were discretized into bins where the firing rates from the cells of the population implement a vector **n** of spikes counts, with an observed probability P(**n**). The probability of the occurrence of different stimuli has a known probability P(s). Finally the joint probability distribution is the probability of a global response **n** and a stimulus s, P(s,**n**).

The information provided by the population of neurons about the stimulus is given by:

$$I(t) = \sum_{s \in S} \sum_{n} P(s,n) \log_2 \frac{P(s,n)}{P(s)P(n)} \qquad (1)$$

This information is a function of the length of the bin, *t*, used for digitizing the neuronal ensembles and the number of the stimuli in the dataset P(s).

To study redundancy, first the information transmitted for aisle each cell is calculated. Also the information conveyed by a group if cells, that is, jointly. If neuron were independent the relation between the joint information, and the sum of the information of the aisle cells, which form the group, should be equal to unity. If the joint information related to the sum of aisle cells is greater that one there exists a synergistic code, and finally if the joint information related to the summatory of individual cell information is lower than one, that is the sum of the aisle cells carry more information than the joint population, denotes redundancy.

In this paper, equation (1) was computed to determine the information contained in the firing trains of isolated retinal ganglion cells for 7 different stimuli and this data was compared to the information carried out by the whole population. The information contained in an increasing set of ganglion cells was also computed in order to determine if the information grows linearly with the number of cells or if it

saturates at a given value. And finally the relation between the aisle cells information is compared with the joint information for determining the characteristic, independent, synergistic, or redundant of the coding.

4. Results

For both experiments shown on this results, neural activity was recorded in most of the electrodes. The cells were selected by pattern matching algorithms for separating different signal sources. The firing rate vectors were computed and finally the stimulus-response table was constructed for the task of discriminating between seven different light intensities. In Figure 1, the information, in bits, is plotted for single cells in the population versus the whole population. Cells with more variability in their response show a higher information capability. The average information for single cells (dotted line), is much lower than the whole population transmitted information in both cases.

The analysis of the saturation limit is plotted in Figure 2. The information for an increasing cell population is show for increasing cell datasets. If initially, for small groups, information rises linearly with the number of cells, it saturates with groups bigger than certain number of cells for both experiments. This means that adding more new cells to the analysis does not provide more information. The degree to which the rise of information with the number of cells deviates from linearity is related to the redundancy of the code. A redundant representation will provide robustness, or fault tolerance to the system.

Finally Figure 3, shows the relation between the joint information transmitted and the sum of the information for each aisle cell in increasing size groups. It can be seen in booth experiments that the values are below unity, that is the behavior of the coding is not synergistic, neither independent but redundant, providing robustness to the code, and fault tolerance to the system.

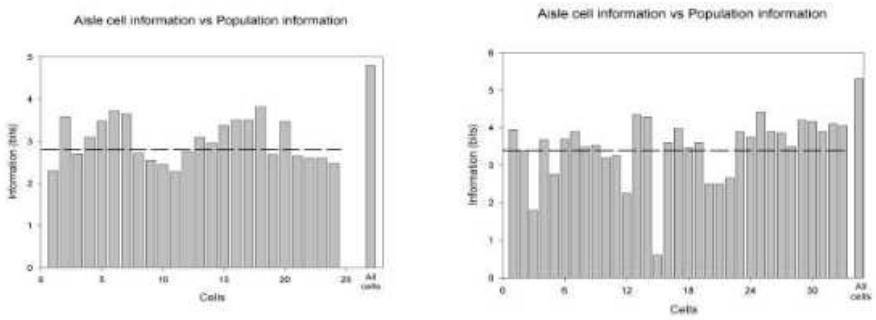

Fig. 1. Single cell coding versus population coding

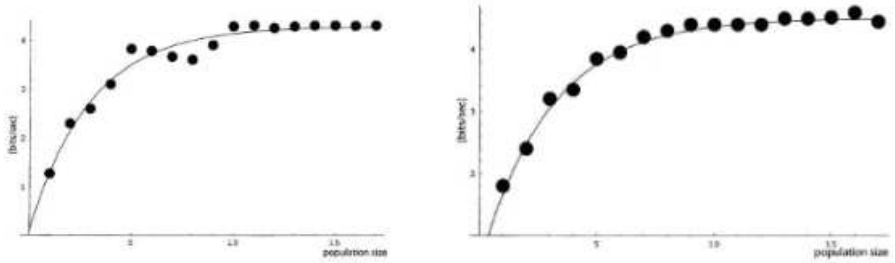

Fig. 2. Information transmitted for an increasing population of retinal ganglion cells in discriminating intensities.

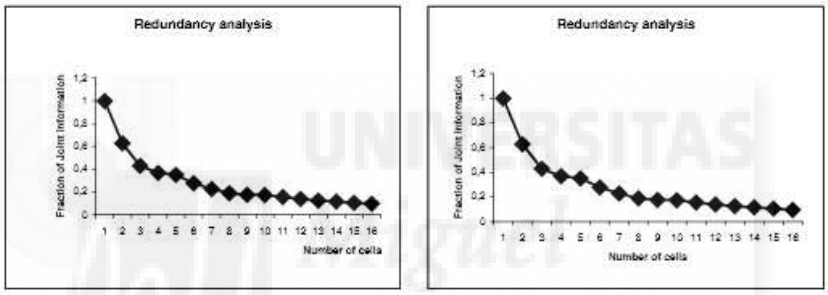

Fig. 3. Redundancy analysis for an increasing population of retinal ganglion cells.

5. Conclusions

Information Theory has been applied for analyzing the neural code of retinal ganglion cells. The information transmitted by the population of cells is always higher than the information contained in the responses of aisle cell, suggesting a population code instead of a single cell code. The overall information registered may vary, it depends on the experiment, number of cells recorded, discriminative character of this cells, location of the multielectrode array, size of the bins, etc., however the overall behavior does not change significantly.

The information on the population grows linearly with number of cells until certain limit, where information saturates. Adding more cells to the set does not provide more information. The redundant characteristic of this scenario has been proved by relating the joint transmitted information versus the addition of the singles cell transmitting rate. Redundancy could be useful to achieve the robustness required for the retina to maintain its performance under adverse environments.

This analysis may be also applied to color coding as well as coding of natural scenarios, where synergistic behaviors may appear. The cooperation between new multichannel acquisition system and innovative analysis tools will provide new insights in neural coding.

Acknowledgements. This research is being funded by E.C. QLK-CT-2001-00279, Fundación Séneca PI-26/00852/FS/01, a grant from the National Organization of the Spanish Blind (ONCE), and Fellowship from the Spanish Ministerio de Educacion to M.B.

References

1. Secker H. and Searle C.: "Time Domain Analysis of Auditory-Nerve Fibers Firing Rates". J. Acoust. Soc. Am. 88 (3) pp. 1427–1436, 1990.
2. Buck L.B.: "Information Coding in the vertebrate olfactory system". Ann. Rev. Neurosci. 19, pp. 517–544, 1996.
3. Fitzhugh, R. A.: "A Statistical Analyzer for Optic Nerve Messages". J. Gen. Physiology 41, pp. 675–692, 1958.
4. Warland D., Reinagel P., Meister M.: " Decoding Visual Information from a Population of Retinal Ganglion Cells". J. Neurophysiology 78, pp. 2336–2350, 1997.
5. Fernández E., Ferrández J.M., Ammermüller J., Normann R.A.: "Population Coding in spike trains of simultaneously recorded retinal ganglion cells Information". Brain Research, 887, pp. 222–229, 2000.
6. Ferrández J.M., Bolea J.A., Ammermüller J. , Normann R.A. , Fernández E.: "A Neural Network Approach for the Analysis of Multineural Recordings in Retinal Ganglion Cells: Towards Population Encoding". Lecture Notes on Computer Science 1607, pp. 289–298, 1999.
7. Shoham S., Osan R., Ammermuller J. Branner A., Fernández E., Normann R.: "The Classification of the Chromatic, and Intensity Features of Simply Visual Stimuli by a Network of Retinal Ganglion Cells". Lecture Notes on Computer Science 1607, pp. 44–53, 1999.
8. Rieke F., Warland D., van Steveninck R., Bialek W.: "Spikes: Exploring the Neural Code". MIT Press. Cambridge, MA, 1997.
9. Jones, K.E., Campbell, P.K. and Normann, R.A.:"A glass/silicon composite intracortical electrode array". Annals of Biomedical Engineering 20, 423-437 (1992).
10. Shannon C.E..: "A Mathematical Theory of Communication". Bell Sys Tech J. 27. pp. 379–423 , 1948.

Formulation and Validation of a Method for Classifying Neurons from Multielectrode Recordings

M.P. Bonomini[1,*], J.M. Ferrandez[2], J.A. Bolea[1], and E. Fernandez[1]

[1] Instituto de Bioingeniera, Univ. Miguel Hernández, Alicante
[2] Dept. Electrnica y Tecnologa de Computadores, Univ. Politécnica de Cartagena

Abstract. The issue of classification has long been a central topic in the analysis of multielectrode data, either for spike sorting or for getting insight into interactions among ensembles of neurons. Related to coding, many multivariate statistical techniques such as linear discriminant analysis (LDA) or artificial neural networks (ANN) have been used for dealing with the classification problem providing very similar performances. This is, there is no method that stands out from others and the right decision about which one to use is mainly depending on the particular cases demands. Therefore, we developed and validated a simple method for classification based on two different behaviours: periodicity and latency response. The method consists of creating sets of relatives by defining an initial set of templates based on the autocorrelograms or peristimulus time histograms (PSTHs) of the units and grouping them according to a minimal Euclidian distance among the units in a class and maximizing it among different classes. It is shown here the efficiency of the method for identifying coherent subpopulations within multineuron populations.

1 Introduction

Understanding how information is coded in different sensory systems is one of the most interesting challenges in neuroscience today. Technology is now available that allows to acquire data with more accuracy both in the temporal and the spatial domains. However this process produces a huge neural database which requires new tools to extract the relevant information embedded in neural recordings.

While the neural code is partially understood in the auditory [1] and olfactory systems [2], the visual system still presents a challenge to neuroscientists due to its intrinsic complexity. Different studies have used different analysis tools to approach the decoding objective. Fitzhugh [3] applied a statistical analyzer to the neural data in order to estimate the characteristics of the stimulus, whereas Warland used linear filters [4] for the decoding task. Other approaches used

* Corresponding author: p.bonomini@umh.es

J. Mira and J.R. Álvarez (Eds.): IWINAC 2005, LNCS 3561, pp. 68–76, 2005.

to get insights into the coding process are discriminant analysis [5], principal component analysis [6] and supervised and non-supervised neural networks [7].

The nearest neighbour clustering decomposes the whole population in disjoint groups, minimizing the distance betwween the elements of a group and maximizing the avaraged squared distance between the centroids of different clusters. This division will achieve temporal boundaries for classificating the neural responses according to their periodicity or PSTH schemes.

In this paper, it is developed and validated a simple method for classification based on two different parameters: periodicity and latency response. The process consists of creating sets of relatives by defining an initial set of templates based on the autocorrelograms or PSTHs of the neural population response and grouping them according to a minimal Euclidian distance among the units in a class and maximizing it among different classes.

The method was implemented using the K-means algorithm [8]. This clustering method was found to be slightly more robust to large amounts of noise in neuronal data than others [9].

It will be shown here the efficiency and robustness of the method for identifying coherent subpopulations within multineuron populations.

2 Materials and Methods

Experimental data was obtained from rabbit retina recordings using a one hundred multielectrode array (Cyberkinetics Inc.)[10]. Visual stimulus consisted of full-field flashes at 0.5 Hz with a 300 ms ON period. Units were sorted using a free open-source program, Nev2lkit, (source code and documentation is freely available at http://nev2lkit.sourceforge.net) by means of principal component analysis (PCA), specifically the correlation method.

Afterwards, the autocorrelograms and PSTHs were calculated on each of the cells in the dataset at two different bin sizes, 50 ms and 100 ms respectively. For the autocorrelation, a maximum lag of 200 was used such that the complete occurrence of a flash transition at any of the former bin widths were included. Accordingly, a 2 second window was chosen for the PSTH computation. For each bin size, either the autocorrelograms or the PSTHs fed a partitional clustering method for the creation of a number of clusters which varied between two and five. For the clustering method, the nearest-neighbour or k-means approach was used. This approach decomposes the dataset into a set of disjoint clusters and then minimizes the average squared distance from a cluster centroid among the elements within a cluster, while maximizes this distance when regarding the centroids of the different clusters. This defines a set of implicit decision boundaries that separate the clusters or classes of units according to their periodicity when clustering their autocorrelograms or to its response delay when clustering their PSTHs. In this way, we end up with groups of relatives that are a subset of the entire array.

In order to validate the efficiency of the method, a first graphical arrangement of the units was accomplished for a fast visualization of the coherence in the clas-

sification among different number of classes and bin widths. Then, a quantitative analysis based on population responses was done. On each class, a population response was build up by summing up all the single response trials from each item within the class at a 5 ms bin size. On these signals, the autocorrelation and correlation with stimulus was calculated.

3 Results

In order to test the accuracy of the method either for an autocorrelation-based or PSTH-based classification, we first arranged the classified units in a graphical way for an appropriate first visual inspection. For both of the two bin sizes used for the analysis, a diagram as the one in Fig. 1 showing the classification performance, was built up for each of the autocorrelation and PSTH approach as well as for each number of clusters.

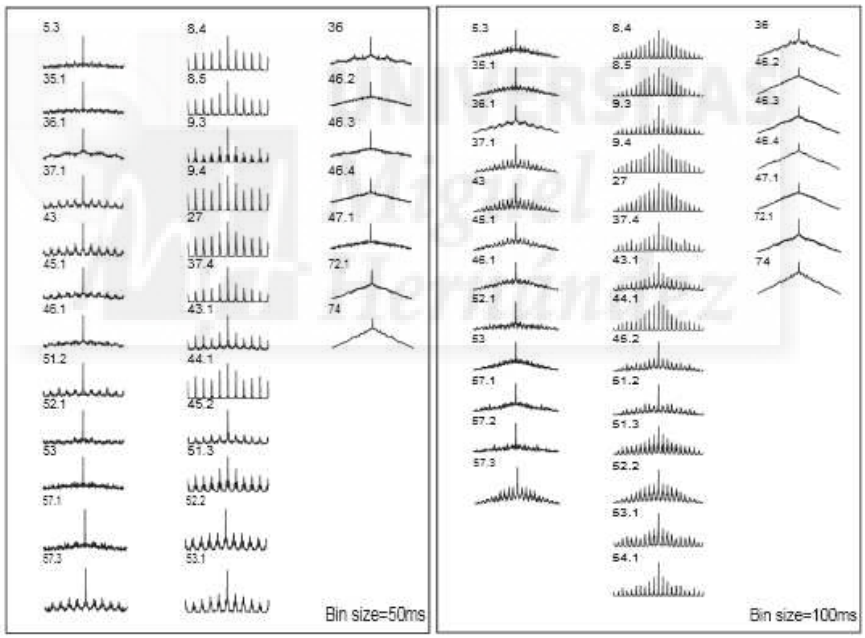

Fig. 1. Graphical representation of the k-means output for five different classes. On each column it is shown the autocorrelograms of the classified units belonging to a same class. Left panel: autocorrelation calculated at a bin size of 50 ms. Right panel: autocorrelation calculated at a bin size of 50 ms. Maximum lag used: 200. Legends on top of the autocorrelograms describe unit identifiers. For clarity reasons not all the units of the original dataset are presented

Specifically, Fig. 1 shows in a graphical fashion the output of the k-means method for the autocorrelograms of a number of units at two bin sizes; 50 and 100

ms respectively, both of them with a maximum lag of 200. All the units belonging to the same class are aligned in the same column. Legends on top of each plot represent the unit identifiers. In the case shown in Fig.1, the dataset was disjoint into three different clusters while in Fig. 2 original data were split into five sets of relatives. Not all of the units are shown for clarity reasons. Notice that units belonging to the class represented by the middle column in both panels present a strong periodicity, following the periodic stimulation while units grouped on the third column do not respond consequently to, at least, the applied stimulation. The same holds when increasing the number of classes, as seen in Fig. 2, with the advantage that the cell periodicities can be clustered in a more graded fashion.

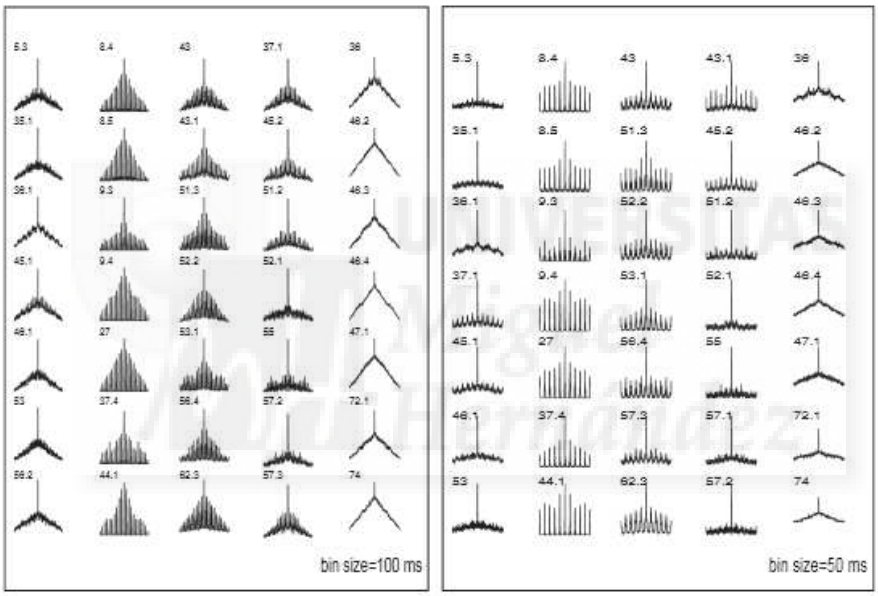

Fig. 2. Graphical representation of the k-means output for five different classes. On each column it is shown the autocorrelograms of the classified units belonging to a same class. Left panel: autocorrelation calculated at a bin size of 50 ms. Right panel: autocorrelation calculated at a bin size of 50 ms. Maximum lag used: 200. Legends on top of the autocorrelograms describe unit identifiers. For clarity reasons not all the units of the original dataset are presented

Once the qualitative assessment of the performance for different bin sizes and number of classes was done as explained above, a more quantitative analysis of how efficiently the method separated units was carried out. Firstly, it was calculated as many subpopulation responses as number of classes were chosen in the K-means algorithm for the classification task. For each class, the activity of all the units belonging to that class were summed up in order to create a population response for that class. Population responses were computed as follows: a bin

width of 5 ms was defined and the activity of all the cells in the subpopulation was summed up at each bin. Afterwards, the signals were smoothed by convolving them with a Gaussian function with a standard deviation of 0.5. Then, both the autocorrelation and correlation to stimulus of these signals were calculated. For an appropriate comparison with the original entire population, Fig. 3a shows the raster of the original population while Fig. 3b shows its smoothed population response. Accordingly, Fig. 3c shows the autocorrelation of the population response normalized so that at zero lag the autocorrelations are identically one, and Fig. 3d shows the population response correlated to stimulus without any scale applied, this is, non normalized. For both the autocorrelation and cross-correlation computation, the entire signal was lagged. Continuous trace on top of Fig. 3a represents the temporal evolution of the stimulus, a 2 second full-field flash with a 300 ms ON period.

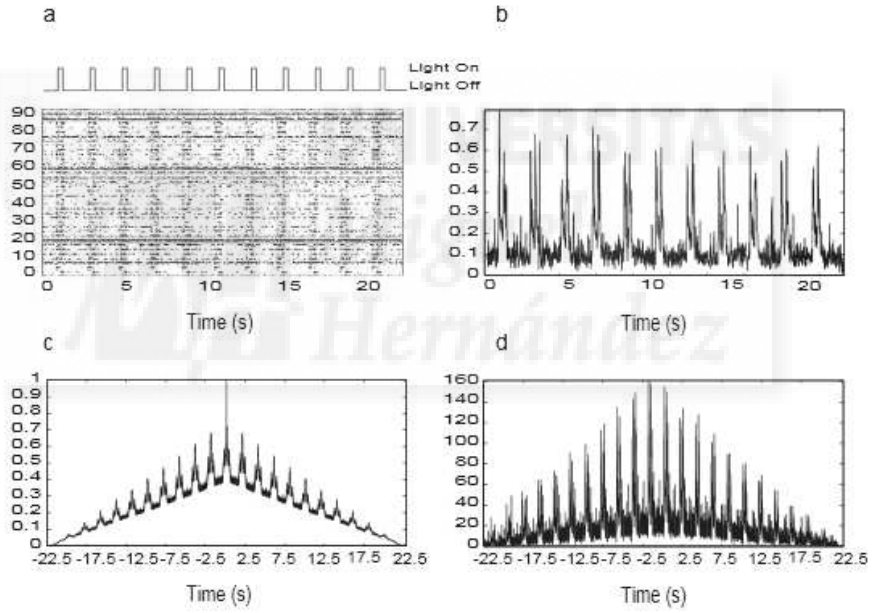

Fig. 3. Representation of the original data. a) Raster plot of the original dataset. Stimulus evolution is represented in the continuous top trace. b) response population resulting from summing up the activity across all the units in the recording for every bin (5 ms). c) normalized population signal autocorrelogram and d) population signal correlated to stimulus. For both correlations the entire signal was lagged

The same analysis as the one done to the original population was applied to every subpopulation in order to highlight the properties that were kept or removed from the original dataset in each of the subpopulations created. As an example, Fig. 4 displays the rasters, population responses, autocorrelation and correlation to stimulus (Fig .4a, 4b, 4c and 4d respectively) of three different

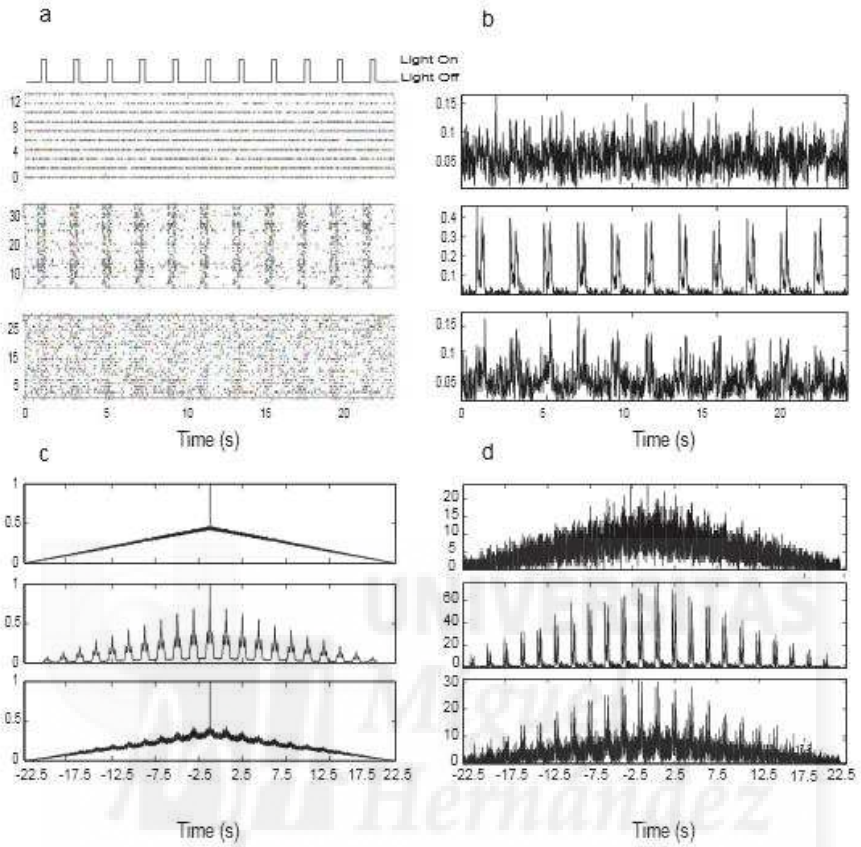

Fig. 4. Representation of the classified data by means of the autocorrelation approach. a) Raster plots of the three subpopulations found by defining the number of classes three. Stimulus evolution is represented in the continuous top trace. b) response populations resulting from summing up the activity across all the units in each subpopulation for every bin (5 ms). c) normalized population signal autocorrelograms and d) population signals correlated to stimulus for each filtered population. For both correlations the entire signal was lagged

subpopulations found by means of the autocorrelation approach using a bin size of 100 ms and a maximum lag of 200.

Consistently, the number of classes set in the classification task was three. The processes were calculated as explained above for the original data. Here, each subpopulation is represented in a subplot across every panel respecting the order through out the different panels for a clear visualization. Notice the clean temporal pattern of the subpopulation represented as a raster (Fig. 4a, middle panel), which is also reflected on its response population (Fig. 4b, middle panel) as well as on both of the correlograms (Fig. 4c and Fig. 4d, middle panels), where either of them turned out improved with respect to the correlograms from the

original entire population (Fig. 3c and Fig. 3d), which display certain amount of noise.

In the same direction, Fig. 5 shows other three different subpopulations obtained from the same original data but using the PSTH approach.

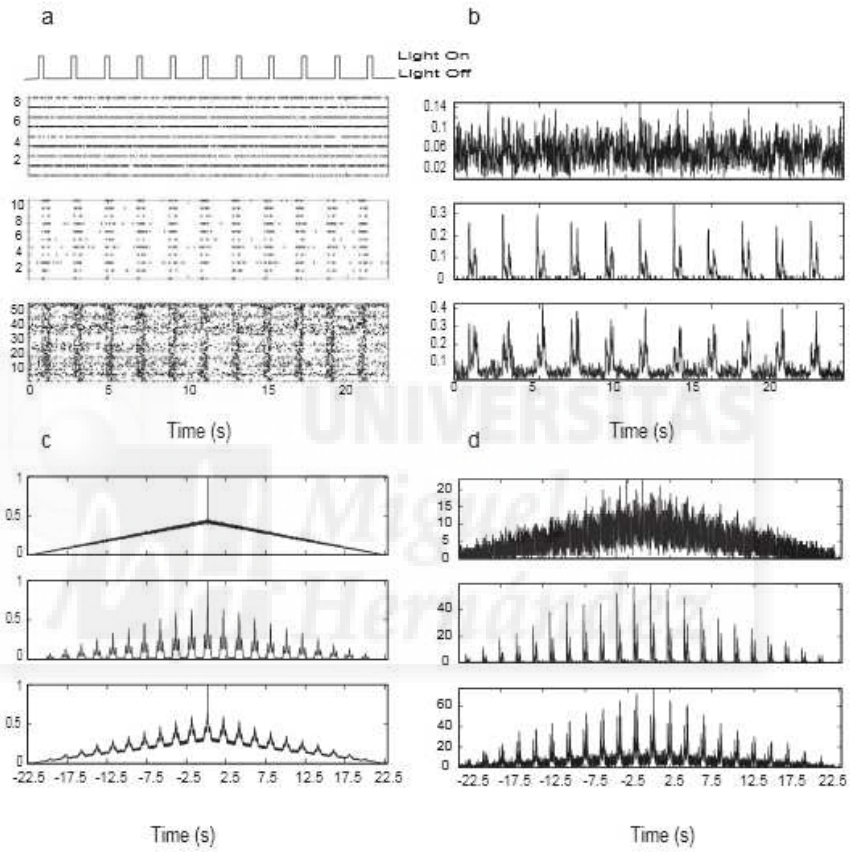

Fig. 5. Representation of the classified data by means of the PSTH approach. a) Raster plots of the three subpopulations found by defining the number of classes three. Stimulus evolution is represented in the continuous top trace. b) response populations resulting from summing up the activity across all the units in each subpopulation for every bin (5 ms). c) normalized population signal autocorrelograms and d) population signals correlated to stimulus for each filtered population

Notice that the purity of the filtered populations depends strongly on the number of classes defined. For instance, in this example three classes are not enough for getting pure ON or pure OFF subpopulations but is enough for getting predominant ON (Fig. 5b, middle subplot) and predominant OFF (Fig. 5b, lower subplot), since one class is reserved for noisy units. The ON and OFF

predominance is also noticed in Fig. 4c, middle and lower subplots respectively when showing correlated activity to stimulus.

4 Conclusions

Two different approaches for an automatic classification of electrophysiological multineuron data were developed and validated. It was established that both approaches worked satisfactorily at splitting original datasets although temporal dynamics of filtered populations vary from one approach to another. When using the autocorrelation approach, units will cluster according to its periodicity while when using the PSTH approach, they will do according to its latency response. The number of classes defined by the experimenter also contribute to the purity within each class, since the more clusters are defined, the more specificity will be achieved. The method turns out to be robust and effective whereas simple and versatile. Even though this is an automatic method, the experimenter has to keep track of the parameters applied in the processing stage as well as the number of classes that would expect to be generated at every particular case.

Acknowledgements

This research is being funded by E.C. QLK-CT-2001-00279, and Ministerio de Ciencia y Tecnologa TIC 2003-09557-C02-02.

References

1. Secker, H. and Searle, C.: Time Domain Analysis of Auditory-Nerve Fibers Firing Rates. J. Acoust. Soc. Am. 88 (1990) 1427-1436
2. Buck, L.B.: Information Coding in the vertebrate olfactory system. Ann. Rev. Neurosci. 19 (1996) 517-544
3. Fitzhugh, R. A.: A Statistical Analyzer for Optic Nerve Messages. J. Gen. Physiology 41 (1958) 675-692
4. Warland, D., Reinagel, P., Meister, M.: Decoding Visual Information from a Population of Retinal Ganglion Cells. J. Neurophysiology 78 (1997) 2336-2350
5. Fernndez, E., Ferrndez, J.M., Ammermller, J., Normann, R.A.: Population Coding in spike trains of sinultaneosly recorded retinal ganglion cells Information. Brain Research 887 (2000) 222-229
6. Tovee, M.J., Rolls, E.T., Treves, A. and Bellis, R.P.: Encoding and the Responses of Single Neurons in the Primate Temporal Visual Cortex. Journal of Neurophysiology, 70 (1993) 640-654
7. Ferrndez, J.M., Bolea, J.A., Ammermller, J. , Normann, R.A. , Fernndez E.: A Neural Network Approach for the Analysis of Multineural Recordings in Retinal Ganglion Cells: Towards Population Encoding. IWANN 99, Lecture Notes on Computer Science 1607 (1999) 289-298

8. MacQueen, J.: Some methods for classification and analysis of multivariate observations. Le Cam, L. M. and Neyman, J., editors, Proceedings of the Fifth Berkeley Symposium on Mathematical Statistics and Probability. University of California Press, Berkeley and Los Angeles, CA (1967)
9. Sim A. W. K., Jin C., Chan L. W., and Leong P. H. W.: A comparison of methods for clustering of electrophysiological multineuron recordings. IEEE Engineering in Medicine and Biology Society (1998) 1381-1384
10. Jones, K.E., Campbell, P.K. and Normann, R.A.: A glass/silicon composite intracortical electrode array. Annals of Biomedical Engineering 20 (1992) 423-437

UNIVERSITAS
Miguel
Hernández

ELSEVIER

Journal of Neuroscience Methods 148 (2005) 137–146

JOURNAL OF NEUROSCIENCE METHODS

www.elsevier.com/locate/jneumeth

DATA-MEAns: An open source tool for the classification and management of neural ensemble recordings

María P. Bonomini[a], José M. Ferrandez[a,b], Jose Angel Bolea[a], Eduardo Fernandez[a,*]

[a] *Instituto de Bioingeniería, Universidad Miguel Hernández, Elche, Spain*
[b] *Department Electrónica y Tecnología de Computadores, University Politécnica de Cartagena, Spain*

Received 24 January 2005; received in revised form 19 April 2005; accepted 22 April 2005

Abstract

The number of laboratories using techniques that allow to acquire simultaneous recordings of as many units as possible is considerably increasing. However, the development of tools used to analyse this multi-neuronal activity is generally lagging behind the development of the tools used to acquire these data. Moreover, the data exchange between research groups using different multielectrode acquisition systems is hindered by commercial constraints such as exclusive file structures, high priced licenses and hard policies on intellectual rights. This paper presents a free open-source software for the classification and management of neural ensemble data. The main goal is to provide a graphical user interface that links the experimental data to a basic set of routines for analysis, visualization and classification in a consistent framework. To facilitate the adaptation and extension as well as the addition of new routines, tools and algorithms for data analysis, the source code and documentation are freely available.

Keywords: Multielectrode recordings; Microelectrode arrays; Data classification; Open-source toolbox

1. Introduction

To achieve a better understanding of the parallel information processing that takes place in the nervous system, many researchers have recently begun to use multielectrode techniques to obtain high spatial- and temporal-resolution recordings of the firing patterns of neural ensembles. These techniques have been used to demonstrate that a population code can provide a more accurate prediction of performance than the individual elements that constitute the population (Ferrandez et al., 1999; Meister, 1996; Warland et al., 1997). However, besides the difficulties of acquiring and storing single unit responses from large numbers of neurons, the standard techniques for the analysis of the neuronal activity recorded simultaneously with numerous electrodes are often insufficient to detect and represent the complexities of neural ensemble data. On the other hand, although it is widely accepted that our understanding of neural coding, information transmission and brain processes would be aided if such data could be shared among individual laboratories (Gardner, 2004), the data exchange between research groups using different multielectrode acquisition systems is hindered by commercial constraints such as exclusive file structures, high priced licenses and hard policies on intellectual rights. Furthermore some commercial software tends to have only limited possibilities to incorporate new tools or to modify existing ones and share them with colleagues (Egert et al., 2002).

To facilitate the analysis of multielectrode data several freely available tools have been developed, but most of them are only intended to very specific processing task such as spike sorting (Bongard et al., 2004; Segev, 2000; Shoham et al., 2003) or on-line detection of spike amplitudes (Gholmieh, 2004). Only one general-purpose toolbox based on Matlab environment has been developed for the analysis of multielectrode data (Egert et al., 2002), but it is mostly oriented to the analysis of files recorded with MCRack (Multi Channel Sys-

* Corresponding author at: Universidad Miguel Hernández, Department of Histology and Institute of Bioengineering, Fac. Medicina, San Juan 03550, Alicante, Spain. Tel.: +34 96 591 9439; fax: +34 96 591 9434.
E-mail address: e.fernandez@umh.es (E. Fernandez).

0165-0270/$ – see front matter © 2005 Elsevier B.V. All rights reserved.
doi:10.1016/j.jneumeth.2005.04.008

tems, Reutlingen, Germany). Thus, there is a need to develop standards for data archiving and tools that allow users to share and analyse data acquired with different hardware systems.

This report introduces a new free open-source software for the classification and management of neural ensemble data. It works on ASCII files, since all commercial systems offer the option of translating their binary files to ASCII. The main idea is to supply a graphical user interface that links the experimental data to a basic set of routines for analysis, visualization and classification in a consistent framework. As an example of its possibilities, it incorporates a dedicated algorithm for noise reduction and simplification of the data based on the occurrence of conditioned spikes within a temporal window, providing a basic method of evaluating high-order neural interactions (Ortega et al., 2004). To facilitate the adaptation and extension as well as the addition of new routines, tools and algorithms for data analysis, the source code and documentation are freely available. Furthermore, although the program includes its own graphics, it also has the option of exporting the data in ASCII format for using by any other graphical, mathematical or statistical package.

2. Methods

2.1. Experimental procedures

Extracellular recordings were obtained from ganglion cell populations in isolated superfused albino rabbit (*Oryctolagus cuniculus*) retina using a rectangular array of 100, 1.5 mm long electrodes, as reported previously (Fernández et al., 2000; Normann et al., 2001; Ortega et al., 2004). Briefly, after enucleation of the eye, the eyeball was hemisected with a razor blade, and the cornea and lens were separated from the posterior half. The retinas were then carefully removed from the remaining eyecup with the pigment epithelium, mounted on a glass slide ganglion cell side up and covered with a Millipore filter. This preparation was then mounted on a recording chamber and superfused with bicarbonate-buffered Ames medium at 35 °C.

For visual stimulation we used either an optical bench with a standard halogen (100 W) light source, neutral density and interference color filters, or a 17″ NEC high-resolution RGB monitor. Pictures were focused with the help of lens onto the photoreceptor layer. The retinas were flashed periodically with full field white light whereas the electrode array was lowered into the retina until a significant number of electrodes detected light evoked single- and multi-unit responses. This allowed us to record with 60–70 electrodes (on average) during each experiment. The retinas were then stimulated with different spatio-temporal patterns.

The electrode array was connected to a 100 channel amplifier (low and high corner frequencies of 250 and 7500 Hz) and a digital signal processor based data acquisition system. Neural spike events were detected by comparing the instantaneous electrode signal to level thresholds set for each data channel using standard procedures described elsewhere (Fernández et al., 2000; Normann et al., 2001; Shoham et al., 2003). When a supra-threshold event occurs, the signal window surrounding the event is time-stamped and stored for later, offline analysis. All the selected channels of data as well as the state of the visual stimulus were digitized with a commercial multiplexed A/D board data acquisition system (Bionic Technologies Inc.) and stored digitally.

For spike sorting we used a free program, NEV2kit, which has been recently developed by our group (Bongard et al., 2004) and runs under Windows, MacOSX and Linux (source code and documentation is freely available at: http://nev2lkit.sourceforge.net/). NEV2kit load multielectrode data files in various formats (ASCII based formats, LabView formats, Neural Event Files (NEV), etc.) and is able to sort extracted spikes from large sets of data. Furthermore, it incorporates tools to identify noise and review individual and groups of spikes. The sorting is done using principal component analysis (PCA) and can be performed simultaneously on many records from the same experiment.

For testing the software capabilities we also used multielectrode recordings that were acquired using other multichannel neural acquisition systems. Thus we used in vivo extracellular recordings provided by Dr. Sanchez-Vives (Institute of Neuroscience, University Miguel Hernández, Alicante, Spain) that were acquired using the Spike 2 system (Spike2 software, CED, Cambridge, UK), data collected using a Multi-Neuron Acquisition Processor (Plexon, Dallas, TX), recordings using barreled micropipettes (De Labra et al., 2005) and recordings from rat somatosensory cortex performed with a customized 16-channel system integrated with an A/D card (National Instruments, PCI_6059M Series).

2.2. Software

The graphical user interface (GUI) of DATA-MEAns was written in Delphi 7.0 (Borland), and designed to make internal calls to stand-alone applications developed in Matlab 6.1 for most of the processing routines. This architecture facilitates the incorporation of new routines, minimizing the work required to change the source code. The software was successfully tested on Windows 98, Windows 2000 and Windows XP, although in principle it is compatible with any Windows operative system without need of any version of Matlab installed.

Following the general-purpose design, we tried to maximize the flexibility allowing the user to:

(i) Select the number of electrodes in the array expressed as number of electrodes along the x- and y-axis. This feature is optimised for rectangular array layouts, but it could be easily adapted to hexagonal or other array shapes.
(ii) Specify the convention and the values used for the monitoring of the stimulus. Specific labels marking stimulus changes or experiment information can be freely defined by the user.

(iii) Configure the units used in the analysis. By default the software loads all the electrodes and units, but they can be individually selected or removed. The settings are configured in the electrode configuration panel and keep for all the later analysis.
(iv) Decide on the number of plots per page. If this feature is the same as the array layout, then direct spatial information can be inferred.
(v) Select the number of classes or groups for the classification algorithm so that "similar" units are in the same class. This maybe useful for data reduction.

2.3. File interface

DATA-MEAns works on ASCII files since all commercial and conventionally used systems offer the option of translating their binary or proprietary formats into an ASCII text file. The input files can contain two columns (separated by tabulations or spaces) or be arranged in a multicolumn table of timestamps where each column in the text file represents either a unit or a stimulus epoch.

Fig. 1A shows an example of the two-columns format for an experiment where the retina was stimulated with random flicker stimulation (Warland et al., 1997). The first column contains the stimulus code or the electrode on which the spike occurred, and the second column the time stamps. According with most used procedures, neural events are identified as XXX.YY where XXX is the channel on which the spike occurred and YY is the unit designation resulting from the spike sorting algorithm. Fig. 1B, displays an example of the multicolumn table of timestamps format. The first element in each column is the neuron identifier (sigXXX*i*), where XXX is the channel descriptor and *i* is the unit derived from the spike sorting algorithm. Last column contains experiment or stimulus information.

2.4. Program structure

The program is structured in three main blocks, *Display, Conditioned Spikes Analysis and Classification,* each designed to perform a specific task, and a principal program which directs the flow of operations. Fig. 2 shows the workflow for the most common routines used with a particular data set.

2.5. Editing and filtering processed units

When recordings are taken from microelectrodes implanted in neural tissues, many electrode channels typically show the activities of more than one neuron. Quite often it is required to trust in spike sorting methods whose accuracy is critical for all subsequent analysis. Thus, even though there have been proposed many sorting algorithms, still arise problematic topics as the variability in the results depending on the

	Channel.unit	Timestamps
stimulus onset --->	2000.0	1.928340
	46.3	1.928390
	56.3	1.939700
	52.2	1.940000
stimulus offset --->	1000.0	1.942939
	94.1	1.943970
	85.0	1.947230
stimulus onset --->	3000.0	1.947360
	73.3	1.947670
	46.2	1.947730
	43.3	1.948370
stimulus offset --->	1000.0	1.950530
	94.0	1.951470
	82.2	1.959870
stimulus onset --->	4000.0	1.967300

(A)

Unit/stimulus identifier --->	sig001a	sig001b	sig002a	sig002b	sig002c	Event001
Timestamps --->	1.018425	0.703250	1.466025	0.756875	2.014850	0.131700
	2.939800	0.821375	1.699325	1.198375	2.790350	0.241700
	2.941375	1.012375	1.977825	1.247950	2.883825	0.351700
	2.973200	1.175200	1.993850	1.303250	2.931225	0.461700
	3.065275	1.186975	2.198825	1.375125	3.270975	0.571700
	3.111275	1.233850	2.262175	1.516125	3.355675	0.681700
	3.985125	1.501150	2.571175	1.902375	3.369850	0.791700
Timestamps --->	3.991775	1.647175	2.882225	1.927200	3.371575	0.901700

(B)

Fig. 1. Input ASCII files. (A) Two-columns format. The left column contains the stimulus code or the electrode on which the spike occurred. By default, numbers under 1000 are interpreted as channel identifiers, whereas numbers equal or greater than 1000 are interpreted as experiment or stimulus codes, but the user can specify customized values in the *General Settings* dialog. Right column contains the timestamps in seconds or time ticks. (B) Multicolumn table of timestamps format. The first line of the file contains the names of all the variables (see text). Data aligned under the columns are numbers representing the neuron firing time (or event time) in seconds or in time ticks.

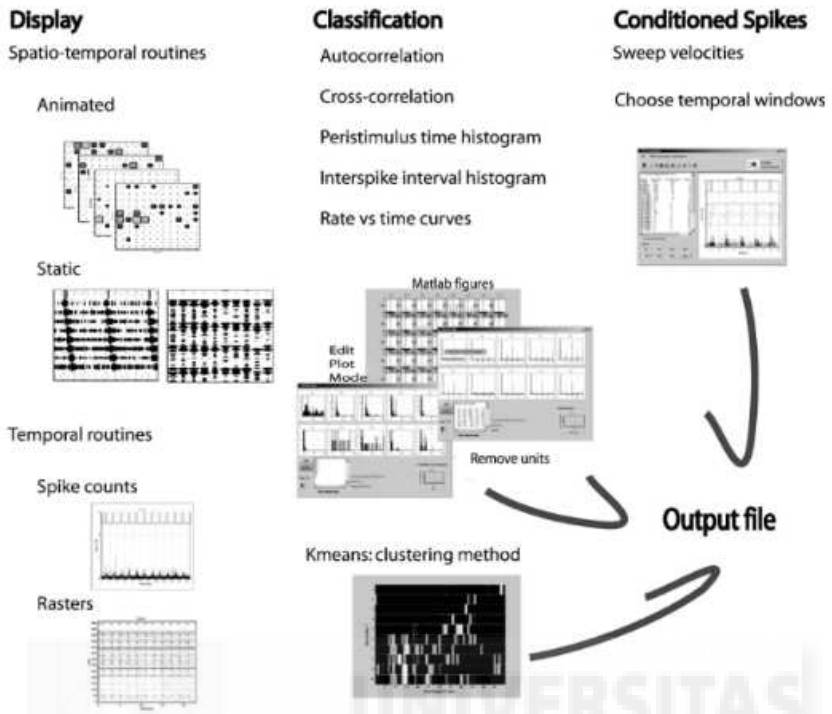

Fig. 2. Program workflow. Screenshots are taken from the program to illustrate the main analysis and routines.

applied method, the effects of spike overlap, the geometry and number of electrodes of the array, etc. (Brown et al., 2004). To facilitate the analysis DATA-MEAns permits to select and/or remove the units and electrodes that will be used in all subsequent analysis. This utility has a double purpose, since it also allows a different way of generating specific populations following well-defined temporal patterns. In addition the classification block can act as a powerful filter that operates on groups of units resulting from these automatic methods.

3. Results

3.1. Display

An important feature of multiple recording methods, besides the simultaneous temporal information supplied by different neurons, is the spatial or anatomical information that can be related to the position of each electrode in the tissue. Thus, in multielectrode experiments it is often desirable to review the results of the recordings with respect to the geometry of the multielectrode array. In order to facilitate these analyses the visualization block has two main branches. One totally aimed at dealing with the timing of the spikes or events, like conventional rasters plots or spike counts, and a second one, which allows to relate spatial and temporal information. Furthermore DATA-MEAns permits to process and represent all the recorded units or just a sub-sample of the whole recording and view the data on user-controlled expanded or contracted time scales.

The display functions allow to represent the results as: (a) the levels of activation in each electrode in an animated frame by frame sequence (a frame is defined as a picture of the electrodes with their activation levels coded in colour and size within the array at a certain time) or (b) the levels of activation across a subset of electrodes in the multielectrode array through a certain time. This subset is delimited by a set of electrodes that define a geometrical element within the array, such as columns, rows or diagonals and works with any type of data as long as it can be represented in a numeric $M \times N$ matrix. As an example, Fig. 3 shows the simultaneously recorded extracellular responses to several consecutive and identical full field white flashes (top trace). Here, a 10 column array is processed along 15 s of regular light flashes applied every 2 s (bin size = 0.06 s). Note that what it is represented in this example is the activity of certain geometrical relation in the array, columns in this case, along a time axis. The routine builds up a population vector composed of the sum over some bin time and among all the units of each column on the electrode array and plots this vector over the time frame given by the user (whole experiment or from a start-time until an end-time). The temporal evolution of each column in the array is represented using a modified hintonw procedure where the levels of activity are represented by changes in size and colours. To simplify the visualization, all the single units derived from a particular channel are

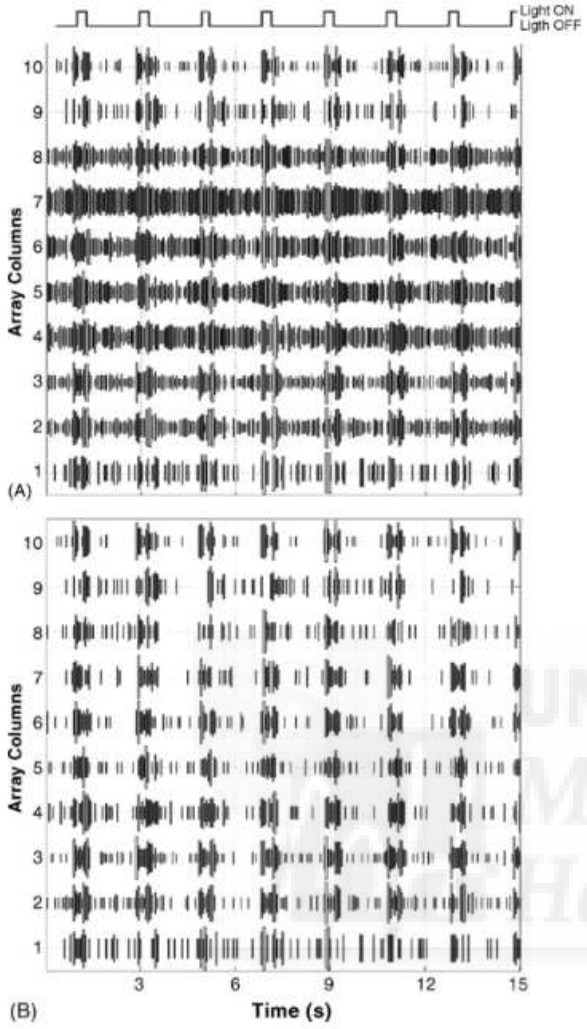

Fig. 3. Output of the display block illustrating the temporal levels of activation across a subset of electrodes through a certain time. In this example, a 10 columns array is processed along 15 s (bin = 0.06 s) of regular light flashes applied every 2 s; (A) raw data. Note the increase of activation (brighter colour and widening of the columns) every 2 s. (B) The same plot after using the edit mode function to remove all those units whose autocorrelograms did not follow a 0.5 Hz pattern. Notice the decrease in the background activity from the raw activity (e.g. columns 4–7). Continuous top trace shows the timing of light stimulus.

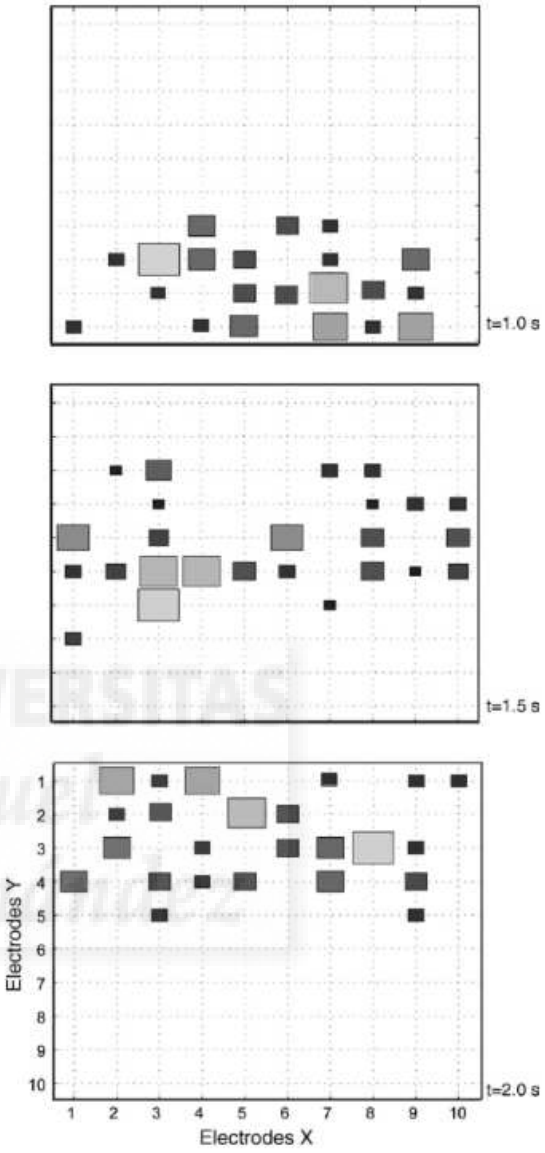

Fig. 4. Example of the animated frame by frame visualization. A sequence of three frames show the response to an upwardly moving bar at different times. Size and colour brightness represent the observed firing rate at a particular electrode location in the array.

represented at the same electrode position. Otherwise, the overlapping of signals in a poorly defined space would hinder the achievement of clear spatio-temporal representations within the array and would blur their advantages.

Fig. 4 shows the responses of a cell ensemble to upwardly moving horizontal bar using the "frame by frame" visualization. Here the temporal evolution of the whole array can be followed in a bin-by-bin animated sequence. The bin size is a user-defined feature and the routine also allows to scan the whole recording or just a period of time between a start-time and an end-time. Again, a colour and size scale grade the firing rate levels at each particular electrode location.

3.2. Classification

In many anatomical structures, it is well known the existence of neurons whose firing patterns are clearly differentiated or depend strongly on the stimuli applied. For instance the tonic and bursting neurons in the basal forebrain (Nunez, 1996), the low-frequency and high-frequency cells in the nucleus gracilis (Panetsos et al., 1997), or the ON, OFF and ON–OFF cells in the retina (Chichilnisky and Kalmar, 2002; Famiglietti and Kolb, 1976). All of them coexists in the same-recorded structure and although the labour involved in the separation of physiologically different

recordings is reasonable if only a few electrodes are used, often requires a considerable amount of time. Thus the problem arises when a significant number of electrodes is used in the recordings. Although the cluster boundaries can be set by hand, the question is how to set them automatically, or better yet optimally. At this point, a tool to facilitate the creation of sub-groups or sub-populations within a given population turns out to be important.

The classification function allows to identify classes or groups of units that behave similarly with respect to a selected spike train analysis method (Rieke et al., 1997). The basic analysis routines, which are actually implemented for the classification tasks are autocorrelations, correlations with stimulus, post-stimulus time histograms (PSTHs), rate curves and interspike interval histograms (ISI). The procedure to achieve the classification is as follows. First the user has to define a predetermined maximum number of groups. Then a spike train analysis method is chosen (i.e., autocorrelations, perievent histograms, rate curves, PSTHs, ISIs, etc.) and the output of this procedure feeds a clustering method, which uses the nearest neighbour or k-means approach. This is a simple clustering method that decomposes the data set into a set of disjoint clusters and then minimizes some measure of dissimilarity in the samples within each cluster, while maximizes the dissimilarity of different clusters. The measure of dissimilarity used in this algorithm is the average squared distance of the data items from their nearest cluster centroids (MacQueen, 1967). This defines a set of implicit decision boundaries that separate the clusters or groups of units according to the selected analysis method (for instance according to their periodicity when clustering their autocorrelations or according to its response delay when clustering their PSTHs). The result is that groups of relatives are formed into classes that are a subset of the entire array. These groups can be exported to an ASCII file for later analysis. Fig. 5 shows an example of five different classes, each containing three units, clustered according to their autocorrelograms. A bin size of 50 ms and a maximum lag of 200 were used for the autocorrelation routines. Notice the coherence among all the units belonging to a same class. Although we chose five classes, the user can specify a different number of groups depending on their particular needs.

With the aim to investigate if the implemented analysis routines were able to extract different subpopulation of cells we used several filters to identify ON and OFF retinal ganglion cells. Fig. 6 shows an example using the PSTH method. For the ON cells, we select all the units whose PSTH peaks fell within the ON period of the light. For the OFF cells we chose those units whose PSTH peaks fell within the OFF period of the stimulus. To test that no changes in the temporal dynamics of the data are produced when filtering, we computed the correlation of the original population response with the stimulus and did the same with the ON-filtered and OFF-filtered populations (Fig. 7). As it can be seen, the three populations shared the same temporal dynamics.

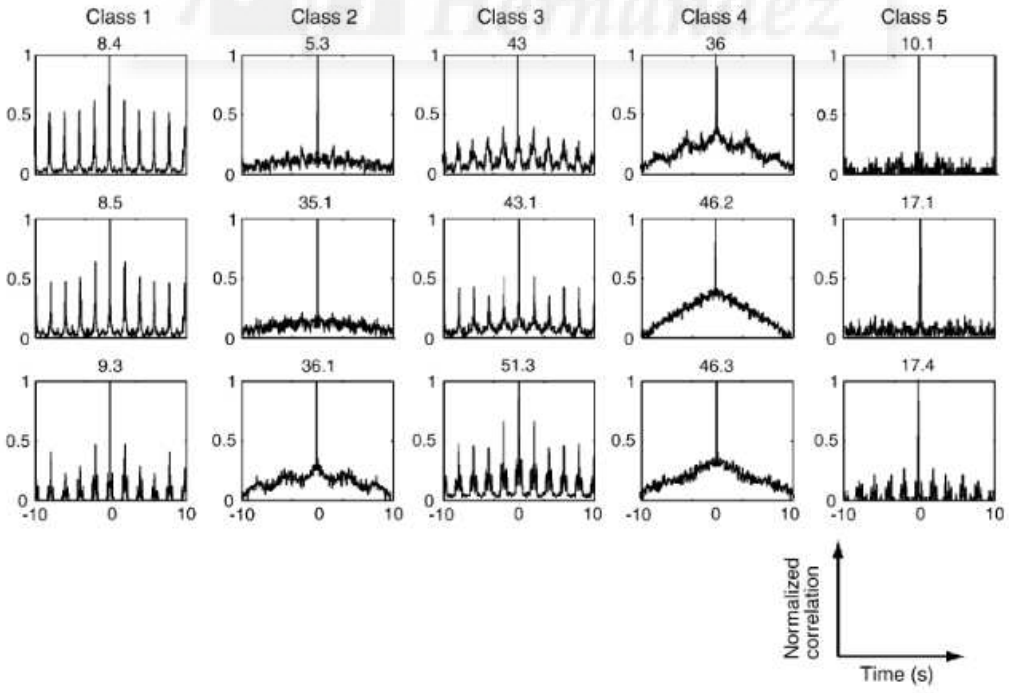

Fig. 5. Classification block. Each column shows a set of units according to the output of the clustering method. In this case, the relatives consisted of autocorrelated units (bin size: 50 ms and lag max: 200) clustered into five different classes. For simplicity, only three units belonging to each class are shown. Class numbers are indicated on top of each column. Unit identifiers are represented as the legends on top of the autocorrelograms panels.

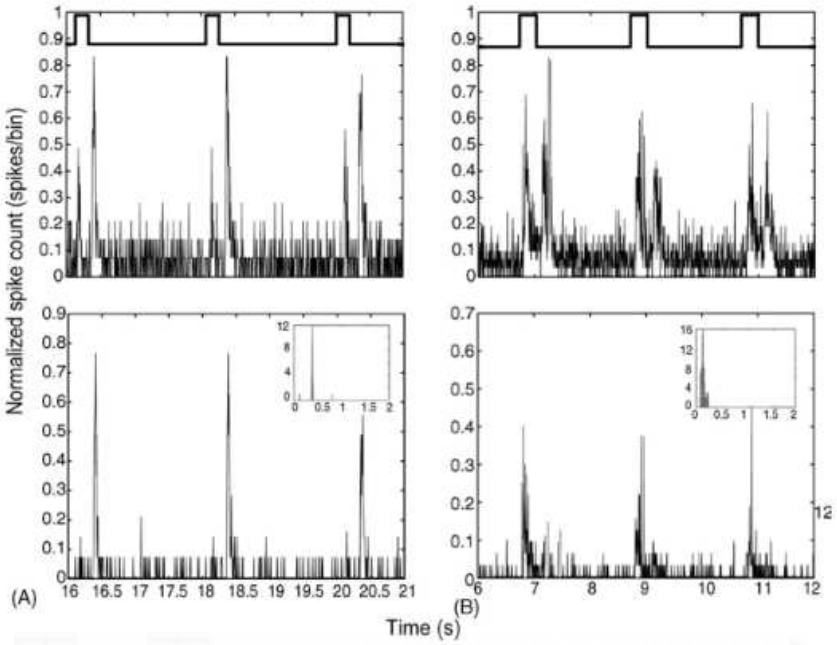

Fig. 6. Selection of units with a particular behaviour. Upper panels show the population responses to several consecutive and identical flashes of light with a light ON period of 200 ms (A) and 300 ms (B). Lower panels show the extracted OFF (A) and ON (B) ganglion cell populations after removing from the dataset all the units whose PSTHs did not present a clear OFF and ON response. Insets on the lower panels show the OFF and ON templates on which we based our selection.

3.3. Conditioned spikes analysis

As an example of the possibilities to implement new code and routines, DATA-MEAns incorporates a new representation of spiking dynamics in multielectrode recordings based on event synchronization. Whereas detailed discussion and application of the algorithm is available elsewhere (Ortega et al., 2004; Quian Quiroga et al., 2002) here we briefly describe for those unfamiliar with the technique the basis of the method. The algorithm consists of finding events that

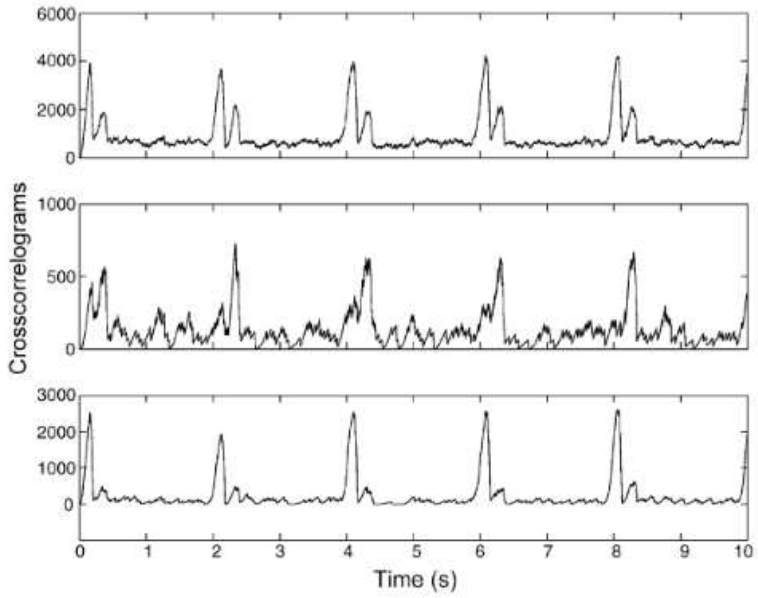

Fig. 7. Preservation of the temporal dynamics after filtering the data. Upper panel: original population response correlated to a periodic stimulation with a 300 ms ON period. Middle panel: filtered OFF population response correlated to the same stimulus. Lower panel: filtered ON population response correlated to the same stimulus. Note the correspondence in the timings for the ON and OFF peaks of activity between the filtered and original populations.

occur within different temporal windows among two or more cells. The events we consider are conditioned spike times, where the condition we impose is the presence of another spike in its temporal vicinity.

In the case of neural ensemble recordings, we call t_i^x the time of the spike i from the x cell. In this way we have a multivariate, discrete time series with the information about the spiking dynamics of the neurons. Now, we shall define new events, τ_i^x, using the above information. Thus the times of these new events are such that:

$$\tau_k^x = t_i^x,$$
$$\text{if } T_1 < (t_i^x - t_{i-1}^x) < T_2 \text{ with } i = 2, m_x, k = 1, n_x \qquad (1)$$

where m_x is the number of spikes the cell x has fired and n_x is the number of events of that cell. Note that index k is incremented every time a new event shows up. The above procedure select discrete "events" between interspike intervals (ISI's) $T_1 = \text{ISI}_{\min}$ and $T_2 = \text{ISI}_{\max}$ and allows to investigate the behavior of multielectrode recordings for different ISIs values. Fig. 8 shows an example of simultaneously recorded extracellular responses to several consecutive and identical full field white flashes (top trace). Close inspection of the firing patterns shows some degree of variability in the responses of each cell to repeated stimulation, introducing uncertainty in the code. Furthermore some cells seem to fire more or less constantly, irrespective of the stimuli. Lower panel of Fig. 8 shows the conditioned events for a window of $\text{ISI}_{\min} = 4$ ms and $\text{ISI}_{\max} = 10$ ms. Each dot represents a spike and its corresponding time with the condition that there must be another precedent spike temporally close to it. Comparing spikes (Fig. 8, upper panel) with conditioned spikes (Fig. 8, lower panel), it can be seen that these events seem to better correlate with the stimuli (top trace), even for those cells with high firing rates. Moreover, the signal to noise ratio (SNR) is highly increased in the latter case. Thus, this procedure allows to study the correlation of different events with the stimuli. Moreover, the method can be also used as a different way of filtering or reducing the noise in the raw recordings.

In order to test that this way of filtering populations gives an equivalent information to that of original populations, we analysed the correlated activity of the different subpopulations in response to light stimulation. Fig. 9 shows the cross-correlograms for the raw spike population (continuous line) and the conditioned spike population (dashed line) for a temporal window of 4–10 ms. Populations were built up by summing the number of spikes of all of the ganglion cells in the recording using non-overlapped bins of 5 ms. The results show that filtered cell responses are within the expected times.

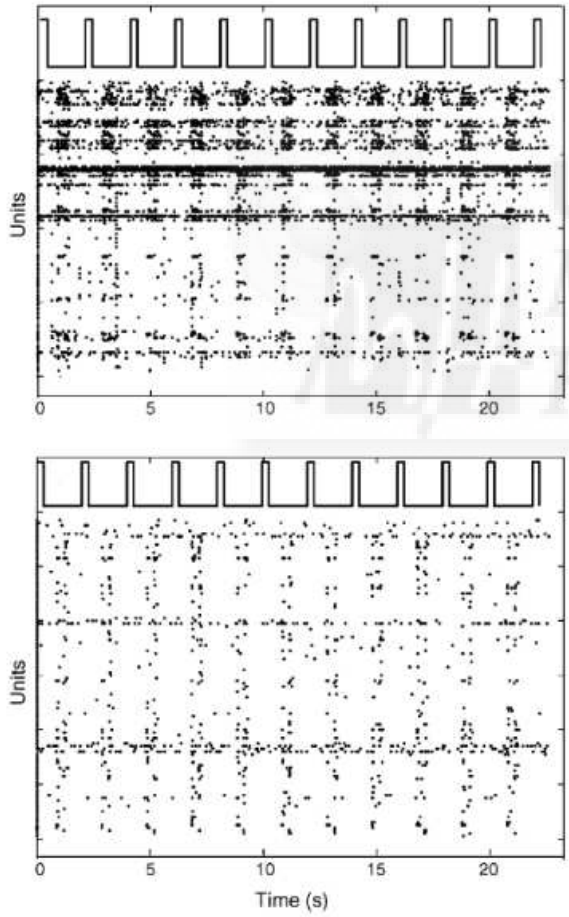

Fig. 8. Simultaneously recorded extracellular responses from a population of retinal ganglion cells to 12 consecutive and identical flashes. Upper panel shows the recorded neuron responses. Lower panel shows the conditioned spikes plot. Each dot represent a spike under the condition that there exist another preceding spike, with a temporal range of 4–10 ms, belonging to the same cell. Although each dot represent a single spike (upper panel) or conditioned spike (lower panel), sometimes spikes that are very close could appear as a single dot due to the printed graph resolution. Top traces show the timing of light stimulus.

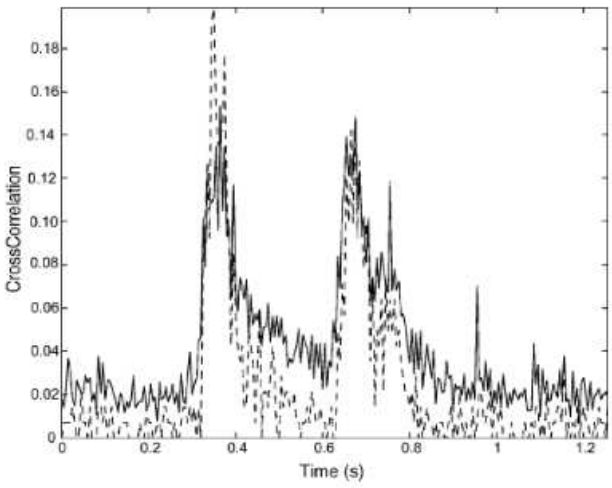

Fig. 9. Correlated activity in response to a periodic stimulus for recorded spikes (continuous line) and conditioned spikes with ISIs in between 4 and 10 ms (dashed line).

4. Discussion

Data sharing requires agreement on techniques and formats, as well as methods for classification and selection, therefore DATA-MEAns provide several visualization and analysis routines, which permit to classify and reduce original datasets for further specific processing. Furthermore to facilitate the adaptation to any particular requirement as well as the addition of new routines, tools and algorithms for data analysis, the source code and documentation is freely available. We hope that it will help new contributors to add functions that are currently not included and that it could be useful for further analysis that allow integrate and compare findings from individual laboratories as well as test new hypothesis.

DATA-MEAns can read ASCII files created by popular data acquisition systems. These files can be easily created and edited using a word processor or any other program for editing text files. Although working with binary files allows to compress information with an optimisation of the memory space used for storage, this approach would require huge and continuous efforts to put together all different file formats, reading them, and updating the "read modules" since the commercial acquisition systems often upgrade their native data files. Moreover, many laboratories use home-made acquisition systems, being excluded from using most of the commercially available software. Our goal is that this toolbox can be useful to the development of standards, all in a common format, which support multiplatform assembly, upload, annotation, search and acquisition that will ease reanalysis of shared data by permitting data upload from within data acquisition applications, and data download directly to standard acquisition routines.

The design based on stand-alone applications offers great flexibility and independence from any other commercial software and represents an easy mechanism for adding new routines altering minimally the source code. This can be particularly useful when the researcher uses their own custom scientific programs. Thus it is possible to write the desired algorithm using a known language, make an executable and link it to the DATA-MEAns application by means of the ShellApi utility from Windows.

Finally, this application was intended only for a preliminary pre-processing of the data, hence only the most generally used routines are implemented. We are aware that numerous functions currently in use, as well as advanced functions used in various labs working with multielectrode data are not included. We hope that the facilities to extend the code and add more specific algorithms and routines can compensates the former and encourages the users to contribute providing ready-made functions useful to the scientific community. Thus, the program and source code are available free of charge upon request from the first author of this paper (email: p.bonomini@umh.es) or directly from the following URL: http://cortivis.umh.es (under the software menu), to academic researches interested in using or enhancing DATA-MEAns.

Acknowledgements

We are very grateful to Markus Bongard for data sharing and helpful advice. We thank Drs. Sanchez-Vives and Carmen De Labra for sharing their multielectrode recordings. This research has been carried out with financial support from the Commission of the European Communities, specific RTD programme "Quality of Life and Management of Living Resource", contract QLK6-CT-2001-00279 and by a Ministerio de Ciencia y Tecnología grant TIC2003-09557-CO2-02.

References

Bongard M, Micol D, Fernandez E. Nev2lkit: a tool for handling neuronal event files; 2004. Available at: http://nev2lkit.sourceforge.net/.

Brown E, Kass R, Mitra P. Multiple neural spike train analysis: state-of-the-art and future challenges. Nat Neurosci 2004;7:456–61.

Chichilnisky EJ, Kalmar R. Functional assimetries in ON and OFF ganglion cells of primate retina. J Neurosci 2002;22:2737–47.

De Labra C, Rivadulla C, Cudeiro J. Modulatory effects mediated by metabotropic glutamate receptor 5 on lateral geniculate nucleus relay cells. Eur J Neurosci 2005;21:403–10.

Egert U, Knott Th, Schwarz C, Nawrot M, Brandt A, Rotter S, et al. MEA-Tools: an open source toolbox for the analysis of multi-electrode data with Matlab. J Neurosci Meth 2002;117:33–42.

Famiglietti EV, Kolb H. Structural basis for ON- and OFF-center responses in retinal ganglion cells. Science 1976;194:193–5.

Fernández E, Ferrandez J, Ammermuller J, Normann RA. Population coding in spike trains of simultaneously recorded retinal ganglion cells. Brain Res 2000;887:222–9.

Ferrandez JM, Ammermuller J, Normann RA, Fernandez E. Management of color and luminance information by a network of ganglion cells in turtle retina. Lect Notes Comput Sci 1999;1607:289–98.

Gardner D. Neurodatabase.org: networking the microelectrode. Nat Neurosci 2004;7:486–7.

Gholmieh G. An algorithm for real-time extraction of population EPSP and population spike amplitudes from hippocampal field potential recordings. J Neurosci Meth 2004;136:111–21.

MacQueen J. Some methods for classification and analysis of multivariate observations. In: Le Cam LM, Neyman J, editors. Proceedings of the Fifth Berkeley Symposium on Mathematical Statistics and Probability. Berkeley and Los Angeles, CA: University of California Press; 1967. p. 281–97.

Meister M. Multineuronal codes in retinal signalling. Proc Natl Acad Sci USA 1996;93:609–14.

Normann RA, Warren DJ, Ammermuller J, Fernandez E, Guillory S. High-resolution spatio-temporal mapping of visual pathways using multi-electrode arrays. Vision Res 2001;41:1261–75.

Nunez A. Unit activity of rat basal forebrain neurons: relationship to cortical activity. Neuroscience 1996;72:757–66.

Ortega G, Bongard M, Louis E, Fernandez E. Conditioned spikes: a simple and fast method to represent rates and temporal patterns in multielectrode recordings. J Neurosci Meth 2004;133:135–41.

Panetsos F, Nunez A, Avendano C. Electrophysiological effects of temporary deafferentation on two characterized cell types in the nucleus gracilis of the rat. Eur J Neurosci 1997;9:563–72.

Quian Quiroga R, Kreuz T, Grassberger P. Event synchronization: a simple and fast method to measure synchronicity and time delay patterns. Phys Rev E 2002;66:0419041–9.

Rieke F, Warland D, de Ruyter van Stevenick R, Bialek W. Spikes: exploring the neural code. New York: MIT Press; 1997.

Segev R. Detection and sorting of neural spikes using wavelet packages. Phys Rev Lett 2000;85:4637–40.

Shoham S, Fellows M, Normann R. Robust, automatic spike sorting using mixtures of multivariate t-distributions. J Neurosci Meth 2003;127:111–22.

Warland DK, Reinagel P, Meister M. Decoding visual information from a population of retinal ganglion cells. J Neurophysiol 1997;78:2336–50.

Towards the Reconstruction of Moving Images by Populations of Retinal Ganglion Cells

Ariadna Díaz-Tahoces[1(✉)], Antonio Martínez-Álvarez[2], Alejandro García-Moll[1], Lawrence Humphreys[1], José Ángel Bolea[3], and Eduardo Fernández[1]

[1] Institute of Bioengineering and CIBER BBN, University Miguel Hernández, Alicante, Spain
adiaz@goumh.umh.es, e.fernandez@umh.es
[2] Department of Computer Technology, University of Alicante, Alicante, Spain
amartinez@dtic.ua.es
[3] Department of Materials Science and Engineering and Chemical Engineering. University Carlos III. Madrid, Spain

Abstract. One of the many important functions the brain carries out is interpreting the external world. For this, one sense that most mammals rely on is vision. The first stage of the visual system is the image processing whose capture takes place in the retina. Here, photoreceptors cells transform light into electrical impulses that are then guided by amacrine, bipolar, horizontal and some glial cells up to the ganglion cells layer. Ganglion cells decode the visual information to be interpreted by the visual cortex. The understanding of the mechanism for decoding the visual information is a major task and challenge in neuroscience. This is especially true for images that change with time, for example during movement. For this purpose, extracellular recordings with a 100 multi-electrode-array (MEA) were carried out in the retinal ganglion cells layer of mice. Different moving patterns and actual images were used to stimulate the retina. Here, we present a new strategy for analysis over the spike trains recorded allowing the reconstruction of the actual stimuli with a reduced number of ganglion cell responses.

Keywords: Retina · Ganglion cells · Natural scene · Receptive fields

1 Introduction

Presently, how the nervous system interprets the outside world using neural messages through a sensory circuit remains a major challenge in neuroscience [1]. In vision, a light stimulus is transduced into an electrical impulse via the photoreceptors. This signal is then transmitted to the inner nuclear and ganglion cell layer which carry out the initial decoding of the stimulus [2].This information is then transmitted through the optic nerve to the visual cortex for further processing.

Normally, visual sensory neurons are characterized in a laboratory setting by their preference to light or dark, intensity, direction and receptive fields. However,

J.M. Ferrández Vicente et al. (Eds.): IWINAC 2015, Part I, LNCS 9107, pp. 220–227, 2015.
DOI: 10.1007/978-3-319-18914-7_23

this has usually been determined using simplified black and white stimuli as a representation of the real world. This is in contrast to the color and motion that we experience.

The problem is not in simulating a realistic visual signal; rather it lies in the interpretation of the various levels of decoding that is concurrently being carried out in the retinal layers [3][4]. This is in part due to the complexity of the signal as well as the many variables that modulate the electrical responses.

For this complicated task we have combined two methods, extracellular recordings from ganglion cell evoked responses under light stimuli using a MEA and a custom designed software to reconstruct complex visual stimuli.

Our software locates the receptive field of each cell based on the response to a moving bar crossing the visual field in 8 orthogonal directions. From this data we can identify their receptive field. Using this information we apply a visual stimuli composed from a natural scene and correlate electrical responses to this image. This allows us to accurately reconstruct our image using only the ganglion cell responses.

This novel method can be used as a tool to characterize electrical responses to complex visual stimuli. Here, we demonstrate with as little as 11 cells we can reconstruct natural images.

2 Material and Methods

Retina Preparation

Wild-type (C57BL/6J strain) mice were bred within a local colony established from purchased breeding pairs (Jackson Laboratories). Following anesthesia with 4% of isoflurane (IsoFlo®, Esteve Veterinaria) inhalational, cervical dislocation was performed. Then both eyes were removed. Animals were dark-adapted for one hour prior to sacrifice. All the experimental procedures were carried out in accordance with the ARVO and European Communities Council Directives (86/609/ECC) for the use of laboratory animals.

The cornea and lens were removed and discarded from the eyeball by a transverse cut along the *ora serrata* with a razor blade. Then, the retinas were removed from the remaining eyecup with the pigment epithelium and mounted on an agar plate with the ganglion cell side facing up. Finally, the tissue was covered with a piece of nitrocellulose paper in order to fix it and maintain the correct moisture. This paper had a small window cut into it to allow placement the electrode on the retinal ganglion cells layer.

This preparation was then mounted on a recording chamber, superfused with oxygenated Ringer medium (124mM NaCl, 2.5mM KCl, 2mM $CaCl_2$, 2mM $MgCl_2$, 1.25mM NaH_2PO_2, 26mM $NaCHO_3$ and 22mM Glucose) at physiological temperature.

These preparations was always performed under dim red illumination.

Multielectrode Recordings and Spike Sorting

Extracellular recordings were obtained from the retinal ganglion cell layer in the isolated mouse retina using an array of 100 electrodes with 400μm inter-electrode distances [5]. The electrical signals captured by the electrodes array were amplified with a 100-channel amplified (Bionic Technologies, Inc) with a gain of 5000 and a bandpass between 250 and 7500 Hz. The selected data from each channel as well as the state of the visual stimulus were digitized with a resolution of 16 bits at a sampling rate of 30 kHz and stored using a signal processor data acquisition system.

All neural spike events recorded exceeded at least 3.25 the standard deviation of noise level. When a supra-threshold event occurred, the waveform and time was stored together with the state of the visual stimulus for later offline analysis.

Each electrode can detect light evoked single- or multi-unit responses making the characterization and grouping of spikes necessary. The spike sorting was carried out by Nev2lkit program, free open source software based on principal component analysis (PCA) method and different clustering algorithms [6]. Time stamps for action potentials of each sorted unit were used to generate inter spike interval histograms (ISI), peristimulus time histograms (PSTH) and peristimulus spike raster analysis using NeuroExplorer®(Nex Technologies) as well as NeurALC software.

Visual Stimuli

All visual stimuli were programmed in Python and reproduced with Vision egg an open source library for real-time visual stimulus generation [7]. For this we used an area of 120×154 pixels of a 16-bit ACER TFT at 60 Hz refresh rate. The patterns displayed on this area were resized to a 4×4mm area with optical lenses and projected through a beam splitter focusing the stimulus onto the photoreceptor layer.

The retinas were then stimulated with three different types of stimuli. Several repetitions of a 700ms flash (196.25 cd/m^2) were displayed followed by darkness for 2300ms to classify the ganglion cells in ON, OFF, ON/OFF or spontaneous with no response to light (NRL) [8].

We then proceeded to stimulate the photoreceptors layer with 250μm wide white bars crossing a black screen at 0.5 & 1Hz. Four pairs of stimuli were used: 0°, 45°,90°,135°, 180°, 225°, 270° and 315°.

This was followed by the presentation of an animated panoramic natural scene projected on a virtual drum for 180 seconds at 0.7Hzfrequency. The image size was 1031×156 pixels grouped into squares of 15×15 pixels and was presented in black and white.

Delimit and Locate the Receptive Field

To determine the size and localization of the cells receptive field [9], the photoreceptor layer was stimulated with 250μm wide white bars crossing the black

screen at 0.5Hz. To automatically map the response for each isolated ganglion cell to the corresponding squared-pixel from the stimulus image projection, an *ad-hoc* Python program was designed. Within this program, the responses to each pair of left-to-right and right-to-left moving-bars are processed separately to calculate their centroids.

To avoid measurement of unwanted firing responses such as noise signals, a custom weighting threshold was defined for filtering them. Then, both signals are set in phase to cancel inherent latency effects and locate the receptive field in every corresponding direction. Fig. 1 represents this automatic phasing process for a given cell response through each mentioned direction. Each phased contribution is added so that four $1 \times N$ matrices of responses are obtained: $M_{0,180}$,$M_{45,225}$, $M_{90,270}$ and $M_{135,315}$. Finally, the receptive field is calculated by multiplying M0,180, by Mt90,270 and M45,225 and Mt135,315 (their transposed orthogonal duals), and averaging the results.

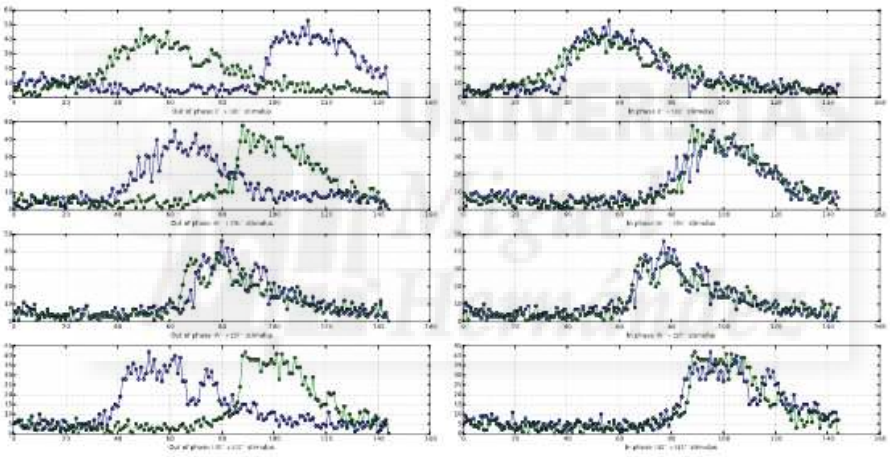

Fig. 1. Automatic phasing for 0°–180°, 45°–225°, 90°–270° and 135°–315° responses

To map the receptive field to the corresponding squared-pixel from the stimulus image, its centroid is calculated. The coordinates from this centroid reveals the actual image location from where the cell is integrating information.

Reconstruction of Natural Scenes

Once the process of determining and mapping every isolated ganglion cell is finished, a weighted set of ganglion cells responses (PSTH) is associated with every squared-pixel. As the original natural scene moves horizontally within a drum, every cell is mapped to a certain squared-pixel process as a $1 \times N$ row of image values in the range 0-255. For reconstructing the natural scene, the data

provided by each different ganglion cells PSTH was normalized between the ranges of the corresponding row by means of a linear regression. In this way, the highest firing rate for a given row corresponds to the highest level of gray within the mentioned row for an ON-type cell. In addition, as some receptive field areas expand to more than one single row, a weighted sum of each rows adjacency is taken into account. In this analysis, OFF cells and NRL were rejected.

3 Results

We performed extracellular recordings in three wild-type adult mice retina. A minimum of 40 retinal ganglion cells were recorded in each animal during each experiment. All of these were classified according to their preference to light ON, OFF, ON/OFF and NRL after the flash stimulus (Fig. 2).

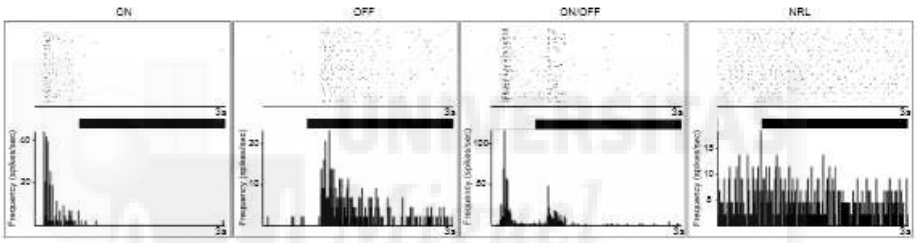

Fig. 2. Raster plot and histogram post stimuli (PSTH) of the four different ganglions cells after a 700ms light stimulus followed by 2300ms of darkness. Each raster plot represents the activity measured in action potentials of individual ganglion cells after a flash stimulus, repeated 30 times. The PSTHs shows the firing frequency (spikes/sec) during this stimulation. Bin size = 14ms.

Although the position and distance between electrodes is known, the location of each cell that they recorded from is not. Our goal was to identify the spatial position of each cell and outline the area of their receptive field. This was done using the responses recorded after light stimulation with bars (Fig. 3). The average value of the receptive field in our population was 0.201μm ± 0.026 SE. From this information we established the actual stimulus area that each cell was able to decode.

The ganglion cells responses were recorded during the motion of the actual scene stimulus repeated 30 times within 3 minutes. After spike sorting, 11 cells were chosen depending on their location to cover the whole image size (Fig 4). The data provided by their PSTH were normalized by a linear regression between the gray values range of the corresponding rows. The image reconstructed with only 11 cells is visually similar to the actual one (Fig 5). Specifically, for lines

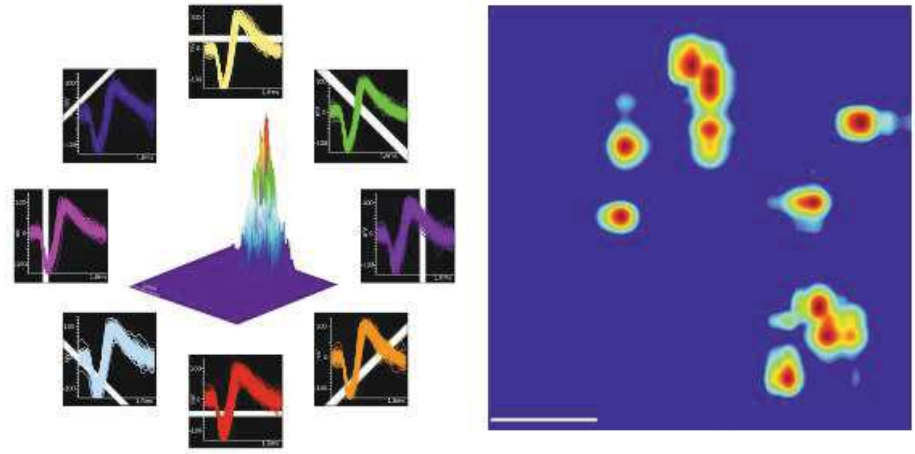

Fig. 3. Left) The action potential waveforms of a ganglion cell for each directional bar stimulus and a 3D plot of their receptive field. X axis = $\pm 100\mu$V; Y axis = 1.6ms. Right) Graphical representation of 11 cell receptor fields and from their responses to the natural scene was reconstructed. Scale bar = 1mm.

Fig. 4. Two examples of ganglion cells receptive fields and how these cells are mapped to the actual scene location during drum rotation. Scale bar = 1mm.

1-6, 7, 10 and 11 ON-type cells responses were selected. The remaining image was reconstructed based on ON/OFF-type responses.

Bhattacharyya distance was calculated between the reconstructions and processed actual images in order to obtain quantifiable information about the similarity of both objects [10]. For this comparative measure the value 1 is assigned to the biggest difference and 0 to an equal distribution. In all experiments we obtained values below 0.35 for this index.

However, nonparametric and parametric statistical tests were also performed using U Mann-Whitney and T student, respectively. In both cases we observed that there are no significant differences between images, $p > 0.05$.

If the actual stimuli are unknown the reconstruction can be performed making the lineal regression between 0-255 gray scale and the ganglion cells responses, regardless of the receptive field location. In these cases Bhattacharyya distance value was within the range 0.4-0.5 (Fig 5D).

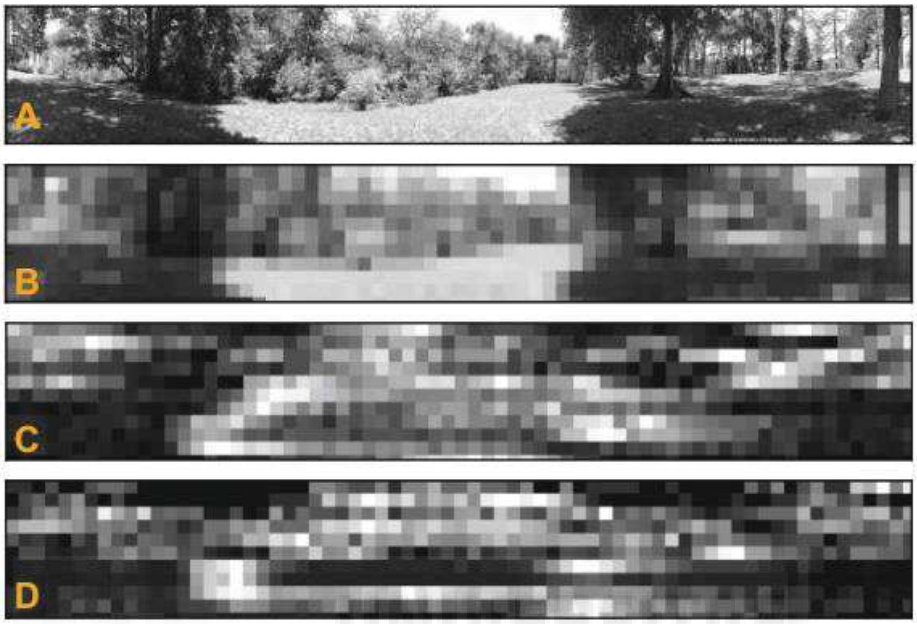

Fig. 5. A) The natural scene, 1031×159 pixels. B) Simplified image with pixels grouped into squares of 15 × 15. C) Image reconstructed based on ganglion cell responses of one animal, Bhattacharyya distance = 0.32. D) Image reconstructed without weighting between rows, Bhattacharyya distance = 0.42.

4 Conclusions

As a first approach, our preliminary results suggest that with the responses of only 11 ganglion cells we are able to reconstruct accurately a complicated natural image. This allows room for improvement for more accurate reconstruction if we were to incorporate more cells into our analysis. Moreover, using the proposed method it is not necessary to know what the natural image actually looks like for carrying out reconstructions as this can be done blind using the gray scale values to achieve reliable results. These experiments need to be repeated and analyzed using natural images presented at different frequencies of motion as well as in color to extend our knowledge for a more complete characterization of ganglion cell function. As this method is robust it can be adapted easily for characterization in other species.

Our ultimate goal is to apply the date acquired from this procedure and begin to compare ganglion cell visual responses in healthy retinas to those suffering from injury or neurodegenerative visual diseases. This could provide valuable information to the processes underlying the functional degradation of ganglion cells in visual impairments.

Acknowledgments. We are very grateful to Sonia Andreu for all her help and technical assistance. This work has been supported in part by grant MAT2012-39290-C02-01, by the Bidons Egara Research Chair of the University Miguel Hernández and by a research grant of the Spanish Blind Organization (ONCE).

References

1. Masland, R.H.: The Neuronal Organization of the Retina. Neuron 76(2), 266–280 (2012), http://www.cell.com/article/S0896627312008835/abstract, doi:10.1016/j.neuron.2012.10.002
2. Hoon, M., Okawa, H., Santina, L.D., Wong, R.O.: Functional architecture of the retina: Development and disease. Progress in Retinal and Eye Research 42, 44–84 (2014), http://www.sciencedirect.com/science/article/pii/S135094621400038X, doi:http://dx.doi.org/10.1016/j.preteyeres.2014.06.003
3. Gollisch, T., Meister, M.: Eye smarter than scientists believed: Neural computations in circuits of the retina. Neuron 65(2), 150–164 (2010), http://www.sciencedirect.com/science/article/pii/S0896627309009994, doi:http://dx.doi.org/10.1016/j.neuron.2009.12.00
4. Nirenberg, S., Pandarinath, C.: Retinal prosthetic strategy with the capacity to restore normal vision. Proceedings of the National Academy of Sciences 109(37), 15012–15017 (2012), arXiv:http://www.pnas.org/content/109/37/15012.full.pdf+html, doi:10.1073/pnas.1207035109
5. Fernández, E., Ferrández, J.-M., Ammermüller, J., Normann, R.A.: Population coding in spike trains of simultaneously recorded retinal ganglion cells1. Brain Research 887(1), 222–2229 (2000), http://www.sciencedirect.com/science/article/pii/S0006899300030729, doi: http://dx.doi.org/10.1016/S0006-89930003072-9
6. Bongard, M., Micol, D., Fernández, E.: NEV2lkit: A new open source tool for handling neural event files from multi-electrode recordings. International Journal of Neural Systems 24(04), 1450009, pMID: 24694167 (2014), arXiv:http://www.worldscientific.com/doi/pdf/10.1142/S0129065714500099, doi:10.1142/S0129065714500099
7. Straw, A.D.: Vision egg: An open-source library for realtime visual stimulus generation. Frontiers in Neuroinformatics 2, http://dx.doi.org/10.3389/neuro.11.004.2008, doi:10.3389/neuro.11.004.2008
8. Van Wyk, M., Wässle, H., Taylor, W.R.: Receptive field properties of on- and off-ganglion cells in the mouse retina. Visual Neuroscience 26, 297–308 (2009), http://journals.cambridge.org/article_S0952523809990137, doi:10.1017/S0952523809990137
9. Zhang, Y., Kim, I.-J., Sanes, J.R., Meister, M.: The most numerous ganglion cell type of the mouse retina is a selective feature detector. Proceedings of the National Academy of Sciences 109(36), E2391–E2398 (2012), arXiv:http://www.pnas.org/content/109/36/E2391.full.pdf+html, http://www.pnas.org/content/109/36/E2391.abstract, doi:10.1073/pnas.1211547109
10. Goudail, F., Réfrégier, P., Delyon, G.: Bhattacharyya distance as a contrast parameter for statistical processing of noisy optical images. J. Opt. Soc. Am. A 21(7), 1231–1240 (2004), http://josaa.osa.org/abstract.cfm?URI=josaa-21-7-1231, doi:10.1364/JOSAA.21.001231

3. Discusión y aportaciones

3.1. Aspectos morfológicos

La geometría fractal

Partiendo de la utilidad del análisis fractal como herramienta para identificar y clasificar tipos y clases de neuronas, algunos investigadores comenzaron a usar la metodología de los multifractales para intentar resolver el problema de que neuronas a simple vista muy diferentes tenían una misma dimensión fractal (Smith y Lange, 1996).

Un multifractal es un fractal que, en lugar de tener un único exponente característico de escalamiento -que nos da el valor de su dimensión-, tiene toda una distribución continua de ellos. La idea que subyace en el uso de este concepto en las neuronas es un intento de caracterizar aquellas zonas del árbol dendrítico diferenciadas por tener su propia dimensión fractal, que puede ser distinta a la global de la neurona.

En el primero de los artículos presentados en esta tesis (Fernández *et al.* 1999) estudiamos los aspectos teóricos y prácticos del cálculo de estas dimensiones multifractales, Dq, en las neuronas. Para contrastar los métodos utilizados -y conseguir así una mejor interpretación de los resultados obtenidos - los aplicamos también al estudio de los modelos de agregación por difusión limitada (DLA). Estas estructuras tienen una cierta semejanza morfológica

con algunas neuronas y, además, su geometría multifractal ya había sido analizada.

Con el procedimiento de recuento de cajas obtuvimos, tanto en las neuronas como en los DLA, unos resultados anómalos, debidos a efectos de tamaño que inciden en los cálculos que se realizan. Estos resultados son incompatibles, (Opheusden *et al.* 1996), con la definición y las propiedades básicas de la multifractalidad ya conocidas lo que nos indicaba lo inapropiado de este método.

Con el método *sand-box* aplicado a las neuronas sí que obtuvimos el comportamiento esperado (Witten y Sander, 1983) de las dimensiones generalizadas *Dq*, lo que aparentemente significaba que las neuronas son multifractales. Pero al tener en cuenta los resultados obtenidos en los DLA y compararlos con los de otros autores, (Vicsek *et al.* 1990), observamos importantes diferencias y hubo que reconsiderar esta conclusión. Nuestros resultados más bien confirmaban la hipótesis de Lam (1995), quien afirma que la aparente multifractalidad de los DLA obtenida en el estudio citado se debe a un efecto por el uso de tamaños finitos, que produce la desviación observada en las dimensiones con respecto a lo que sería un escalamiento único.

Esta interpretación aporta una descripción verosímil de todos los resultados numéricos obtenidos en los DLA finitos y en las neuronas y es una explicación suficiente de su aparente multifractalidad; se ha demostrado que conduce, al menos en el caso de los DLA, a predicciones erróneas. Como consecuencia tampoco en el caso de las neuronas la interpretación de la presencia de un conjunto de dimensiones distintas -un escalamiento

complejo- está suficientemente fundamentada, y por lo tanto no podemos concluir, a partir de los resultados obtenidos, que las neuronas sean multifractales.

Los mosaicos en la retina. La V-proporción

Continuando con los estudios morfológicos pasamos después a estudiar cómo se distribuyen los diferentes tipos celulares dentro de la retina. Para evaluar cómo están formados los mosaicos retinianos hay disponibles varias técnicas cuantitativas: cálculo de densidades, autocorrelación, índices de regularidad, etc. Nosotros desarrollamos un nuevo método basado en el diagrama de Voronoi o teselación de Dirichlet que permite el análisis de los patrones de interacción entre las poblaciones celulares. Le pusimos el nombre de V-proporción.

En su versión inicial aplicamos este método para determinar la correlación espacial entre los conos azules y las células horizontales sin axón de los felinos (Ahnelt *et al.* 2000). En la mayoría de los mamíferos los conos azules representan aproximadamente un 10% total de conos y están organizados de forma poco regular (Anhelt, 1987), (Kouyama and Marshak, 1997), (Galli-Resta *et al.*, 1999). Por el contrario, las células horizontales sin axón que conectan solo con conos se distribuyen regularmente. El hecho de que estas células horizontales presenten formas alargadas e irregulares y realicen contactos sinápticos con la mayor parte de los conos dentro de sus campos dendríticos hizo que nos planteáramos este estudio.

La razón de basar el diseño de la V-proporción en el diagrama de Voronoi es que los polígonos que con él se obtienen se aproximan mejor a la distribución

de los campos dendríticos de las células horizontales que las áreas circulares. Una vez construido el diagrama para la población de estas células, nuestra referencia en este caso, incorporamos alrededor de sus lados unas bandas cuya anchura es proporcional a la distancia al centro del polígono (el soma de la célula). La proporción de neuronas del otro mosaico que está en esas bandas cuantifica y, en cierto modo, localiza la correlación existente.

Al aplicar el método a nuestros datos, el mosaico de conos azules mostró una correlación espacial negativa con respecto al de las células horizontales. Se observó un gradiente en la distribución de conos azules que tienden a evitar el cuerpo y las dendritas primarias de las células horizontales y predominan en los límites de los polígonos de Voronoi. Esto da lugar a que la proporción de conos azules/no azules sea diferente en el centro y la periferia de estas células horizontales, hecho que puede tener importantes implicaciones en el procesamiento de la información del color en la retina.

Comprobada la utilidad del método que habíamos ideado decidimos profundizar en su desarrollo efectuando varias mejoras, comparándolo con otros métodos que estudian las relaciones espaciales entre diferentes poblaciones celulares y evaluando los resultados que proporciona tanto en simulaciones como en datos reales (Martínez *et al.*, 2010).

Solventamos el problema de los efectos de borde característicos de métodos similares considerando para el estudio el área comprendida en el recubrimiento convexo de la población de referencia. Añadimos la posterior construcción de simulaciones aleatorias de la distribución de las dos poblaciones para poder contrastar así la significancia de los resultados mediante un test de Montecarlo. Esto permite -además de comprobar si hay

atracciones, repulsiones o ninguna relación- asociar un intervalo de confianza al comportamiento resultante en los distintos anchos de banda considerados, consiguiendo así información adicional al detectar en qué zonas se producen mayores desviaciones con respecto a las simulaciones.

Para validar el método lo aplicamos a poblaciones simuladas, generadas siguiendo distribuciones de probabilidad matemática que reflejaran correlaciones positivas, negativas o independencia. En todos los casos la V-proporción detectó certeramente dichas interrelaciones. Por último, lo usamos también en poblaciones reales de células comparando nuestros resultados con trabajos previos en los que se analizaron los mismos datos. La similitud entre las conclusiones obtenidas en nuestro estudio y las de dichos trabajos confirma la efectividad del método de la V-proporción que, como ya hemos comentado, presenta la ventaja adicional de aportar más información sobre la situación de las neuronas de las poblaciones.

3.2. Codificación y decodificación

El código neuronal

Otro de los problemas estudiados fue el del código neuronal: analizar los trenes de potenciales de acción con los que las células ganglionares de la retina responden a los estímulos para dilucidar cuales son los parámetros más relevantes con los que transmiten la información visual.

En un primer trabajo los analizamos usando redes neuronales artificiales (Ferrández *et al.* 1999) como alternativa novedosa a los diversos tipos de análisis estadístico utilizados habitualmente.

Las redes neuronales artificiales intentan simular procesos mentales como el aprendizaje, la memoria asociativa, la generalización, etc. por medio de modelos matemáticos simples que imitan la actividad funcional del sistema nervioso sin descender a considerar los procesos químicos que la causan.

En nuestro trabajo hemos usado dos redes distintas. La primera fue la de propagación hacia atrás (*BackPropagation*) de tres capas con 20 nodos en la capa oculta. La capa de salida consistía en tantas unidades como clases se querían reconocer. Con esta arquitectura cada unidad de la capa de salida solo dispara para un cierto estímulo mientras el resto no se activa.

El sistema de entrenamiento en este tipo de red consiste en el siguiente proceso: empezar con unos pesos sinápticos cualquiera e introducir unos datos iniciales de entrada (en la capa de entradas) elegidos al azar entre los que se van a usar para el entrenamiento; la red genera entonces un vector de datos de salida (propagación hacia delante) usando una determinada función de activación; se compara la salida generada con la deseada y la diferencia obtenida (error) se usa para ajustar los pesos sinápticos de los nodos de la capa de salida; de un modo similar el error se propaga hacia atrás, hacia la capa anterior, ajustando los correspondientes pesos sinápticos y así hasta que se alcance la capa de entradas. Este proceso se repite con los diferentes datos de entrenamiento.

La otra red usada fue la LVQ (*Learning Vector Quantization*) de Kohonen supervisada, con 16 unidades en la capa competitiva y una tasa de aprendizaje de 0.05. Pertenece a la categoría de las redes competitivas o mapas de autoorganización. En ellas los nodos más parecidos al vector de entrada incrementan su peso como respuesta a esa entrada, mientras el peso

del resto disminuye -salvo el de sus vecinas más cercanas-. Esto establece una relación topológica en el mapa. El tamaño de la vecindad disminuye a lo largo del entrenamiento; en eso consiste la autoorganización. La principal ventaja de usar el tipo LVQ es que se necesita menos tiempo para alcanzar los criterios de convergencia.

Ambas redes neuronales indican que el cerebro puede potencialmente obtener información sobre las características del estímulo de las respuestas de la población, pero no tanto de las de las células aisladas. Los parámetros más relevantes en la codificación del estímulo han resultado ser el número de espigas (la tasa media) y el tiempo exacto de la primera espiga tras el estímulo. El hecho de que con ambos estímulos se obtengan similares -y elevados- índices de estimación parece indicar redundancia en la transmisión de la información, lo que está relacionado con la robustez del sistema para transmitir datos.

En el siguiente trabajo (Ferrández *et al*., 2002) abordamos las mismas cuestiones, pero usando herramientas propias de la Teoría de la Información de Shannon-Weaver, (Shannon, 1949), porque permiten cuantificar la transmisión del código.

En este estudio hemos ido cambiando el número de neuronas de la población para observar si la cantidad de información crece linealmente con el tamaño de la población o se satura produciendo un fenómeno de redundancia. Observamos que las células con más variabilidad en su respuesta transmiten más información y que, nuevamente, la población transmite mucho más que las células individuales.

Al analizar la información contenida en poblaciones de tamaño creciente se vio que al principio el número de bits transmitido crece linealmente con el tamaño pero que a partir de cierto número de células deja de hacerlo debido a que la información se satura. El comportamiento no es sinérgico, ni independiente, sino redundante: siempre hay un número de células que es capaz de transmitir casi el 100% de la información; por tanto, añadir más células al conjunto no proporciona más información. Nuevamente observamos redundancia, que puede ser útil para conseguir la robustez requerida para que la retina mantenga sus funciones en circunstancias adversas.

Distinguir grupos de neuronas sincrónicas

Estas conclusiones de saturación y robustez del sistema nos condujeron al intento de clasificar las respuestas neuronales de la población para poder detectar interacciones entre subgrupos de neuronas que permitieran reducir los datos manteniendo la información relevante sobre el estímulo.

Así en Bonomini *et al.* (2005a) desarrollamos y validamos un método para este propósito basado en dos comportamientos distintos: periodicidad y respuesta del estado latente. Consiste en crear grupos de neuronas relacionadas definiendo un conjunto inicial basado en los autocorrelogramas o los histogramas del tiempo periestímulo de las unidades y después agrupando las neuronas minimizando la distancia entre las de una clase y maximizando por el contrario las distancias entre diversas clases. Comprobamos su eficiencia para identificar subpoblaciones coherentes dentro de la población registrada, a pesar de ser sencillo y versátil.

Este método de clasificación lo incorporamos en DATA-MEAns, un programa libre de código abierto explicado en Bonomini *et al.*, (2005b) y puesto a disposición de la comunidad científica para facilitar un análisis sencillo de los datos registrados con multielectrodos. Su principal ventaja es que utiliza ficheros ASCII, lo que facilita que pueda ser usado por cualquier paquete gráfico, estadístico matemático con el que un laboratorio de neurociencia esté habituado a trabajar.

Decodificación: evaluar resultados

Finalmente hemos intentado estudiar mecanismos para decodificar la información visual que las células ganglionares de la retina transmiten cuando se estimulan con imágenes que no son estáticas, que se mueven y que son lo más realistas posible. Ello ha dado lugar al último de los artículos que incluimos (Díaz-Tahoces *et al.* 2015) y a otro artículo que actualmente se encuentra en fase de preparación.

Básicamente hemos presentado un procedimiento que permite reconstruir con cierta precisión una imagen compleja tomada de la naturaleza a partir de las respuestas, registradas simultáneamente, de varias células ganglionares de la retina. De hecho, hemos conseguido reconstruir una imagen compleja con tan sólo 11 células ganglionares. Para medir de algún modo dicha precisión hemos comparado las imágenes original y reconstruida mediante diversos métodos, optando finalmente por el de calcular la distancia de Bhattacharyya. Esta cuantificación nos permite contrastar los resultados con los que se obtengan al incorporar más células al análisis o al utilizar otros posibles procedimientos de reconstrucción del estímulo, evaluando así si son más exactos.

También puede resultar útil para comparar los datos obtenidos con este procedimiento de decodificación al aplicarlo a retinas sanas con los que resulten al estudiar retinas dañadas o que sufran enfermedades visuales neurodegenerativas, permitiendo conocer mejor los deterioros que se hayan producido en los aspectos funcionales de las células ganglionares.

4. Conclusiones y líneas futuras

Conclusiones.

A partir de los resultados de los trabajos que presentamos en esta memoria de tesis podemos extraer varias conclusiones, unas relacionadas con el procesamiento de la información en la retina y otras sobre la validez e interés de los métodos matemáticos desarrollados y utilizados para su estudio. Teniendo en cuenta ambos aspectos consideramos que las conclusiones principales son las siguientes:

1. No se puede concluir que las neuronas son multifractales debido a la incidencia en los cálculos de efectos de tamaño que impiden una interpretación exacta de los resultados numéricos.

2. La V-proporción es un método útil y eficaz para estudiar las relaciones espaciales entre dos conjuntos distintos de células que indiquen posibles dependencias funcionales entre ellos.

3. El código poblacional posee una mayor capacidad discriminativa de los estímulos que la codificación individual, proporcionando una determinada inmunidad al ruido a través de la redundancia en la codificación, ya que la tasa de acierto de la población se satura a partir de un número determinado de células.

4. Es posible desarrollar métodos efectivos para clasificar las neuronas según su respuesta, identificando así subgrupos coherentes en la población registrada que permitan reducir la cantidad de información significativa.

5. Se pueden obtener valores cuantitativos de la semejanza entre las escenas naturales utilizadas en los estímulos y las reconstruidas a partir de las respuestas de grupos de células ganglionares. Esto permite analizar y entender mejor los procesos de decodificación de la información visual.

Líneas futuras

1.- Generalizar el método de la V-proporción a tres dimensiones

Los avances técnicos en microscopia electrónica permiten conocer y estudiar mejor la morfología tridimensional de las neuronas individuales y las células glía, lo que hace posible utilizar el cálculo de estadísticos espaciales asociados a objetos tridimensionales (Eglen *et al.*, 2008) y estudiar la disposición espacial de las neuronas que están disparando sincrónicamente. En este sentido sería interesante generalizar el método de la V-proporción a tres dimensiones y por otro lado intentar localizar con más precisión los circuitos neuronales que subyacen en la actividad sincrónica de grupos de células retinianas.

2. El papel de las células glía

Tradicionalmente se ha asumido que la función de las células de Müller en la retina de los vertebrados es fundamentalmente dar soporte a las neuronas que transmiten la información. Sin embargo, los trabajos de Reichenbach y sus colegas en la Universidad de Leipzig han mostrado que además facilitan la transmisión de los fotones a través de la retina hasta los fotorreceptores (Franze et al., 2007) y mejoran la relación señal/ruido minimizando la dispersión de luz intrarretiniana (Reichenbach y Bringmann, 2013). También se conoce que contribuyen a la generación de la onda b del electrorretinograma mediante la regulación de la distribución de potasio a través de toda la retina (Newman y Odette, 1984). Cabe preguntarse pues si estas células glía tienen algún papel en la transmisión de las imágenes y en ese caso cómo se puede implementar en el diseño de la retina artificial.

3.- Uso de técnicas de Big Data.

En los experimentos con el uso de multielectrodos cada vez se registra una mayor cantidad de células. Para estudiar las interacciones entre un gran número de ellas se necesitan utilizar herramientas estadísticas capaces de gestionar el procesado y análisis de datos de tamaño ingente. Esta situación se está produciendo también en otros campos científicos porque los dispositivos electrónicos y las redes sociales son una fuente inagotable de datos. Ha aparecido así el concepto de *Big Data*. Los científicos e investigadores especializados en el análisis de datos se enfrentan al reto y la necesidad de describir de un modo

eficiente grandes cantidades de datos con nuevas herramientas ya que usar los procedimientos tradicionales sería excesivamente costoso y tardaría mucho tiempo computacional.

Recientemente la revista *Nature Neuroscience* (2014) ya ha dedicado un número especial a presentar diferentes tipos de *big data* en neurociencia, así como a discutir distintos aspectos controvertidos sobre su uso y utilidad.

Desde el punto de vista de nuestros estudios puede ser de gran interés utilizar con los datos neuronales registrados en los experimentos las nuevas técnicas y estrategias que se están desarrollando como consecuencia de este fenómeno, aunque, como ya se ha dicho por varios expertos (Lloret-Villas *et al*., 2016), ello requerirá que los datos sean más abiertos e integrados.

4.- Uso de wavelets.

La actividad neuronal es variable. Las respuestas ante presentaciones repetidas de un mismo estímulo presentan variaciones, debidas en parte a la plasticidad neuronal. Nos planteamos intentar utilizar en futuros trabajos métodos matemáticos más específicos que sean capaces de decodificar información en procesos no estacionarios con características que varían con el tiempo. Una posibilidad es analizar las señales obtenidas de los registros multicelulares mediante transformaciones basadas en ondículas (*wavelets*, en inglés, es el término con el que son más conocidas).

Aunque se han desarrollado principalmente gracias a su eficacia para codificar imágenes de un modo eficiente ya se han comenzado a usar para estudiar la dinámica de los sistemas neuronales. Se han aplicado fundamentalmente al problema de clasificar los potenciales de acción según su forma (Hulata *et al.* 2000), (Letelier y Weber 2000), (Pavlov *et al.* 2007), y al análisis de electroencefalogramas (Hramov *et al.* 2015), obteniéndose hasta el momento resultados bastante prometedores. Dado que permiten comprimir grandes cantidades de información creemos que puede ser interesante explorar los resultados que nos proporcione utilizarlas en los registros neuronales obtenidos con multielectrodos.

5.- Consecuencias de un código fuertemente dinámico.

Un trabajo reciente (Tikidji-Hamburyan *et al.* 2015) ha mostrado que la actividad combinada de las células ganglionares de la retina depende de la luminosidad ambiental: con cada cambio en el nivel de luz la respuesta de una gran fracción de células ganglionares cambia cualitativamente. Incluso las características de las respuestas neuronales que se consideran fundamentales como las que permiten clasificarlas en ON, OFF u ON-OFF dependen dinámicamente de las condiciones globales del estímulo.

Esto obliga a explorar las potenciales consecuencias que un código retiniano fuertemente dinámico tiene para nuestra actual comprensión de la función y el procesamiento visual de la retina. A la vista de esta dependencia de los patrones de respuesta de las células ganglionares de la retina con respecto a las condiciones ambientales parece

necesario reevaluar tanto las teorías sobre cómo codifica la retina los estímulos visuales como los modelos de decodificación de los estímulos por áreas cerebrales superiores.

5. Referencias

Ahnelt, P.K., Fernández, E., Martínez, O., Bolea, J.A. y Kubber-Heiss, A. (2000) "Irregular S-cone mosaics in felid retinas. Spatial interaction with axonless horizontal cells revealed by cross correlation" *Journal of the Optical Society of America A*, 17(3), pp. 580–588.

Bongard, M., Micol, D. y Fernández, E. (2014) "NEV2lkit: A new open source tool for handling neural event files from multi-electrode recordings" *International Journal of Neural Systems* 24(04), 1450009.

Bonomini M.P., Ferrández J.M., Bolea J.A. y Fernández E. (2005a) "Formulation and Validation of a method for classifying Neurons from multielectrode recordings". En *Mechanisms, Symbols and Models Underlying Cognition*, pp. 68- 76, Heidelberg/Berlin, Ed. Springer.

Bonomini, M.P., Ferrández, J.M., Bolea, J.A. y Fernández E., (2005b) "DATAMeans: An open source tool for the classification and management of neural ensemble recordings" *Journal of Neuroscience Methods*, 148 pp. 137-46.

Boycott, B.B., y Wassle, H. (1974) "The morphological types of ganglion cells of the domestic cat's retina" *Journal of Physiology*, 240, pp. 397–419.

Brindley, G.S. (1982) "Effects of electrical stimulation of the visual cortex" *Human neurobiology*, 1, pp. 281-283.

Brindley, G.S., Donaldson, P.E.K., Falconer, M.A. y Rushton, D.N. (1972) "The extent of the region of occipital cortex that when stimulated gives phosphenes fixed in the visual field" *Journal of Physiology,* 225(2), pp. 57-58.

Brindley, G.S. y Lewin, W.S. (1968) "The sensations produced by electrical stimulation of the visual cortex" *Journal of Physiology,* 196(2), pp. 479-493.

Cook, J.E. (2003) "Spatial regularity among retinal neurons". En: Chalupa, L.M. y Werner, J.S., (eds.) *The Visual Neurosciences*. (pp. 477-491). Cambridge, MA, MIT Press.

Crick, F. (2000) *La búsqueda científica del alma, una revolucionaria hipótesis para el siglo XXI*. (Francisco Páez, trad.) Madrid: Ed. Debate. (Obra original publicada en 1994).

Daubechies, I. (1992) *Ten Lectures on Wavelets*. Philadelphia: Society for Industrial and Applied Mathematics.

Dayan, P. y Abbott, L.F. (2001) *Theoretical neuroscience: computational and mathematical modeling of neural systems*. Massachusetts, The MIT Press.

Díaz-Tahoces, A., Martínez-Álvarez, A., García-Moll, A., Humphreys, L., Bolea, J.A. y Fernández, E. (2015) "Towards the Reconstruction of Moving Images by Populations of Retinal Ganglion Cells" En *Artificial Computation in Biology and Medicine*, pp 220-227, London, Springer-Verlag.

Dobelle, W.H. (2000) "Artificial vision for the blind by connecting a television camera to the visual cortex" *ASAIO Journal,* 46(1) pp. 3-9.

Dobelle, W.H. y Mladejovsky, M.G. (1974) "Phosphenes produced by electrical stimulation of human occipital cortex, and their application to the development of a prosthesis for the blind" *Journal of Physiology (Lond),* 243 pp. 553-576.

Dobelle, W.H., Mladejovsky, M.G., Evans J.R., Roberts T.S. y Girvin J.P. (1976) "'Braille' reading by a blind volunteer by visual cortex stimulation" Nature, 259 pp. 111-112.

Dobelle, W.H., Mladejovsky, M.G. y Girvin J.P. (1974) "Artificial vision for the blind: electrical stimulation of visual cortex offers hope for a functional prosthesis" *Science,* 183 pp.440-444.

Duyckaerts, C. y Godefroy, G. (2000) "Voronoi tessellation to study the numerical density and the spatial distribution of neurones" *Journal of Chemical Neuroanatomy*, 20(1) pp. 83–92.

Eglen, S.J., Lofgreen, D.D., Raven, M.A. y Reese, B.E. (2008) "Analysis of spatial relationships in three dimensions: tools for the study of nerve cell patterning" *BMC Neuroscience*, 9 pp. 68.

Eglen, S.J., Raven, M.A., Tamrazian, E. y Reese, B. E. (2003) "Dopaminergic amacrine cells in the inner nuclear layer and ganglion cell layer comprise a single functional retinal mosaic" *Journal of Comparative Neurology*, 466(3) pp. 343–55.

Falconer, K. (2003) *Fractal Geometry: Mathematical Foundations and Applications.* John Wiley, New York.

Fernández, E. (2008) "A Cortical Visual Neuroprosthesis for the Blind" *mst|news*, 4(08) pp. 8-11.

Fernández, E., Bolea, J.A., Ortega, G. y Louis, E. (1999) "Are neurons multifractals?" *Journal of Neuroscience Methods*, 89(2) pp. 151–157.

Fernández, E., Eldred, W.D., Ammermüller J., Block A., von Bloh W. y Kolb H. (1994) "Complexity and scaling properties of amacrine, ganglion, horizontal and bipolar cells in the turtle retina" *Journal of Comparative Neurology*, 347(3) pp. 397–408.

Fernández, E., Pelayo. F., Romero, S., Bongard, M., Marín, C., Alfaro, A. y Merabet L. (2005) "Development of a cortical visual neuroprosthesis for the blind: the relevance of neuroplasticity" *Journal of Neural Engineering*. 2:R1-12.

Ferrández, J.M., Bolea, J.A., Ammermüller J., Normann R.A. y Fernández E. (1999) "A Neural Network Approach for the Analysis of Multineural Recordings in Retinal Ganglion Cells". En *Engineering Applications of Bio-Inspired Artificial Neural Networks*, pp. 289-298. Berlin/Heidelberg, Ed. Springer.

Ferrández, J. M., Bongard, M., de Quirós, F. G., Bolea, J. A. y Fernández, E. (2002) "Neural coding analysis in retinal ganglion cells using information theory". En *ICANN '02: Proceedings of the International Conference on Artificial Neural Networks*, pp. 174–179, London, Springer-Verlag.

Franze, K., Grosche, J., Skatchkov, S.N., Schinkinger, S., Foja, C., Schild, D., Uckermann, O., Travis, K., Reichenbach, A. y Guck, J. (2007) "Müller cells are

living optical fibers in the vertebrate retina" *Proceedings of the National Academy of Sciences*. 104 (20): 8287–8292.

Galli-Resta, L., Novelli, E., Volpini, M. y Strettoi, E. (2000) "The spatial organization of cholinergic mosaics in the adult mouse retina" *European Journal of Neuroscience,* 12(10) pp. 3819–22.

Hanan, W.G. y Heffernan, D.M. (2001) "Geometrical multifractality of the perimeter of DLA clusters" *Chaos, Solitons and Fractals*, 12, pp. 193–195.

Hramov, A.E., Koronovskii, A.A., Makarov, V.A., Pavlov, A.N. y Sitnikova, E. (2015) *Wavelets in Neuroscience*. Springer, Berlin.

Hodgkin, A.L. y Huxley, A.F. (1952) "A quantitative description of membrane current and its application to conduction and excitation in nerve", *Journal of Physiology*, 117, pp. 500-544

Hulata, E., Segev, R., Shapira, Y., Benveniste, M. y Ben-Jacob, E. (2000) "Detection and sorting of neural spikes using wavelet packets" *Physical Review Letters*, 85(21) pp. 4637–40.

Jelinek, H.F., Bolea, J. A. y Fernández, E. (2000) "Towards a useful fractal analysis methodology in biological research" En *IV Congreso Iberoamericano de Biofísica*, pág. 136, Alicante, España.

Jelinek, H.F. y Fernández, E. (1998) "Neurons and fractals: how reliable and useful are calculations of fractal dimensions?" *Journal of Neuroscience Methods,* 81(1-2) pp. 9-18.

Kolb H., Nelson R. y Mariani A. (1981) "Amacrine cells, bipolar cells and ganglion cells of the cat retina: a Golgi study" *Vision Research,* 21 pp. 1081–1114.

Koch, C. (2005) *La consciencia. Una aproximación neurobiológica.* (Joan Soler, trad.). Ed. Ariel, Barcelona. (Obra original publicada en 2004).

Kohonen, T. (1984) *Self Organization and Associative Memory*. New York, Springer Verlag.

Kolb, H., Fernández, E., et al. (1994) "Are there three types of horizontal cell in the human retina?" *Journal of Comparative Neurology*, 343 pp. 370–386.

Lam, C. H. (1995) "Finite-size effects in diffusion-limited aggregation" *Physical Review B*, 52 pp. 2841–7.

Letelier, J. C. y Weber, P. P. (2000) "Spike sorting based on discrete wavelet transform coefficients" *Journal of Neuroscience Methods*, 101(2) pp. 93–106.

Lewicki M.S. (1998) "A review of methods for spike sorting: the detection and classification of neural action potentials" *Network,* 9(4) pp, 53-78.

Lloret-Villas, A., Daudin, R. y Le Novère N. (2016) ""Big Data" in neuroscience: open door to a more comprehensive and translational research" *Big Data Analytics*, 1:5 pp.1-8.

Martínez Mozos, O., Bolea, J. A., Ferrández, J. M., Ahnelt, P. K. y Fernández, E. (2010) "V-Proportion: A method based on the Voronoi diagram to study spatial relations in neuronal mosaics on the retina" *Neurocomputing*, 74 (1-3) pp. 418- 427.

Maynard, E.M. (2001) "Visual prostheses" *Annual Review of Biomedical Engineering*, 3 pp. 145-168.

Meister, M. y Hosoya, T. (2001) "Are retinal ganglion cells independent encoders?" *http://www.variational-bayes.org/~pel/critics/Meister_2001_Encoders.pdf.*

Meister, M., Legando, L. y Baylor, D. (1995) "Concerted signaling by retinal ganglion cells" *Science*, 270 pp. 1207–1210.

Meister, M., Pine, J. y Baylor, D. (1994) "Multineuronal signals from the retina: acquisition and analysis" *Journal of Neuroscience Methods*, 51(1) pp. 95-106.

Newman, E.A. y Odette, L.L. (1984) "Model of electroretinogram b-wave generation: a test of the K+ hypothesis" *Journal of Neurophysiology*, 51 pp. 164–182.

Nirenberg, S., Carcieri, S.M., Jacobs, A.L. y Latham, P.E. (2001) "Retinal ganglion cells act largely as independent encoders" *Nature*, 411 pp. 698–701.

Normann, R.A. y Fernández, E. (2016) "Clinical applications of penetrating neural interfaces and Utah Electrode Array technologies" *Journal of Neural Engineering*, 13(6): 061003.

Normann, R.A., Greger, B., House, P., Romero, S., Pelayo, F. y Fernández, E. (2009) "Toward the development of a cortically based visual neuro-prosthesis" *Journal of Neural Engineering*, 6(3): 035001.

Normann R.A., Maynard, E.M., Guillory, K.S. y Warren D.J. (1996) "Cortical implants for the blind" *IEEE Spectrum*, 33(5) pp. 54-59.

Normann R.A., Maynard E.M., Rousche P.J. y Warren D.J. (1999) "A neural interface for a cortical vision prosthesis" *Vision Research,* 39(15): 2577-2587.

Olshausen, B. y Field, D. (2005) "How close are we to understanding V1?" *Neural Computation* 17, pp. 1665–1699.

Olshausen, B. y Field, D. (1996) "Emergence of simple-cell receptive field properties by learning a sparse code for natural images" *Nature* 381, pp. 607–609.

Opheusden, J.H.J. van, Bos, M.T.A. y Kaaden G. van der (1996) "Anomalous multifractal spectrum of aggregating Lennard-Jones particles with Brownian dynamics" *Physica A*, 227(3) pp. 183–196.

Pavlov, A., Makarov, V.A., Makarova, I. y Panetsos, F. (2007) "Sorting of neural spikes: When wavelet based methods outperform principal component analysis" *Natural Computing*, 6 (3), pp. 269–281.

Penfield, W. y Jaspers, H. (1974) *Epilepsy and the functional anatomy of the human brain*. London, England, Churchill.

Penfield, W. y Rasmussen, T. (1950) *The cerebral cortex of man*. New York, Macmillan.

Polyak, S.L. (1941) *The retina*. Chicago, University of Chicago Press.

Reichenbach, A. y Bringmann, A. (2013) "New functions of Müller cells" *Glia*, 61, pp. 651–678.

Rey H.G., Pedreira C. y Quian Quiroga R. (2015) "Past, present and future of spike sorting techniques" *Brain Research Bulletin*, 119 (Pt B) pp. 106-117.

Rodieck, R.W. (1991) "The density recovery profile: a method for the analysis of points in the plane applicable to retinal studies" *Visual Neuroscience*, 6(2) pp. 95–111.

Rousche, P.J. y Normann, R. (1999) "Chronic intracortical microstimulation (ICMS) of cat sensory cortex using the Utah Intracortical Electrode Array" *IEEE Transactions on Rehabilitation Engineering*, 7(1) pp. 56-68.

Schmidt, E.M., Bak, M.J., Hambrecht, F.T., Kufta, C.V., O'Rourke, D.K. y Vallabhanath, P. (1996) "Feasibility of a visual prosthesis for the blind based on intracortical microstimulation of the visual cortex" *Brain*, 119 pp. 507-522.

Schnitzer M.J. y Meister M. (2003) "Multineuronal firing patterns in the signal from eye to brain" *Neuron*, 37 pp. 499 –511.

Shannon, C.E. (1948) "A mathematical theory of communication" *Bell System Technical Journal*, 27 pp. 379–423.

Tikidji-Hamburyan, A., Reinhard, K., Seitter, H., Hovhannisyan A., Procyk C.A., Allen A.E., Schenk M., Lucas R.J. y Münch T.A.. (2015) "Retinal output changes qualitatively with every change in ambient illuminance" *Nature Neuroscience*, 18(1) pp. 66–74.

Usrey W.M. y Reid R.C. (1999) "Synchronous activity in the visual system" *Annual Review of Physiology*, 61 pp. 435-456.

Vicsek, T. (1992) *Fractal Growth Phenomena*. Singapore: World Scientific.

Vicsek, T., Family, F. y Meakin, P. (1990) "Multifractal geometry of diffusion-limited aggregates" *Europhysics Letters*, 12 pp. 217–222.

Wässle, H., Peichl, L. y Boycott, B.B. (1983) "A spatial analysis of on- and off-ganglion cells in the cat retina" *Vision Research*, 23(10) pp. 1151–60.

Wässle, H. y Riemann, H.J. (1978) "The mosaic of nerve cells in the mammalian retina" *Proceedings of the Royal Society of London. Series B, Biological sciences,* 200(1141) pp. 441–461.

Witten, T. A. y Sander, L.M. (1983) "Diffusion limited aggregation" *Physical Review B*, 27 pp. 5686–97.